University of Southern Queensland
Faculty of Health, Engineering and Sciences

Modelling the behaviour of floodways subjected to flood loadings

A dissertation submitted by

Shane Cummings

In fulfilment of the requirements of

ENG 4111 and ENG 4112 Research Project

Towards the degree of

Bachelor of Engineering (Honours) (Civil) BENH

October 2015

ABSTRACT

This research investigates the behaviour of floodways when subjected to extreme flood loadings. Queensland floods of 2010 / 11 and 2013 indicated many floodways failed to meet performance requirements to withstand such events. Current floodway design guidelines primarily focus on hydraulic design aspects for determining a floodways capacity, similar to that of a broad crested weir. This approach fails to consider additional loadings such as drag, debris, impact and lifting forces. Therefore, the loadings utilised in this research are adapted from AS 5100.2-2004: Bridge Design. Strand7 software is used to perform a 2D plane strain finite element analysis to identify the potential failure mechanisms and areas of vulnerability within floodway structures and surrounding soils. This analysis focused on the Left Hand Branch Road (LHBR) floodway located in the Lockyer Valley region, one of the worst-affected areas in Queensland.

Due to limited historical flood data available for this region, a parametric study was conducted and identified the worst loading combination with respect to flow velocities and flow depths. Analysis concluded the stress imposed by the worst load combination did not exceed the 32 MPa compressive strength of the concrete used in the LHBR structure even once a damage simulation had been performed. Therefore the floodway is adequate to withstand all stresses resulting from flow velocities less than 10 m/s, however displacement within the structure, surrounding soils and rock protection appeared to be of more concern. Areas of vulnerability and displacement magnitudes have been identified, however, quantifying the significance of this displacement is difficult without an Australian Standard for floodway design to compare to.

Based on the structural adequacy of the floodway, the most critical failure mechanisms are most likely attributed to erosion or scour in and around the immediate area of the floodway.

University of Southern Queensland

Faculty of Health, Engineering and Sciences

LIMITATIONS OF USE

The Council of the University of Southern Queensland, its Faculty of Health, Engineering & Sciences, and the staff of the University of Southern Queensland, do not accept any responsibility for the truth, accuracy or completeness of material contained within or associated with this dissertation.

Persons using all or any part of this material do so at their own risk, and not at the risk of the Council of the University of Southern Queensland, its Faculty of Health, Engineering & Sciences or the staff of the University of Southern Queensland.

This dissertation reports an educational exercise and has no purpose or validity beyond this exercise. The sole purpose of the course pair entitled "Research Project" is to contribute to the overall education within the student's chosen degree program. This document, the associated hardware, software, drawings, and other material set out in the associated appendices should not be used for any other purpose: if they are so used, it is entirely at the risk of the user.

CERTIFICATION

I certify that the ideas, designs and experimental work, results, analyses and conclusions set out in this dissertation are entirely my own effort, except where otherwise indicated and acknowledged.

I further certify that the work is original and has not been previously submitted for assessment in any other course or institution, except where specifically stated.

Shane Cummings
Student Number: U1024662

Signature

29th October 2015

Date

ACKNOWLEDGEMENTS

I would like to acknowledge everyone who contributed to and assisted me throughout this research. In particular I would like to make mention of:

My supervisors, Professor Karu Karunasena, Dr Weena Lokuge and Dr Buddhi Wahalathantri for their ongoing support, feedback and encouragement.

A special mention to Dr Buddhi Wahalathantri for his patience, generosity of time and imparted knowledge during the finite element analysis stage of this project.

Lockyer Valley Regional Council who supplied the Left Hand Branch Road Floodway information and drawings which made this research possible.

To my wife Janine, friends and family, thank you for all your patience, understanding, encouragement and support over the last few years.

TABLE OF CONTENTS

LIST OF FIGURES

LIST OF TABLES

LIST OF APPENDIX FIGURES

LIST OF APPENDIX TABLES

NOMENCLATURE

A	cross sectional area of flow (m^2)
A_{deb}	projected area of debris (m^2)
A_L	area lift force is applied on structure (m^2)
A_s	wetted area of structure (m^2)
c	cohesion
C_d	drag coefficient
C_f	free flow coefficient of discharge
C_L	lift coefficient
C_s	flow with submergence coefficient of discharge
d_{sp}	the wetted depth of the superstructure
d_{ss}	wetted depth of the superstructure
d_{wgs}	the vertical distance from the girder soffit to the flood water surface upstream
$F^*_{debris\ service}$	serviceability design force (kN)
$F^*_{debris\ ultimate}$	ultimate design debris force (kN)
F_{drag}	drag force (kN)
F_{Impact}	impact force (kN)
F^*_{Ls}	serviceability design lift force (kN)
F^*_{Lu}	ultimate design lift force (kN)
g	gravity (9.81 m/s^2)
H	specific head or specific energy (m)
h	depth of flow (m)
hw	height of headwater above floodway crest (m)
L	length of floodway (m)
l	width of floodway (m)
n	Manning's roughness coefficient
P	wetted perimeter (m)
ρ	density (1,000 kg/m^3)

$\emptyset$	angle of internal friction (°)
P_r	proximity ratio
Q	discharge over floodway (m^3/s)
R	hydraulic radius (m)
S	stream hydraulic gradient (m/m)
$\sigma_{11}, \sigma_{22}, \sigma_{33}$	principal stresses such that $\sigma_{33} \leq \sigma_{22} \leq \sigma_{22} \leq \sigma_{11}$
σ_n	normal stress (MPa)
S_r	relative submergence
V	velocity (m/s)
y_{gs}	the vertical distance from the girder soffit to the bed (m)
V_u	mean velocity of water for ultimate limit state (m/s)

GLOSSARY

2D	Two Dimensional
ARI	Average Recurrence Interval
FEA	Finite Element Analysis
FEM	Finite Element Method
LHBR	Left Hand Branch Road
LVRC	Lockyer Valley Regional Council
PPE	Personal Protective Equipment
USQ	University of Southern Queensland
X	Horizontal Axis
Y	Vertical Axis

CHAPTER 1. INTRODUCTION

1.1 Overview

This chapter introduces the reader to the basic concept of a floodway and details the motivation behind this project. The aims and objectives are clearly defined to provide a general understanding of the approach and goals this research endeavours to achieve.

1.2 Definition of a Floodway

A floodway is a roadway which traverses shallow depressions such as creeks and rivers which are subjected to flood events. These types of structures are specifically designed to withstand the damaging effects caused by overtopping floodwaters. The reoccurrence of such overtopping is generally infrequent and of short duration. These types of structures are implemented in regional areas where the volume of motor vehicle traffic is too low to justify the construction of major infrastructure such as bridges (Main Road Western Australia 2006).

1.3 Research Motivation

During the summer of 2010 / 11 and throughout January 2013, Queensland experienced a variety of extreme weather events. Category 5 cyclones like that of Yasi in combination with intensive rainfall periods resulted in tidal surges ultimately causing widespread flooding throughout Queensland (Pritchard 2013). On both occasions, one of the worst-affected areas in the state was the Lockyer Valley region, located at the base of the Great Dividing Range, just 30 minutes from both Toowoomba and Ipswich (Lockyer Valley Regional Council 2012a).

An annual report released in 2011 / 12 by the Lockyer Valley Regional Council (LVRC) reported approximately 77% of the council's road infrastructure sustained some form of damage as a direct result of the 2010 / 11 flood disaster. The cost incurred for restoration works resulting from this flood event was estimated at $280 million. Included in this estimate was damage to 192 of the 330 floodways throughout the region, with 65 requiring complete replacement (Lockyer Valley Regional Council 2012b).

Currently, there are no Australian Standards for ensuring the safe and effective design of floodways in Australia, only guidelines. Many restorations of damaged floodways merely replicated the inadequate floodway design prior to the flood event. As a result, many restored floodways were re-damaged in the wake of the 2013 flood, presenting the LVRC with additional restoration costs of around $8 million. A primary example of this is the East Haldon floodway which was restored post the 2010 / 11 flood event at a cost of $1,418,841, only to sustain approximately $1 million damage again in 2013 (Lockyer Valley Regional Council 2014). This type of reoccurrence highlights deficiencies in current floodway design throughout this region and more broadly Australia.

1.4 Aim

The aim of this research project is to investigate the performance of current floodway designs when subjected to extreme flood loadings. Research shows these types of flood events have an adverse effect on current floodway structures, with many failing to meet the necessary performance requirements to withstand such events. Utilising Strand7 finite element analysis (FEA), this project aims to understand the failure mechanisms and areas of vulnerability within floodway structures. The results of this analysis will highlight areas where improvements for future floodway design could be made. This will not only reduce the financial impacts sustained by councils throughout Australia in the

wake of such events, but also provide a greater level of safety and benefit to the local community.

1.5 Objectives

Conducting a two dimensional (2D) plane strain Strand7 FEA, this project investigates the stresses and displacements incurred on floodway structures during extreme flood conditions. The model itself is based upon a case study of the Left Hand Branch Road (LHBR) floodway located in Queensland's Lockyer Valley region. Current design guidelines primarily focus on hydraulic aspects of design and determine a floodways capacity in a similar manner to that of a broad crested weir. Therefore, this project performs a parametric study to investigate the behaviour of the floodway when subjected to additional loadings such as drag, debris, impact and lifting forces. This parametric study includes three alternative loading combinations which are analysed for a range of different water depths and flow velocities. In the absence of an Australian Standard for floodways, all loadings have been calculated in accordance with the Australian Standard Bridge design Part 2: Design loads (AS 5100.2-2004) (Standards Australia 2004).

The primary objective is to identify the structural adequacy of the LHBR floodway when subjected to these additional loadings and identify those loading combinations that have the most adverse effect on the structure. A comprehensive Strand7 FEA aims to identify as many areas of vulnerability or potential failure mechanisms within the structure and surrounding soil as possible.

CHAPTER 2. LITERATURE REVIEW

2.1 Introduction

This chapter presents the comprehensive literature review conducted to identify why this project is of significance from a financial and community perspective. It investigates typical floodway design characteristics and the current floodway design guidelines being utilised by engineers throughout Australia. Since the primary focus of this research is to conduct a FEA of a floodway using Strand7 software, this chapter details the finite element method (FEM) and the material yield criterions necessary for analysis.

2.2 Project Feasibility

As a result of the 2010 / 11 Queensland flood, almost 60% of floodways across the Lockyer Valley region were damaged, with over 19% requiring complete replacement (Lockyer Valley Regional Council 2012a). The estimated cost to replace more than 2,000 square meters of damaged floodways was approximately $1.45 million (Lockyer Valley Regional Council 2012b). These estimations appear to have been inadequate with Queensland Bridge and Civil procured to reconstruct nine damaged floodways on Black Duck Creek Road alone at an estimated cost of $2 million (Queensland Bridge and Civil 2015). The Sandy Creek floodway on Woodlands Road is another example of reoccurring damage. This 40 m long reinforced concrete floodway required four new box culverts and a concrete overlay, estimated at cost of $500,000 (Queensland Government n.d.).

The concerning factor with the repairs and maintenance of these floodways is the fact they are only required to be repaired to their pre-disaster state (Lockyer Valley Regional Council 2012b). This practices is supported by a submission to

the Australian Government Productivity Commission Inquiry into Natural Disaster Funding Arrangements, highlighting repairs are to be a similar standard to that of the pre-existing floodway, rather than a new and improved or a more permanent structure. This like for like replacement has the potential to cause exponential ongoing costs and further isolate the community in similar future flood events (Lockyer Valley Regional Council 2014).

Many of these floodways act as a primary link between Lockyer Valley regional suburbs and local communities. The Woodlands Road floodway connects approximately 5,000 rural properties making it a vital piece of infrastructure to the local community. Substantial damage to this floodway would significantly impact local residents, causing potential long or short term isolation. Not only are there financial, commercial and community impacts associated with floodway damage, there are also significant risks to human life. During the 2011 and 2013 floods, two lives were tragically lost at Sandy Creek on Woodlands Road between Laidley and Gatton (Crisafulli 2014). Improving floodway design has the potential to provide a more robust and safer form of infrastructure for the local community.

2.3 Typical Floodway Design

In many circumstances floodway design considerations are attained based upon the characteristics associated with each individual floodways location. In general terms there are three different categories of floodways, Types 1, 2 and 3. All three designs have similar components but are differentiated by how the components are utilised to combat varying flow velocities.

Type 1 floodways as shown in Figure 2.1 below and are designed specifically for low velocity water flow and consists of three main components. The roadway itself is constructed using a cement-stabilised pavement with a double layer of sealant for further safeguard. Rock protection combined with geofabric underlay

is used to protect the downstream batter slope from the effects of scour. The application of geofabric underlays is dependent upon the velocity of flow and is only successfully utilised under low velocity flow conditions.

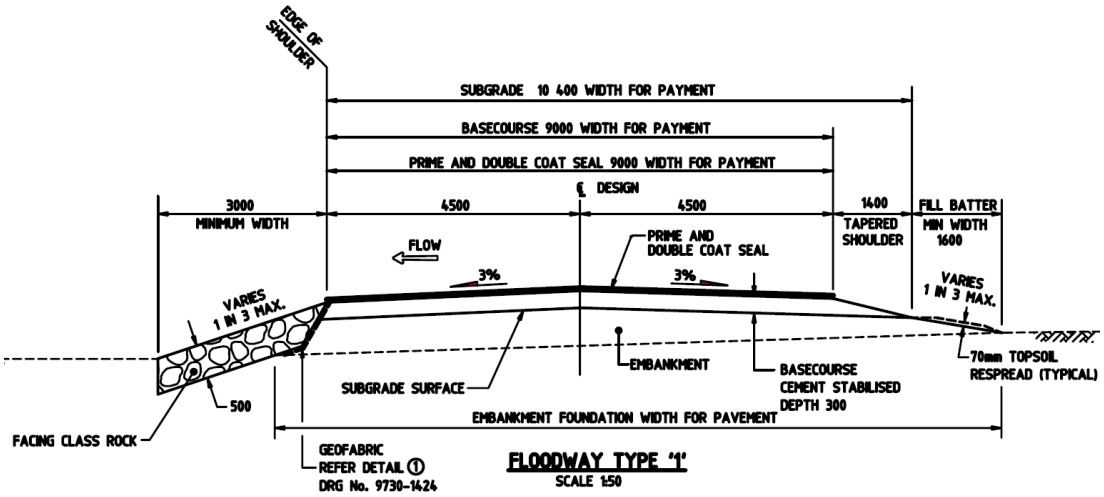

Figure 2.1: Floodway Type 1
(Main Road Western Australia 2006)

Type 2 floodways are designed to withstand medium flow velocities and are very similar in design to the Type 1 floodway. To withstand the effects of scour which occur as result of an increase in flow velocity, two additional modifications have been made. Firstly, a concrete cut-off wall has been added to the downstream shoulder of the floodway and the rock protection extended, both highlighted below in Figure 2.2 below:

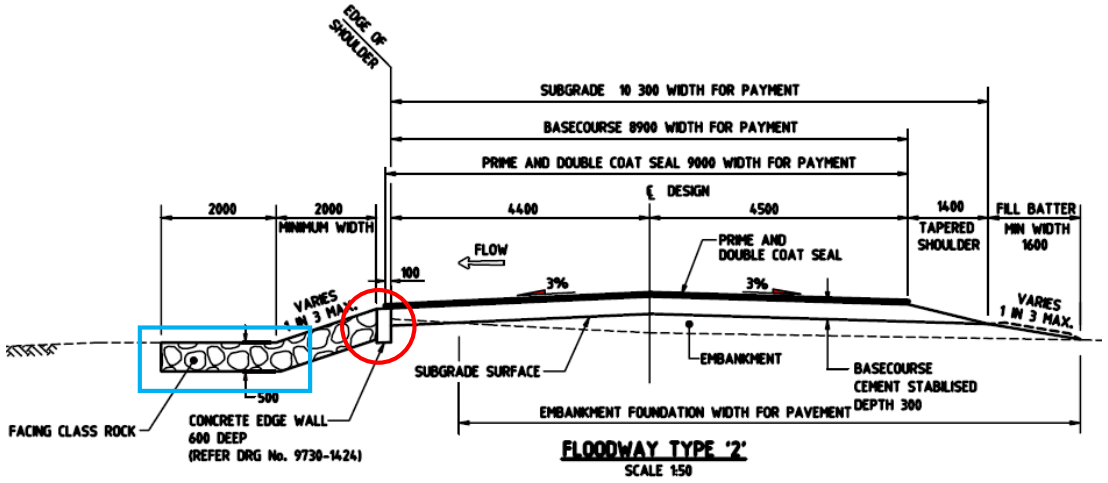

Figure 2.2: Floodway Type 2
(Main Road Western Australia 2006)

Type 3 floodways are similar to the Type 2 floodway design, however provide a greater level of performance in high velocity flow environments. Achieving this level of performance is done by extending the concrete cut-off wall further into the ground in combination with heavier and thicker rock protection highlighted in Figure 2.3 below:

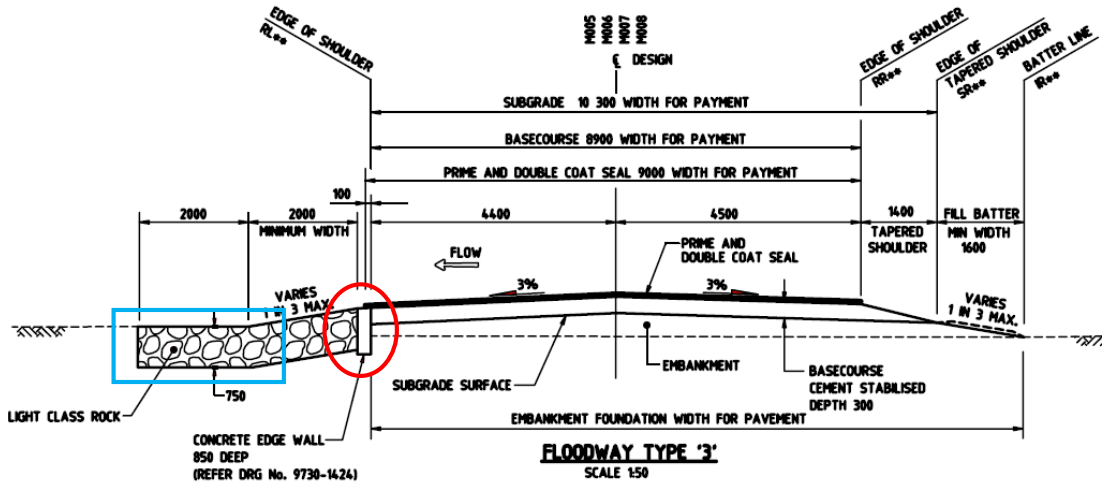

Figure 2.3: Floodway Type 3
(Main Road Western Australia 2006)

2.4 Types of Floodway Protection

Currently the Department of Transport and Main Roads (2010) detail five successful types of floodway protection, Types 1, 2, 4, 5 and 7. Types 3 and 6 have previously been used, however are no longer recommended.

Type 1 is a reinforced concrete floodway and is the most common type of floodway protection currently being used. The selected reinforcement used needs to satisfy strength requirements and limit cracks caused by temperature and shrinkage. This type of floodway is recommended for all crossings where grassed protection is not adequate. Refer to Figure 2.4 below for visual representation:

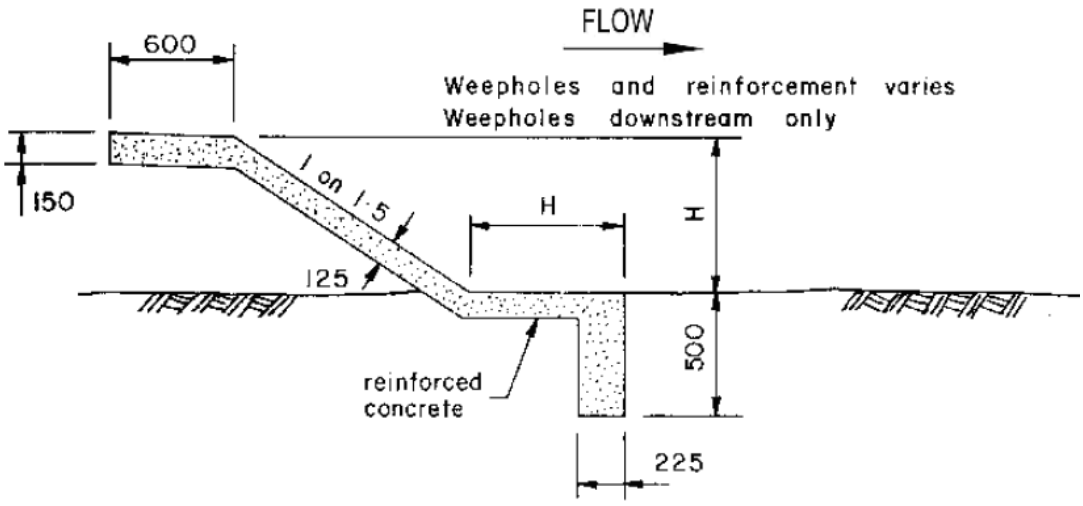

Figure 2.4: Type 1 Floodway Protection
(Department of Transport and Main Roads 2010)

Type 2 is a reinforced concrete floodway which performs well but requires specialised design and therefore costs need to be justified as they are generally higher than Type 1. This type of floodway is recommended where tailwater depths are unknown but generally less than 700 mm below the downstream edge of the formation. Refer to Figure 2.5 below for visual representation:

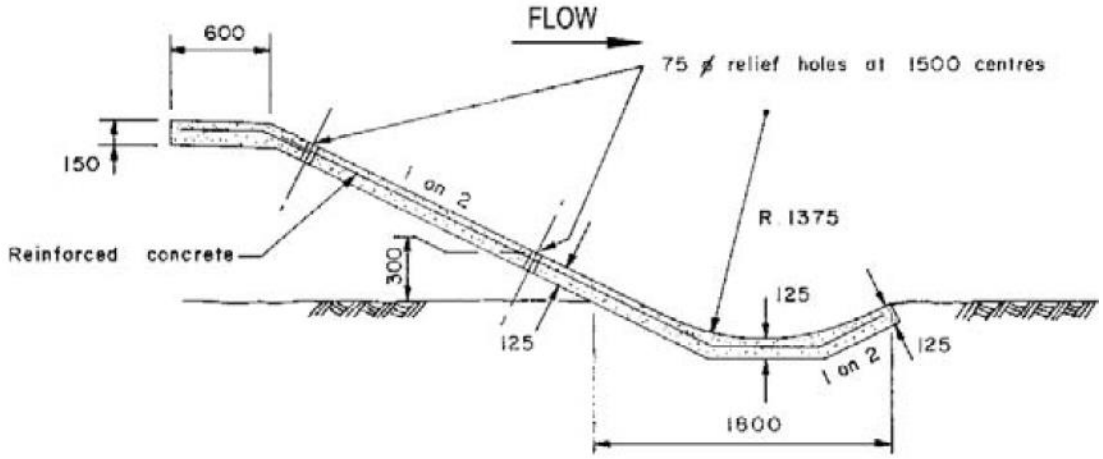

Figure 2.5: Type 2 Floodway Protection
(Department of Transport and Main Roads 2010)

Type 4 is an alternative to the reinforced concrete types used in Type 1 and Type 2 and shown in Figure 2.6 below. It is constructed using a fabric filter underlay, pinned or anchored stone mattresses and gabions. Considerations can be made for a cut-off wall, however once the rock mattress protection has settled it provides sufficient protection against scour.

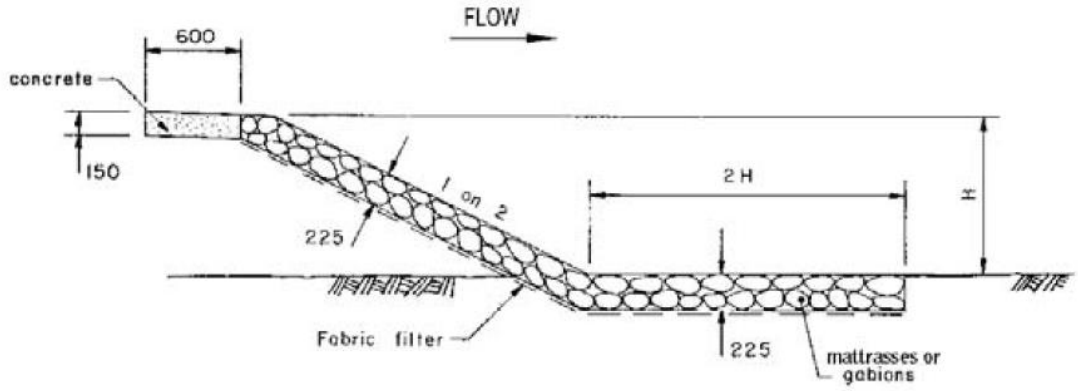

Figure 2.6: Type 4 Floodway Protection
(Department of Transport and Main Roads 2010)

Type 5 as seen in Figure 2.7 below utilises a bituminous seal and is commonly used due to its cost effectiveness. It is recommended only to be used when the following criteria is satisfied:

- fill height is less than 900 mm
- less than 300 mm of tailwater at overtopping
- minimal submergence time (hours)
- low flow velocities.

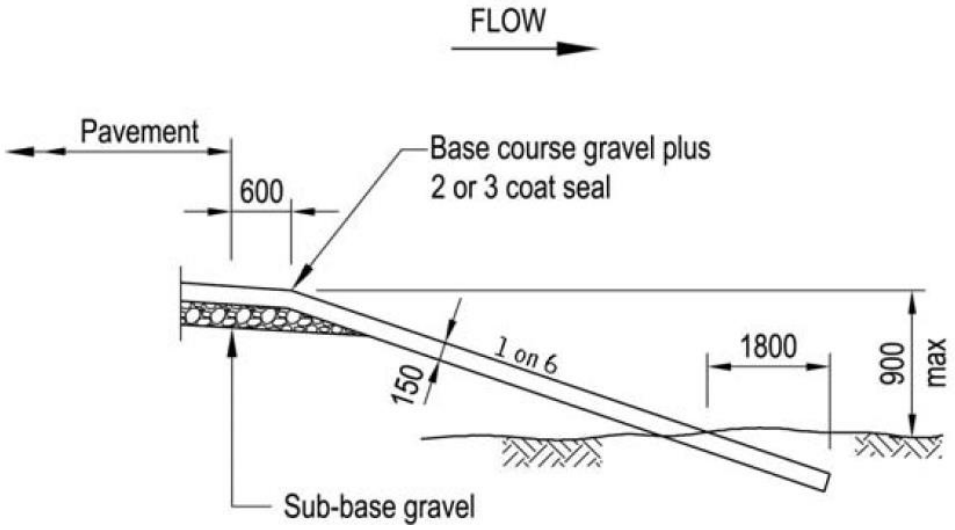

Figure 2.7: Type 5 Floodway Protection
(Department of Transport and Main Roads 2010)

Type 7 is a variation to Type 4, where mattresses are not readily available. This type of floodway is not commonly used throughout Queensland as the rock material required for riprap is not easily attainable. This type is represented in Figure 2.8 below:

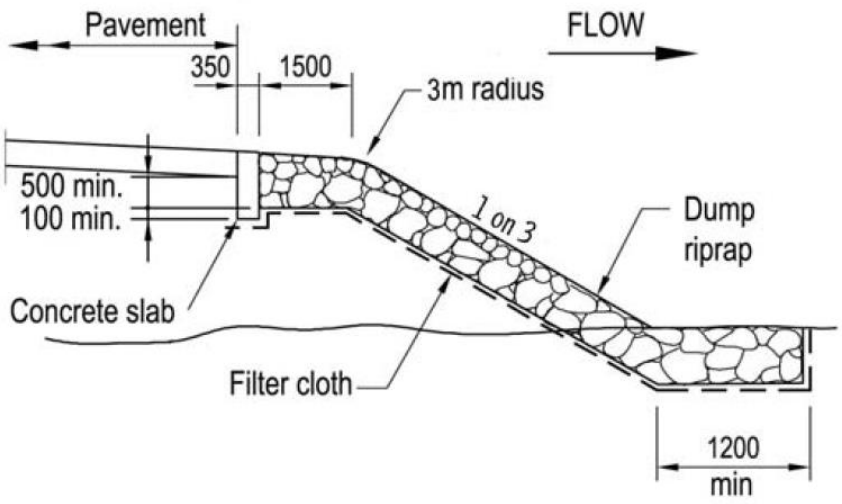

Figure 2.8: Type 7 Floodway Protection
(Department of Transport and Main Roads 2010)

2.5 Current Design Guidelines

Current guidelines into floodway design are detailed in three key documents:

1. Department of Transport and Main Roads Road Drainage Manual Chapter 10 Floodway Design (Department of Transport and Main Roads 2010)

2. Main Roads Western Australia's Floodway Design Guide (Main Road Western Australia 2006)

3. Austroad's Guide to Road Design Part 5B: Drainage – Open Channels, Culverts and Floodways (Austroads Ltd 2013).

The aim of these design criteria's is to determine the configuration of the floodway and evaluate the need for the inclusion of scour protection and / or culverts into the design. Floodway structures are generally located in rural areas where traffic volumes are low. For this reason the design criteria allows for floodways to be submerged by flood waters, but only during floods with a low Average Recurrence Interval (ARI) of between 10 and 20 years.

2.5.1 Hydraulic Design

Hydraulic design aims to accommodate both the flow over and beneath the floodway. The inclusion of culverts into floodway design performs many different functions which impact upon the surrounding areas and the floodway structure itself. The primary benefits of including culverts are to reduce the afflux or rise in water level upstream caused by the floodway embankment and to eliminate any ponding of water. Culverts also have the ability to increase the tailwater level which reduces the amount of batter protection required on the downstream side of the floodway (Austroads Ltd 2013; Department of Transport and Main Roads 2010; Main Road Western Australia 2006).

2.5.2 Types of flows

Analysis of floodways follow the same principles as those utilised for broad crested weirs with flows across the roadway typically categorised as free flow or submerged flow. During the early stages of overtopping the condition of flow is considered free flowing, meaning the height of the upstream flood level determines the discharge. Alternatively, submerged flow indicates the discharge is controlled by both the height of the tailwater and the height of the headwater.

Two examples of free flowing conditions are shown in images A and B in Figure 2.9 below. Image A demonstrates how velocities of flow are likely to be high as the water passes over the shoulder of the roadway and onto the surface of the downstream embankment batter. This condition has the potential to cause substantial erosion or scouring at the downstream toe of the floodway. However this potential for erosion decreases when the velocity of flow across and over the shoulder of the roadway increases. Image B in Figure 2.9 shows as this velocity increases the flow over the shoulder of roadway begins to separate with a percentage of the flow riding over the surface of the tailwater, reducing the amount of flow onto the surface of the downstream embankment batter.

Submerged flow conditions occur when the overtopping flow depth exceeds the critical depth across the entire roadway, as shown in image C Figure 2.9. The velocity of the flow passing the downstream embankment batter is less than those under free flow conditions in the same location.

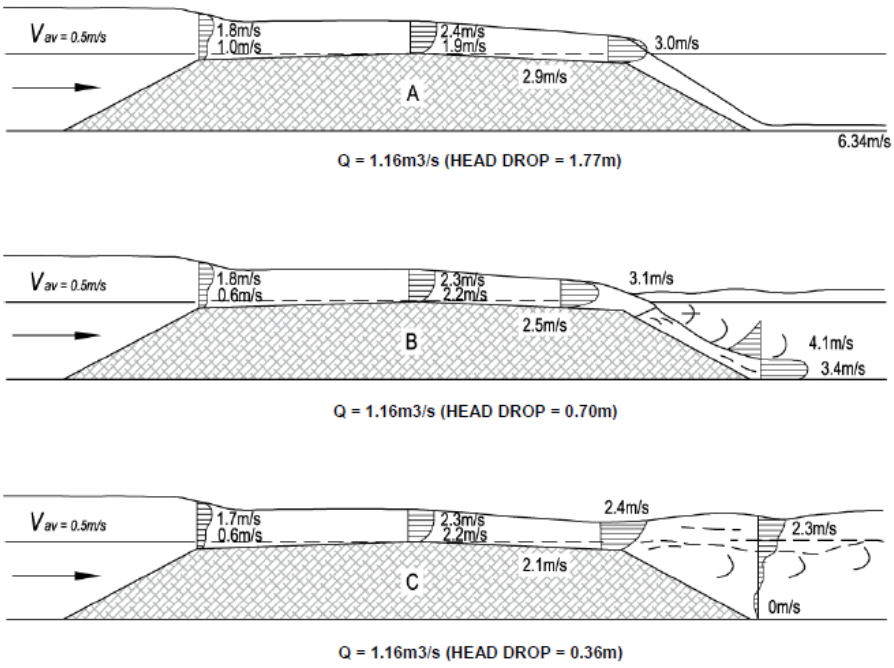

Figure 2.9: Flow Velocities over a Typical Floodway
(Department of Transport and Main Roads 2010; Main Road Western Australia 2006)

2.5.3 Floodway Capacity

Austroads Ltd (2013), Department of Transport and Main Roads (2010) and Main Road Western Australia (2006) all calculate the discharge across the floodway for both submerged and unsubmerged flows as if it were flow passing over a broad crested weir:

$$Q = C_f L H^{1.5} \left(\frac{C_s}{C_f} \right) \qquad (2.1)$$

where:

Q = discharge over floodway (m^3/s).

C_f = free flow coefficient of discharge.

C_s = flow with submergence coefficient of discharge.

L = length of floodway (m).

H = specific head or specific energy (m).

The procedure for determining the discharge over the floodway is as follows:

Step 1. Calculate the discharge using open channel analysis from which you can identify the height of the tailwater and the approaching average velocity. Using Manning's equation determine the stage discharge curve for the stream based on the natural section:

$$V = \frac{1}{n} R^{\frac{2}{3}} S^{\frac{1}{2}} \qquad (2.2)$$

where:

V = velocity (m/s).

n = Manning's roughness coefficient.

A = cross sectional area of flow (m^2).

R = hydraulic radius (m).

$$R = \frac{\text{Area (A)}}{Wetted\ Perimeter\ (P)} \qquad (2.3)$$

S = stream hydraulic gradient (m/m).

Q = flow (m^3/s).

$$Q = VA \qquad (2.4)$$

Step 2. Identify the crest level of the floodway and the floodways length as shown in Figure 2.10 below. Note the length of the floodway is the distance between sag curves and not between crest curves. This is primarily because the extra capacity gained from the side ramps is generally cancelled out by the loss of capacity due to the sag curves. Once this is determined assume the headwater height above the crest of the floodway. In doing so be aware once the water level exceeds the ramps and the approaching embankments of the floodway and spreads out over the road, the upstream water level will begin to increase, especially for larger flows. This will result in an upper limit to the amount of backwater that can ensue.

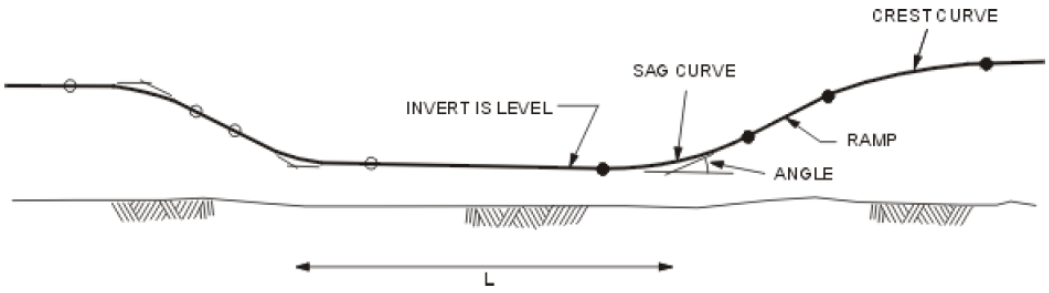

Figure 2.10: Long Section of a Typical Floodway
(Main Road Western Australia 2006)

Step 3. Calculate H/l.

$$H = hw + \frac{V^2}{2g} \tag{2.5}$$

where:

H = total head (static plus velocity) (m).

hw = Height of headwater above floodway crest (m).

V = average velocity of approaching flow (m/s).

g = acceleration due to gravity = 9.81 m/s^2.

l = width of floodway (m).

Step 4. If the H/l value is greater than 0.15 determine the free flow coefficient (C_f) from curve B in Figure 2.11. If less than 0.15 C_f should be determined from curve A of the same figure.

Step 5. If D/H > 0.76 submergence is present and the percentage of submergence needs to be calculated. The submergence factor C_s/C_f is then determined from curve C in Figure 2.11 below:

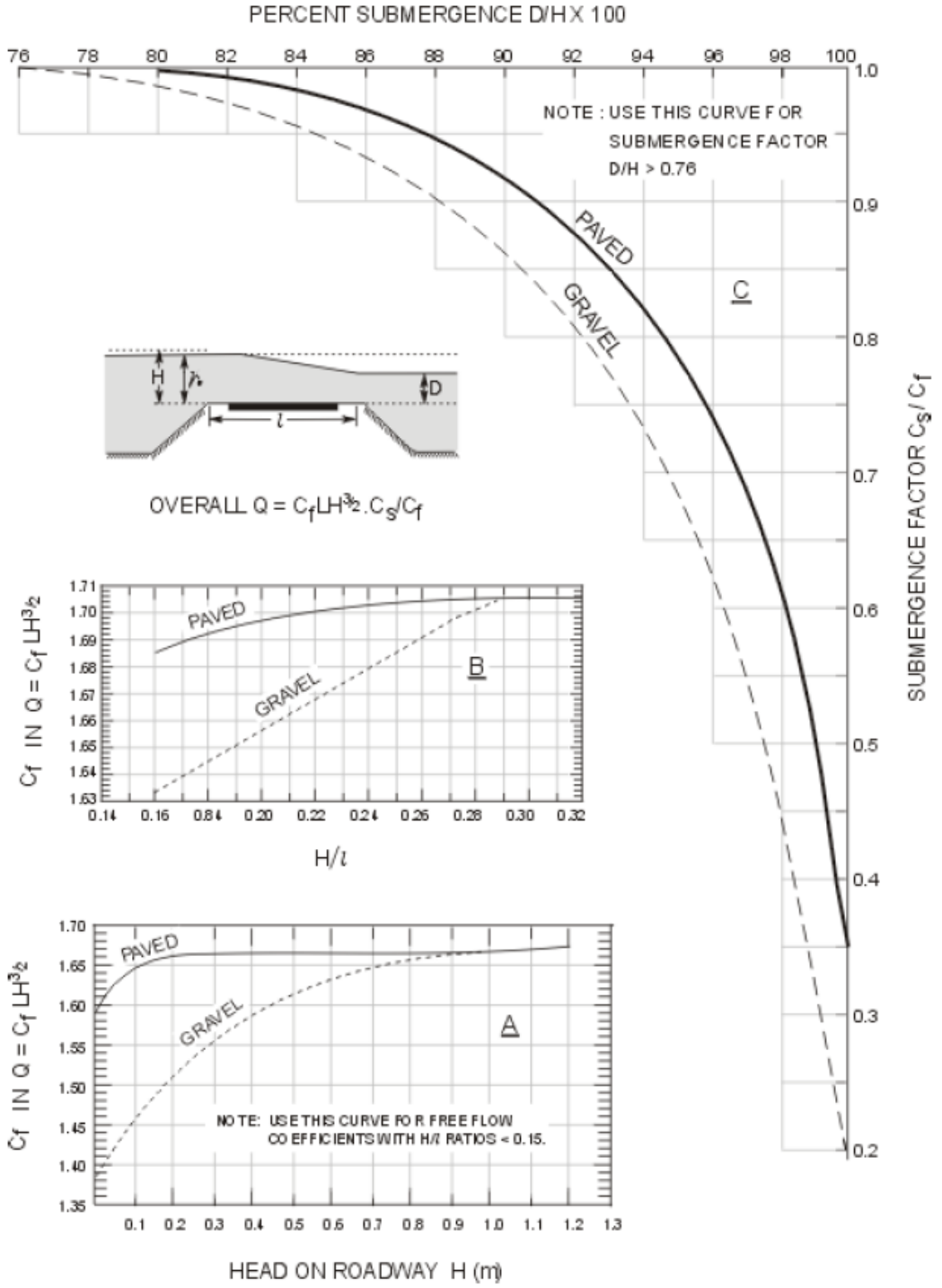

Figure 2.11: Discharge Coefficients for Floodways

(Main Road Western Australia 2006)

Step 6. Utilising the broad crested weir formula previously stated in Equation (2.1), calculate the discharge over the floodway.

Step 7. When submergence is present a final check must be made to confirm the discharge over the floodway is equivalent to the design discharge. For instance, where this criteria is not satisfied adjustments must be made to the depth of flow above the crest of the floodway and repeat steps 2 – 7.

For circumstances where floodways are designed with culverts, the performance contribution of the culvert must be taken into account. The flow downstream of the floodway should equate to the summation of the flow over the floodway and through the culvert. Therefore a backwater versus discharge curve needs to be established for the culvert. The iterative procedure above is once again utilised to determine the combined flows once the floodway is overtopped. Once this overtopping takes place the backwater generally decreases, reducing the flow through the culverts.

2.6 Forces Acting on Bridges

Structures such as bridges, floodways and culverts crossing varying bodies of water need to be designed to withstand the adverse effects of water flow. In combination with these fluid forces, other influences such as debris accumulation, impact, drag and lifting forces need to be considered (Standards Australia 2004). Since all the current Australian floodway guidelines exclude these types of forces as part of their floodway design criteria, this research considers these forces in the same manner as those outlined in the AS 5100.2-2004 for bridges (Standards Australia 2004).

2.6.1 Hydrostatic Forces

Hydrostatics is the study of how a pressure contained within a fluid at rest impacts upon a defined surface or plane. Fluids at rest generate no shear stresses within

the fluid and therefore the resulting force will always act orthogonal (90 degrees) to the surface area in which it is in contact. Figure 2.12 below demonstrates Pascal's Law and how pressure acting at any point within a resting body of fluid is the same in all directions, irrespective of orientation of the surface surrounding that point:

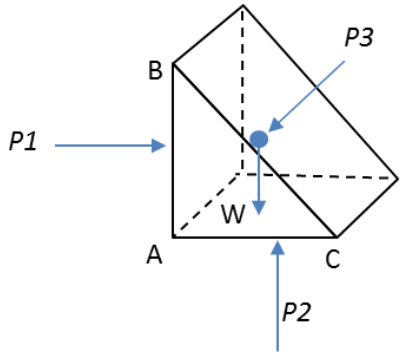

Figure 2.12: Pascal's Law
(Nalluri & Featherstone 2009)

For incompressible fluids such as water, we know the relationship between pressure and water depth is distributed linearly:

$$Hydrostatic\ Pressure = \rho g h \qquad (2.6)$$

where:

ρ = density (1,000 kg/m^3).

g = gravity (9.81 m/s^2).

h = depth of flow (m).

In the case of a fully submerged vertical surface this linear relationship is generally represented by a triangular pressure prism. However, a submerged

horizontal surface will yield a rectangular pressure prism, both of which are represented in Figure 2.13 below:

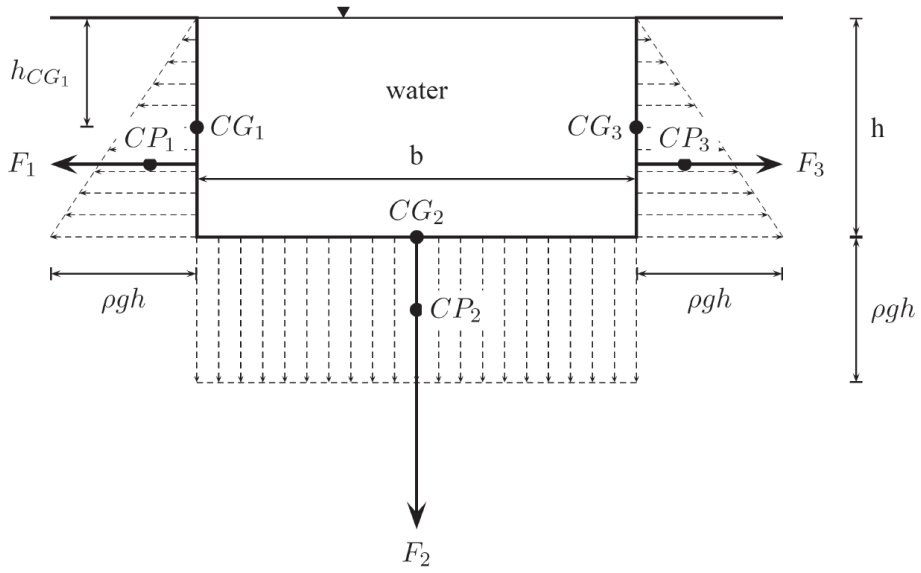

Figure 2.13: Hydrostatic Pressure Prisms
(Moore 2013)

2.6.2 Drag Forces

Drag forces with respect to bridges are present when there is an interaction between a structure and the velocity of a water. The magnitude of these types of forces are dependent on the following:

- flow velocity
- direction of the water flow
- viscosity of the water
- geometry of the structure.

In accordance with AS 5100.2-2004 for bridges (Standards Australia 2004) drag forces are calculated using Equation (2.7) below:

$$F_{drag} = 0.5 C_d {V_u}^2 A_s \quad (2.7)$$

where:

C_d = drag coefficient.

V_u = mean velocity of water (m/s).

A_s = wetted area of structure (m^2).

In order to calculate the drag coefficient the relative submergence and proximity ratios need to be established. Relative submergence is the ratio of the vertical distance from the girder soffit to the flood water surface upstream (d_{wgs}) to the wetted depth of the superstructure (d_{sp}) based on Figure 2.14 below and shown in Equation (2.8):

$$S_r = \frac{d_{wgs}}{d_{sp}} \quad (2.8)$$

Similarly the proximity ratio is determined based on the vertical distance from the girder soffit to the bed (y_{gs}) to the wetted depth of the superstructure (d_{ss}) based on Figure 2.14 below and shown in Equation (2.9):

$$P_r = \frac{y_{gs}}{d_{ss}} \quad (2.9)$$

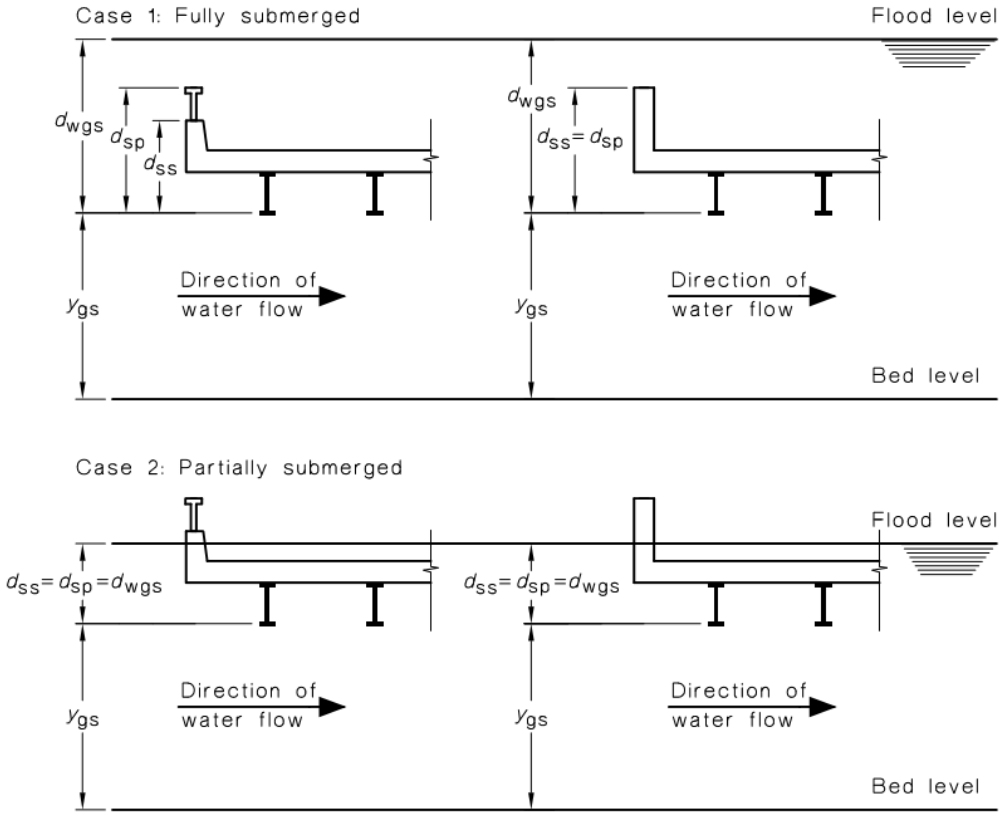

Figure 2.14: Dimensions

(Standards Australia 2004)

Once these ratios have been determined the final drag coefficient can be identified using Figure 2.15 below:

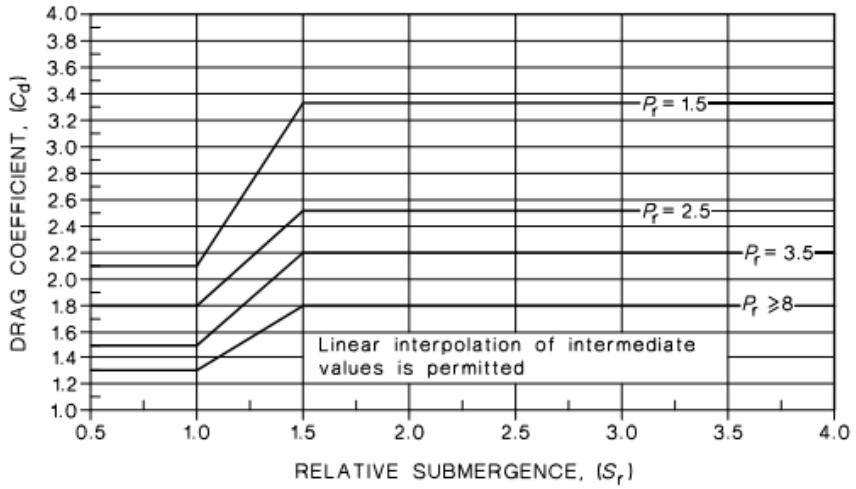

Figure 2.15: Relative Submergence

(Standards Australia 2004)

2.6.3 Lifting Forces Caused by Scour

Scour is referred to as the erosion of soil and sediment of river beds and embankments at critical floodplain structures and is generally caused by drag or sheer resistance, uplift forces and super-critical water flow velocity (Akan 2006; Department of Transport and Main Roads 2013; Hamill 1999; Main Road Western Australia 2006). Similar to a debris strike, excessive scour during floods can jeopardise the integrity of the structure and potentially cause catastrophic failure (Akan 2006; Hamill 1999). This is evident in research conducted by LVRC who identified damage sustained to floodways post the Queensland flood events stating 23% of damage was attributed to washouts and 11% suffering damage to approaches (Wahalathantri et al. 2015).

The Western Australian Floodway Design Guidelines (Main Road Western Australia 2006) identify the following areas of a floodway which are vulnerable to scour in order of severity:

a) toe of the downstream batter slope

b) surface of batter slope

c) at the edge of downstream shoulders

d) on the road surface

e) on the upstream batter slope

f) additionally, scour below the floodway can cause failure.

Figure 2.16 represents these areas of vulnerability graphically:

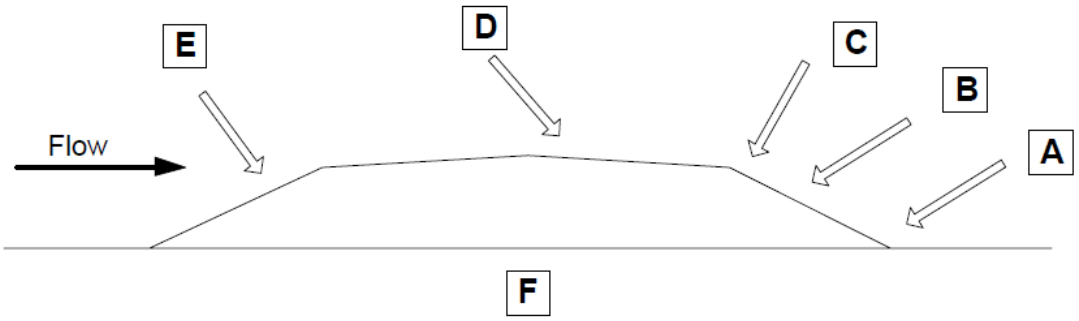

Figure 2.16: Vulnerabilities of a Floodway to Scour
(Department of Transport and Main Roads 2013)

Some of these vulnerabilities identified above, directly correlate to Figure 2.17 below which shows the effects of scouring in these locations based on a Queensland floodway post flood events:

Figure 2.17: Floodway Damage (Scour)
(Queensland Reconstruction Authority n.d.)

The Western Australian Floodway Design Guidelines (Main Road Western Australia 2006) outlines multiple countermeasures to reduce the impacts of scouring on floodways which include:

- appropriately designed rock protection

- pump-up concrete revetment mattresses
- cut-off walls (end walls)
- rock fill below embankment
- cement stabilised batter slope / embankment fill
- cement stabilised subgrade / basecourse
- two-coat bituminous seal.

The methods used to determine the magnitude of scour is complicated yet critical to ensuring community safety and minimising long term infrastructure costs. The complexity of considering different types of scour such as contraction scour and local scour means this dissertation does not have the provision to conduct a full analysis of scour and therefore it falls outside the scope of this project. However, this research identifies areas in the soil surrounding the floodway which may be vulnerable to scour.

In the absence of Australian Standards for floodways, lifting forces are based on that described in AS 5100.2-2004 for bridges (Standards Australia 2004). Clause 15.4.3 of AS 5100.2-2004 (Standards Australia 2004) details how to calculate the lifting force for both ultimate limit state and serviceability limit state design using Equation (2.10) and Equation (2.11) below:

Ultimate design lift force (F^*_{Lu}):

$$F^*_{Lu} = 0.5 C_L {V_u}^2 A_L \qquad (2.10)$$

where:

C_L = lift coefficient.

V_u = mean velocity of water for ultimate limit state (m/s).

A_L = area lift force is applied on structure (m^2).

Serviceability design lift force (F^*_{Ls}):

$$F^*_{Ls} = 0.5 C_L {V_s}^2 A_L \qquad (2.11)$$

where:

C_L = lift coefficient.

V_s = mean velocity of water for serviceability limit state (m/s).

A_L = area lift force is applied on structure (m^2).

Note: An upper and lower value for lifting coefficients need to be identified from Figure 2.18 to determine the direction in which the lifting force is applied. Resultant forces less than the self-weight of the structure are applied in the downward direction whilst forces greater than the self-weight of the structure generate uplift.

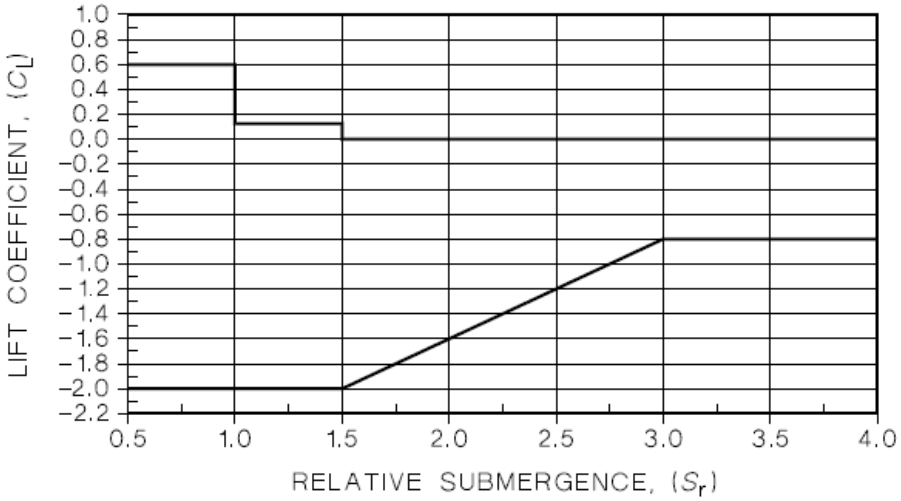

Figure 2.18: Superstructure C_L
(Standards Australia 2004)

2.6.4 Debris Forces

During a flood, floating debris and debris accumulation is transported downstream impacting on floodplain structures such as bridges, culverts, weirs and floodways. The strikes and accumulation caused by this debris impact upon the natural flow of water adversely affects residential and commercial infrastructure, floodways and other critical structures located close to the floodplain (Haehnel & Daly 2004; Schmocker & Hager 2013). The result of such impacts can cause significant structural damage and has the potential to jeopardise the integrity of the structure, even cause catastrophic failure (Haehnel & Daly 2004; U.S. Department of Transportation 2012).

Schmocker and Hager (2013) and Austroads Ltd (2013) identify debris as a result of one of two reasons, debris is accumulated in the river or stream due to natural erosion (i.e. vegetation, soil and uprooted trees) or it is entrained into the rivers or streams by flood waters (i.e. logs, cars and manmade objects). Figure 2.19 below is a demonstration of why both manmade objects and natural vegetation accumulation must be considered when designing floodways:

Figure 2.19: Debris Impact and Accumulation Sustained During Floods (Gold Coast Bulletin 2014)

Debris accumulation contributes to the existing hydraulic forces imposed by the water flow and therefore substantially increases the forces acting on floodplain structures (Schmocker & Hager 2013; U.S. Department of Transportation 2012). Schmocker and Hager (2013) further state debris accumulation reduces the cross section at the floodplain structure, increasing the level of water upstream potentially causing damage to nearby infrastructure.

In the absence of Australian Standards for floodways, debris loading considerations are based on AS 5100.2-2004 (Standards Australia 2004) for bridges. Clause 15.5.1 of AS 5100.2-2004 (Standards Australia 2004) outlines the forces due to debris for superstructures as a debris mat. This is a variable which approximates the depth of debris to be considered for design and is shown in Figure 2.20 below. The factors influencing the size of the debris mat include the type of vegetation contained within the catchment area and the depth of the water flow. The clause also states in the absence of an accurate estimation, a depth of 1.2 metres should be taken as the depth of the debris mat.

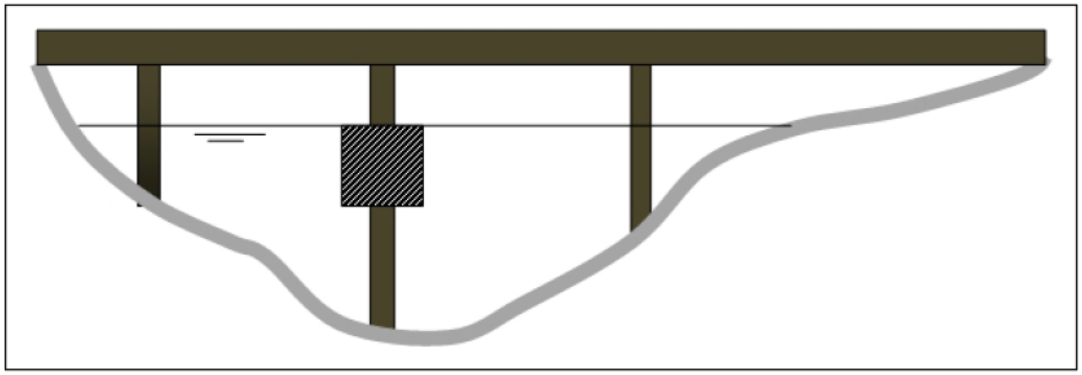

Figure 2.20: Debris Mat on a Single Pier
(U.S. Department of Transportation 2012)

Clause 15.5.4 of AS 5100.2-2004 (Standards Australia 2004) further details how to calculate the accumulation of debris forces for both ultimate limit state and serviceability limit state design using Equations (2.12) and (2.13) below:

Ultimate design debris force ($F^*_{debris\ ultimate}$):

$$F^*_{debris\ ultimate} = 0.5 C_d V_u{}^2 A_{deb} \qquad (2.12)$$

where:

C_d = drag coefficient.

V_u = mean velocity of water for ultimate limit state (m/s).

A_{deb} = projected area of debris (m^2).

Serviceability design force ($F^*_{debris\ service}$):

$$F^*_{debris\ service} = 0.5 C_d V_s{}^2 A_{deb} \qquad (2.13)$$

where:

C_d = drag coefficient.

V_s = mean velocity of water for serviceability limit state (m/s).

A_{deb} = projected area of debris (m^2).

Note: Drag coefficients are determined from Figure 2.21 for debris acting on piers or Figure 2.22 for debris acting on superstructures:

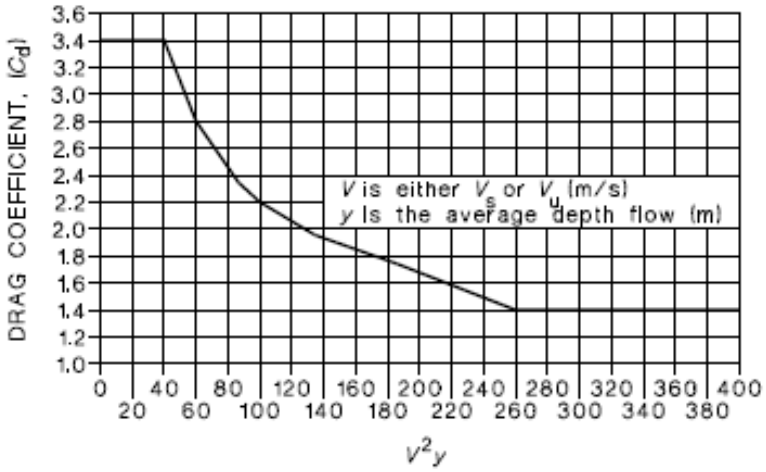

Figure 2.21: Pier Debris Drag Coefficient
(Standards Australia 2004)

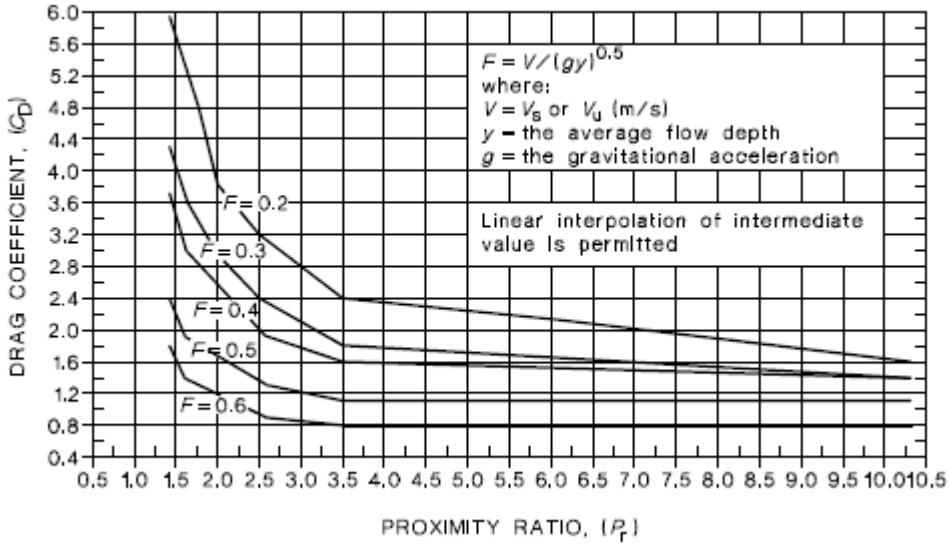

Figure 2.22: Superstructure Debris Drag Coefficient (Standards Australia 2004)

When considering debris strikes, Haehnel and Daly (2004) state there are three different approaches to estimating the maximum debris impact force, all of which they claim to be theoretically equivalent. Each approach calculates the force based on a one-degree-of-freedom system by which only the mass of the debris object is considered.

The contact stiffness approach is based upon the mass of the debris object and the stiffness of the structure (Haehnel & Daly 2004) and aligns with the AS 5100.2-2004 (Standards Australia 2004) approach for analysing forces due to log impacts. Clause 15.6 of AS 5100.2-2004 (Standards Australia 2004) states, where floating logs are possible, the design forces for ultimate limit and serviceability limit state should be calculated based upon the assumption a moving log with a minimum mass of two tonnes is stopped within a specified distance. This distance varies from pier to pier and is dependent upon the piers material and / or construction. The three most common types of piers outlined and their specified stopping distances are:

- timber piers with a stopping distance of 300 mm

- hollow concrete piers with a stopping distance of 150 mm
- solid concrete piers with a stopping distance of 75 mm.

Equation (2.14) below utilises the solid concrete pier with a stopping distance of 75 mm to best represent a concrete floodway in determining the magnitude of these impact loads:

$$F_{Impact} = 0.5 \times 2000kg \times {V_u}^2/0.075m \qquad (2.14)$$

where:

V_u = mean velocity of water for ultimate limit state (m/s).

In accordance with AS 5100.2-2004 (Standards Australia 2004) debris impacts and debris accumulation forces shall not be applied simultaneously.

2.7 Finite Element Method

Engineers, designers and many other professions view the FEM as a critical piece of technology for simulating physical structures and processes. Computer modelling and simulation is generally utilised in the preliminary stages of the design process. It is a critical tool for assisting engineers and designers with the analysis of a system, allowing for a measure of functionality and feasibility to be achieved pre-production. To achieve optimal performance and cost effectiveness an iterative process must be undertaken similar to that shown in Figure 2.23 below:

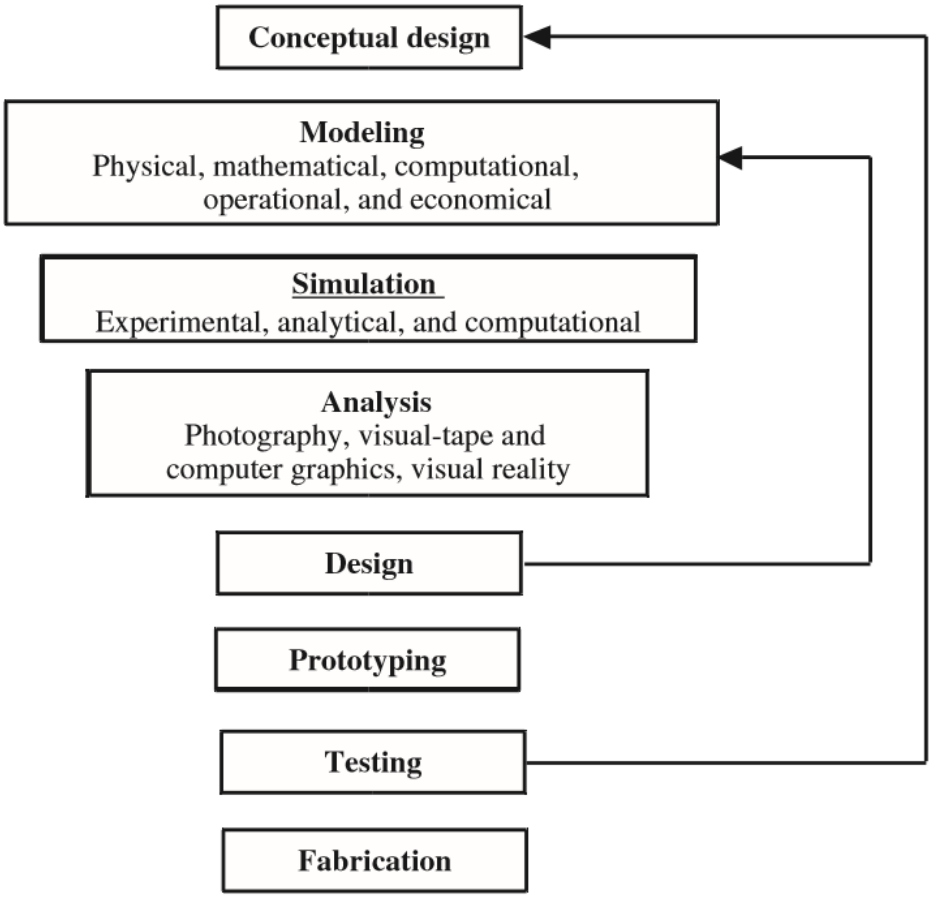

Figure 2.23: Advanced Engineering System Process
(Liu 2003)

The FEM is therefore designed to find solutions to complex problems through the simplification of partial differential equations into a system of simultaneous algebraic equations. The application of this method is strongly utilised throughout multiple engineering disciplines on a range of problems involving structural analysis, heat transfer, fluid flow, mass transport and electrical. This approach allows an approximate solution to a complex problem to be reached much more efficiently than what can be achieved analytically through the utilisation of discretization. Discretization subdivides a body into smaller units known as finite elements which are all interconnected by nodes or boundary lines as seen in Figure 2.24 below:

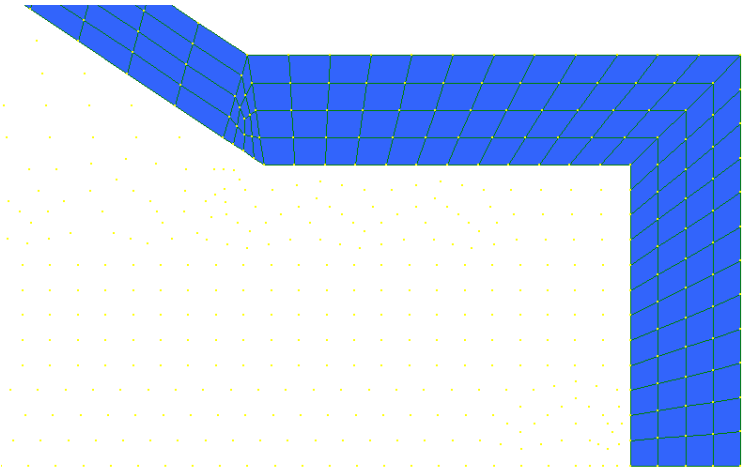

Figure 2.24: Discretization representation from Strand7

It is these smaller elements which make up the simplified system of algebraic equations, eliminating the need to try and solve the problem for the entire body in one operation, hence yielding an approximate solution. The accuracy of this approximate solution is dependent upon the computational effort imposed at the discretion of the analyst. Smaller elements yield a more accurate solution, however this increases the number of equations and ultimately the computational time required to acquire a solution. One way to improve computational time without increasing the element size and compromising the accuracy of the solution is to only model a portion of the overall model. This approach however can only be considered on models of symmetrical geometry subjected to uniform loading conditions. Developing a portion of the overall model dramatically reduces the number of mathematical equations and computational time required to compute the same solution since the behaviour is the same throughout all the individual portions that make up the entire model (Zienkiewicz et al. 2015; Liu 2003; Dhatt et al. 2013).

2.8 Strand7 Yield Criterions

The two main Strand7 material yield criterions relevant for this research include von Mises and Mohr Coulomb. Both of which are detailed further in this section.

2.8.1 von Mises

The von Mises yield criterion is a determination of the distortion of energy within a material. This criterion indicates that yielding of a material will initiate once the second invariant of the deviatoric stress tensor J'_2 reaches a certain value $K_{(k)}$, shown in Equation (2.15) below.

$$\left(J'_2 \right)^{0.5} = K_{(k)} \tag{2.15}$$

Strand7 therefore defines the von Mises yield criteria based on the following Equation (2.16) below:

$$\sigma_{VM} = \sqrt{\frac{1}{2}[(\sigma_{11} - \sigma_{22})^2 + (\sigma_{22} - \sigma_{33})^2 + (\sigma_{33} - \sigma_{11})^2]} \tag{2.16}$$

where:

$\sigma_{11}, \sigma_{22}, \sigma_{33}$ = Principal stresses such that $\sigma_{33} \leq \sigma_{22} \leq \sigma_{22} \leq \sigma_{11}$.

The failure envelope for von Mises is represented as an eclipse established based upon the yielding points of the principal stresses $\sigma 1_{yield}$ and $\sigma 2_{yield}$ shown in Figure 2.25 below. All stress values that fall within the ellipse are considered safe, all those falling outside represent material failure.

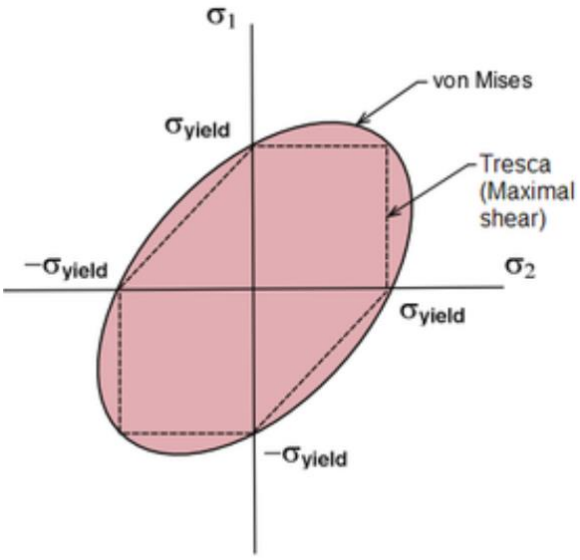

Figure 2.25: von Mises Failure Envelope
(Engineers Edge Solution By Design 2015)

2.8.2 Mohr Coulomb

Strand7 generates contour plots of Mohr Coulomb stress using the expression below:

$$\sigma_{MC} = \frac{1}{2}(\sigma_1 - \sigma_3)cos\emptyset - c + \left[\frac{1}{2}(\sigma_1 + \sigma_3) + \frac{1}{2}(\sigma_1 - \sigma_3)sin\emptyset\right]tan\emptyset \qquad (2.17)$$

where:

σ_n = normal stress (MPa).

c = cohesion.

$\emptyset$ = angle of internal friction (°).

On the yield surface, Mohr Coulomb equivalent stress equates to zero, unlike other yield criterions such as von Mises and Tresca. Figure 2.26 below

demonstrates how the stress quantity output from Strand7 is the difference between current shear stress represented by the circle and failure envelope measured at an angle equal to the internal friction angle from horizontal. Therefore it can be seen in Figure 2.26 that the dashed red line represents the current shear stress and the solid red line indicates the output shown by Strand7. Based on this example, this output would be considered negative as it sits below the failure envelope. However, should the Mohr Coulomb circle eclipse the failure envelope this value will become positive indicating that the material has yielded.

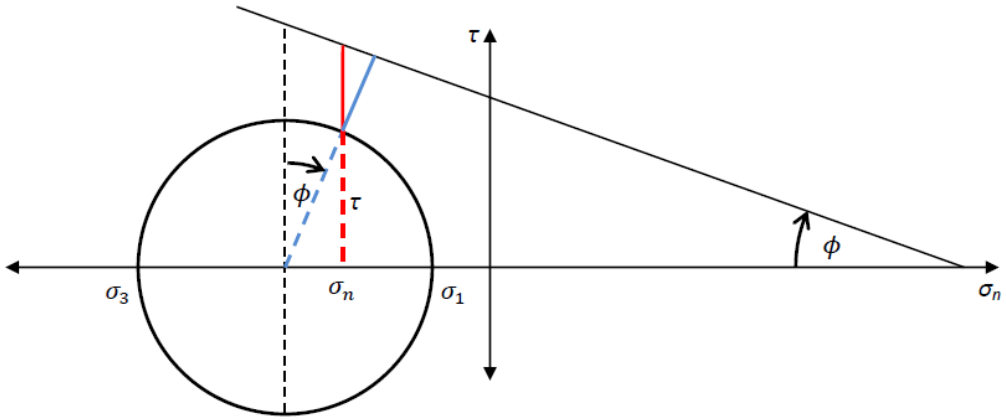

Figure 2.26: Mohr Coulomb Yield Criterion
(Strand7 Pty Ltd n.d.a)

2.9 Literature Review Summary

This literature highlighted deficiencies within the current design guidelines for floodways across Australia. Post flooding, Local Councils and Government Agencies incurred substantial financial costs. These costs are compounded when damaged floodways from the 2010 / 11 flood were repaired like for like meaning further damage was incurred in the wake of the 2013 flood. Furthermore, these floodways are generally located in rural areas and are a vital form of infrastructure providing the local communities with access to and from residential and commercial properties.

In general, there are three different guidelines adopted by various states throughout Australia. Specified within these guides are three different types of floodways and five recommended types of floodway protection. All of these guidelines determine a floodways capacity based on hydraulic design aspects, similar to a broad crested weir. What this literature has proven is there is major gap in the knowledge when it comes to considering additional loadings such as impact, debris, drag and lifting forces acting on a floodway. In the absence of an Australian Standard relevant to floodway design, AS 5100.2-2004: Bridge design Part 2: Design loads Standards (Standards Australia 2004) has been utilised to calculate these forces.

The FEM is based upon an iterative process utilising Strand7 capability to find solutions to complex problems through the simplification of partial differential equations into a system of simultaneous algebraic equations. This process requires the floodway to be modelled using discretization, which subdivides a body into smaller units known as finite elements which are all interconnected by nodes or boundary lines. The accuracy of this approximate solutions is dependent on the element size with smaller elements yielding a more accurate result but requiring more computational time to process the number of equations.

Finally, there are a number of yield criterions available within Strand7. The two which have been identified as most relevant to this research is the von Mises and the Mohr Coulomb yield criterions. The literature revealed Strand7 uses slightly modified versions of these criterions and therefore understanding this will be important to the accuracy of the analysis conducted.

CHAPTER 3. PROJECT METHODOLOGY AND PRELIMINARY STRAND7 MODEL

3.1 Introduction

In accordance with the project specification available in Appendix A, the methodology of this project primarily investigates the stresses and displacements concrete floodways incur as a direct result of extreme flood loadings. These concentrated stresses will identify areas of vulnerability within the structure and allow for comparisons to be made between the compressive strength of the concrete floodway. In addition to the stresses, this project also analyses the nodal displacements to ascertain a level of vulnerability associated with failure mechanism within the structure and surrounding soils.

The primary focus for this research is to construct a 2D Strand7 finite element model based upon the LHBR floodway design specifications detailed in section 3.2.2 below. Whilst the geometry of the structure is in accordance with these drawings, additional research was required to determine sufficient material properties. Due to limited historical flood data available for this region, a parametric study is undertaken to determine the worst loading combinations with respect to flow velocities and flow depths. Utilising the literature from above, three alternative loading combinations consisting of all forces including hydrostatic, drag, lifting, log impact and debris accumulation are calculated and how they act on the model clearly defined. As there is no Australian Standard for determining these loads with respect to floodways our analysis considers the ultimate limit state design for bridges as specified in AS 5100.2-2004 (Standards Australia 2004). Boundary conditions have been identified through an iterative process and a convergence study undertaken to enhance the accuracy and efficiency of the model.

The flow chart below provides a general overview of the methodology adopted with further details below:

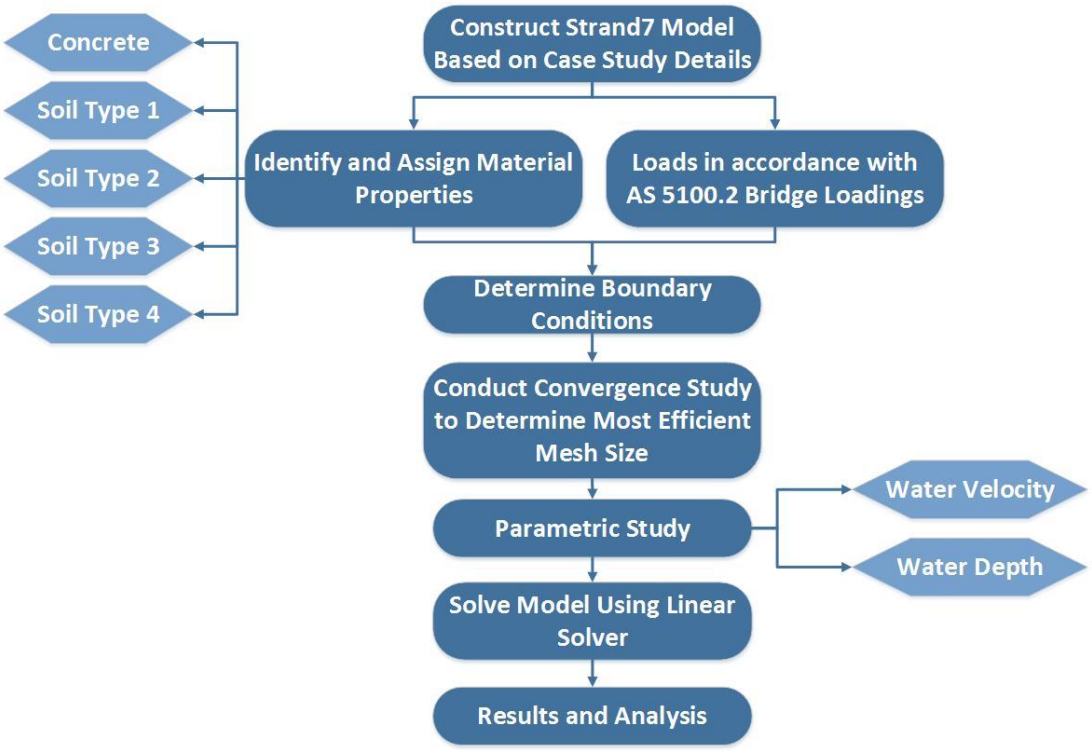

Figure 3.1 Project Methodology

3.2 LHBR Floodway Case Study

The LHBR floodway was selected as the focus for this case study due to its geographical location within southeast Queensland's Lockyer Valley Region shown in Figure 3.2 below:

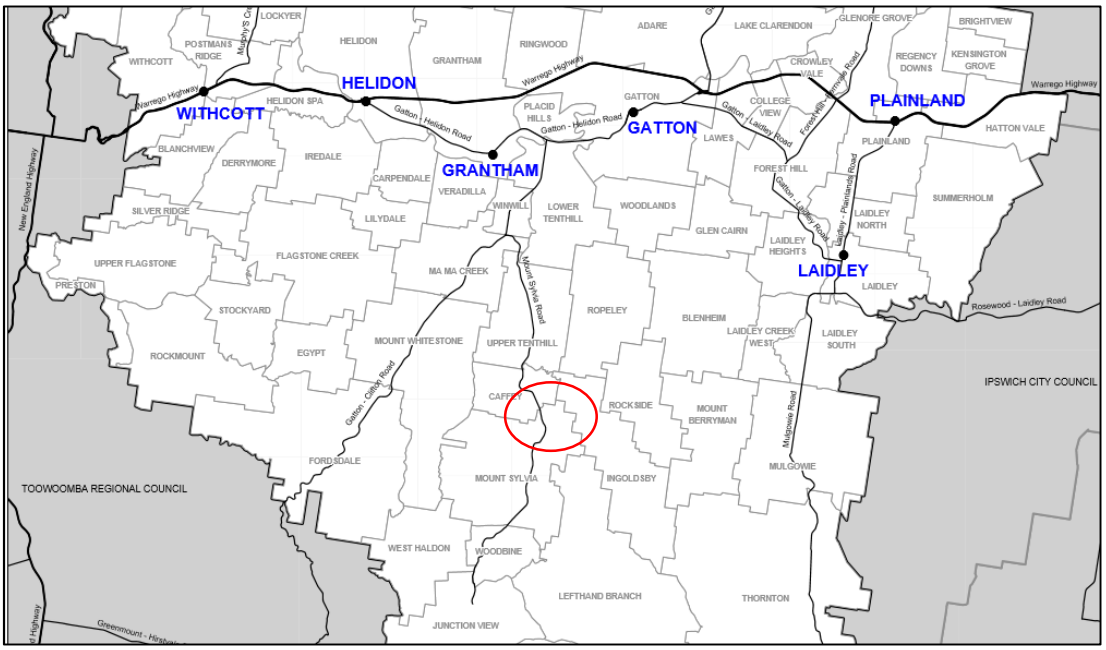

Figure 3.2: Location of LHBR Floodway
(Lockyer Valley Regional Council 2009)

Situated in Mount Sylvia, south of Grantham and southwest of Gatton, the floodway provides the local community with vital motor vehicle access to their regional properties and / or farms. With only two entry points onto LHBR, access is extremely limited and would not be possible without this type of infrastructure. This floodway elevates the roadway, traversing the shallow Tenthill Creek improving the level of access available to residents during periods of rainfall.

Previously outlined in the project background, this region incurred millions of dollars of restoration costs as a result of the 2010 / 11 and 2013 Queensland floods with many floodways sustaining minor or major structural damage, some on more than one occasion. Investment by the LVRC into improving the LHBR floodway has provided an excellent opportunity to investigate the performance of current floodway design practices. The detailed drawing below in Figure 3.3 provides an overview of the LHBR floodway with an enlarged drawing available in Appendix D. This current design incorporates many of the design characteristics detailed in the Chapter 10 guidelines of the Queensland Drainage Manual (Department of Transport and Main Roads 2010). These include concrete

cut-off walls and aprons, rock protection and culverts all of which have been previously discussed.

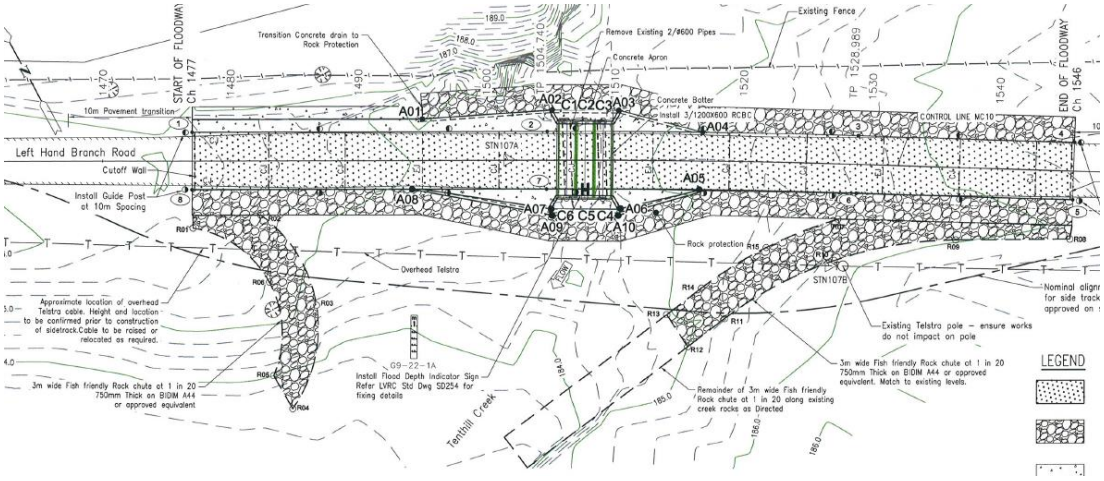

Figure 3.3: LHBR Floodway

3.2.1 Topography

The LHBR floodway used for this analysis is located at the northern end of LHBR at an elevation of approximately 180 m above sea level. Steep mountains forming The Great Dividing Range are situated in close proximity, less than 500 m in some directions and surround the floodway approximately 280 degrees. Majority of the slopes are vegetated with native trees and grass in combination with rocky outcrops. This regions level of vulnerability to flooding is clearly illustrated in the topographical map shown in Figure 3.4. Some mountain peaks surrounding the floodway reach 670 m above sea level and have an elevation difference of approximately 490 m. Upstream of the floodway the constricted and very steep mountain ridges either side of the LHBR demonstrates how rainfall runoff from the southern end would become concentrated in the direction of the LHBR floodway as this is the only natural path available for excess water to travel.

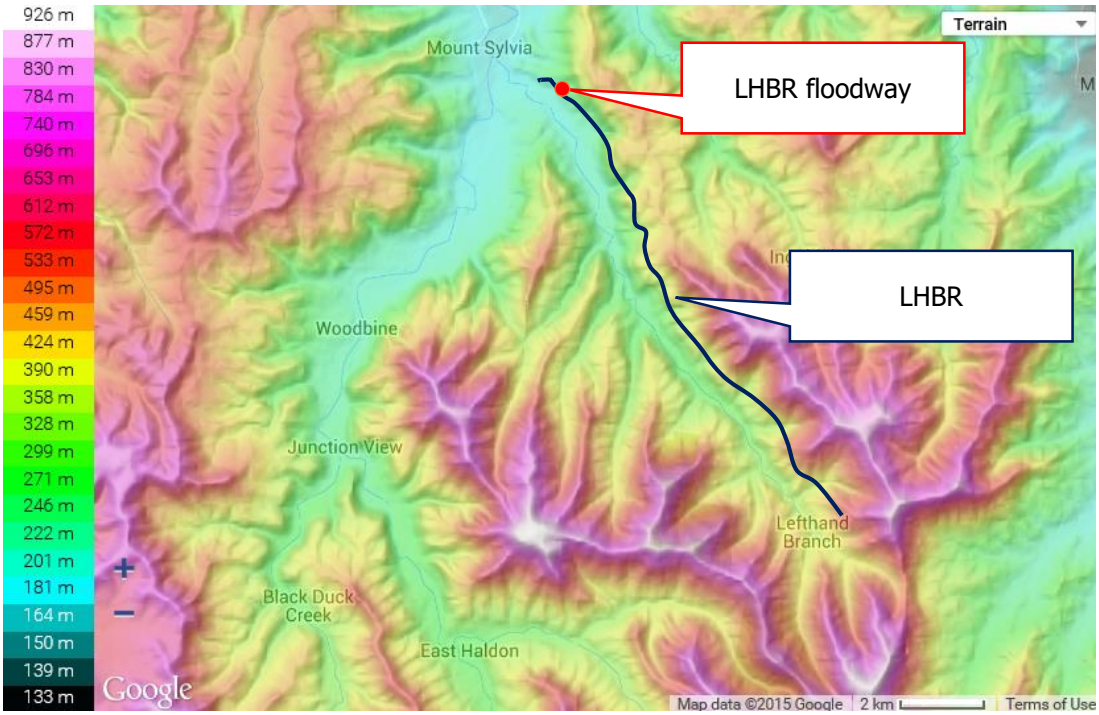

Figure 3.4: Topography Map of LHBR
(topographic-map.com n.d.)

3.2.2 LHBR Floodway Specifications

Based upon detailed drawings supplied by the LVRC, the LHBR floodway is 69.7 m in length and 4.5 m wide, allowing for single lane traffic. A cross section taken of the Tenthill Creek shows the depth of the floodway varies across its length reaching a maximum depression of approximately 1.2 m in the centre of the floodway as shown in Figure D.2 in Appendix D. The floodway design itself is based upon three main cross sections across its length, typical cross sections A, B and C shown in Figure 3.5 below. Section B also contains three 1200 mm x 600 mm concrete box culverts. Complete details and dimensions for all cross sections can be obtained from enlarged drawings shown in Figure D.3, Figure D.4 and Figure D.5 in Appendix D.

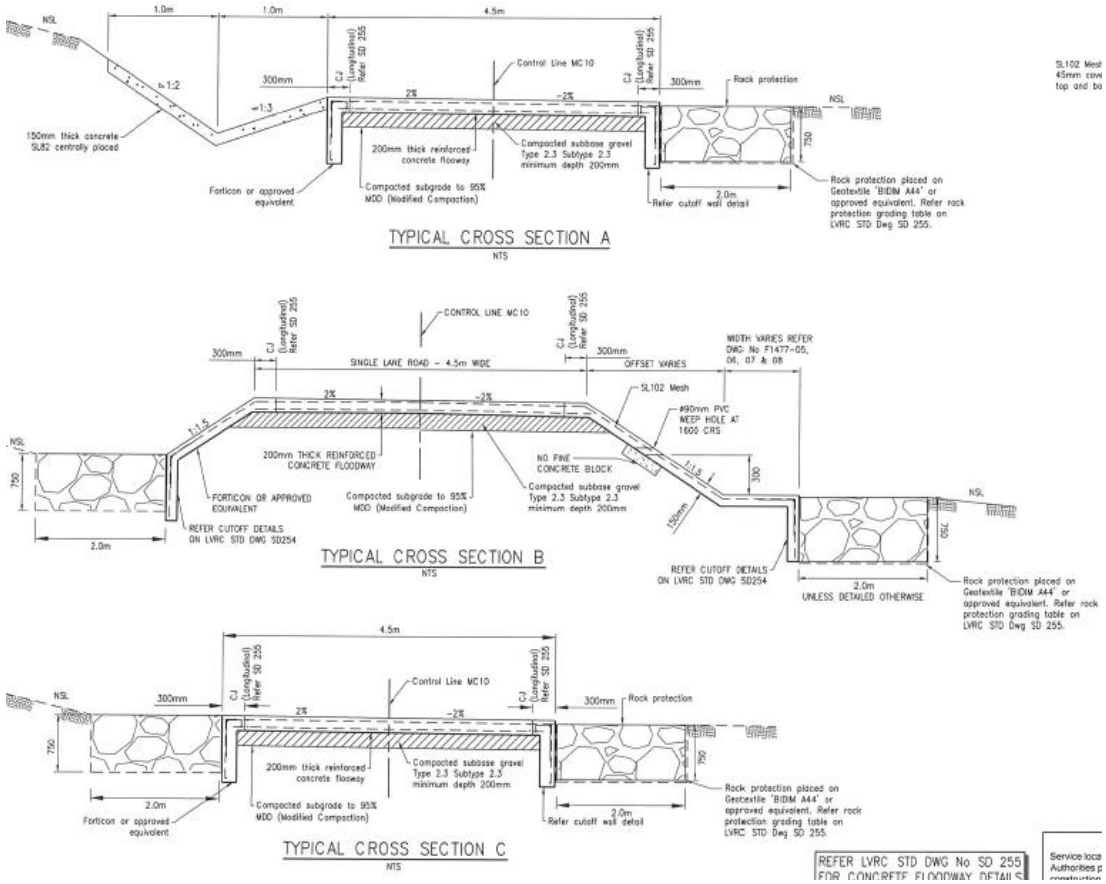

Figure 3.5: Cross Sections A, B and C

3.3 Strand7 Model Development and Geometry

The accuracy and validity of any finite element model is strongly dependent upon how it is developed. Since this research investigates the performance of a floodway structure i.e. stresses and displacements, a 2D plane strain analysis is undertaken. In doing so, the assumption is made that the floodway cross section B to be modelled is of infinite or very long length. The selection to focus on cross section B of the floodway as opposed to sections A or C was determined based on its location in the centre of the Tenthill Creek. This area would experience the greatest flow depths and velocities. Figure 3.6 below shows the typical cross section B to be modelled:

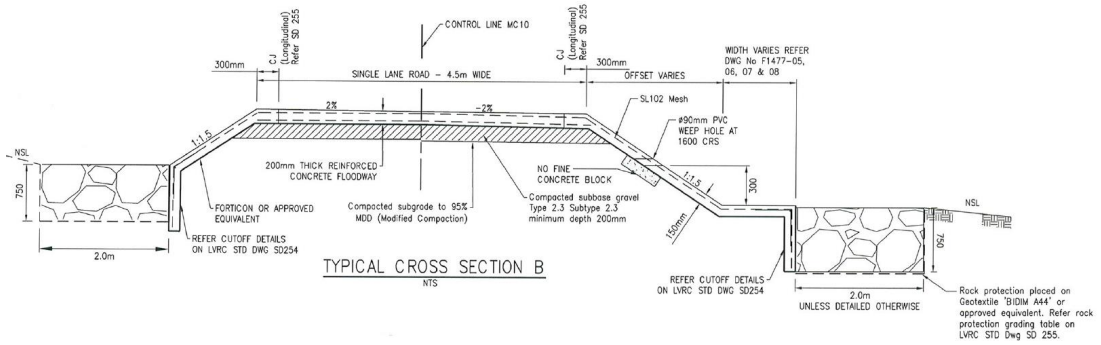

Figure 3.6: Cross Sections B

Since the geometry of cross section B is asymmetric, unbalanced around a central point, a full scale model needs to be constructed. The disadvantage to this approach is that the computational time required to acquire a solution will increase. However, since this project is focussing on conducting a 2D linear static analysis, the time increase will not be significant and is only increased by minutes as opposed to hours.

Construction of the model geometry is done manually by first determining the X and Y coordinates of the points of intersection across the entire model. These critical points called nodes essentially define the perimeter of the concrete floodway structure, rock protection and supporting layers of soils. Once these nodes are established suitable element types need to be identified to connect the nodes and ultimately form the finite elements making up the model. Strand7's inbuilt functions provide five different plate alternatives which are all suitable to perform a 2D plane strain analysis. Of the five alternatives shown in Figure 3.7 below, the Tri3 and Quad4 plates highlighted below were adopted as the most suitable based on the given geometry and analysis required:

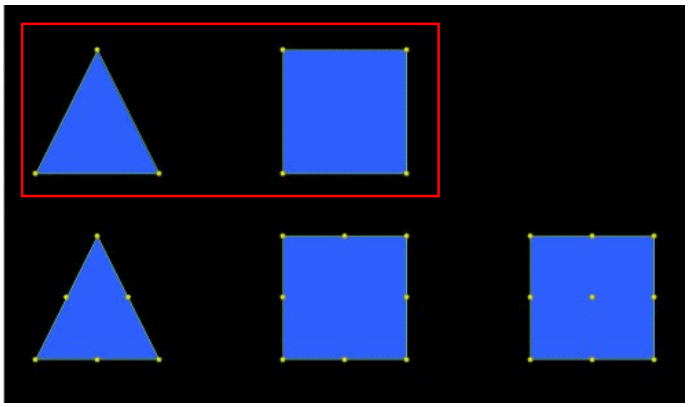

Figure 3.7: Tri3 and Quad4 Plate Legend
(Strand7 Pty Ltd n.d.c)

Figure 3.8 below represents the basic Strand7 model established for cross section B of the LHBR floodway and identifies the flow direction, upstream and downstream zones and axis orientation:

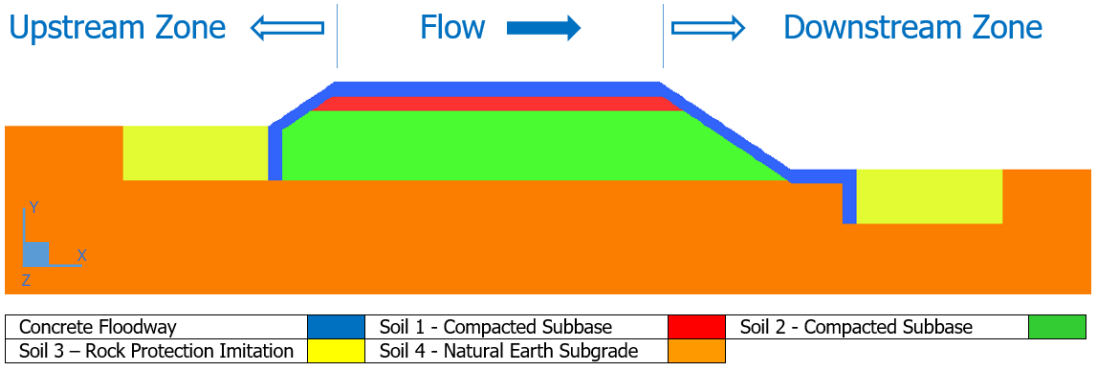

Figure 3.8: Basic model for cross section B

Furthermore, Table 3.1 below identifies the units of measure utilised for the finite element model.

Table 3.1: Unit System adopted for this model

Unit	Unit Quantity
Length	m
Edge Pressure	MPa
Point Load Force	kN

3.4 Material Properties

Detailed drawings of the LHBR floodway indicate five different materials the basic model is comprised of, all of which are stated in the above legend. However, whilst we know the types of material i.e. concrete, rock and soil, we do not know their shear strength parameters required to satisfy the failure criterions for Strand7 analysis. The combination of Strand7 limitations, unavailable information and the financial cost associated with conducting onsite soil investigations meant literature would be necessary to provide the most suitable parameters for analysis. A paper titled Soils and Land Suitability of the Lockyer Valley Alluvial Plains South-East Queensland (Queensland Government Natural Resources and Mines 2002) identified the soil found in the Mt Sylvia region where the LHBR floodway is located to be Alluvium as shown in Figure 3.9 below:

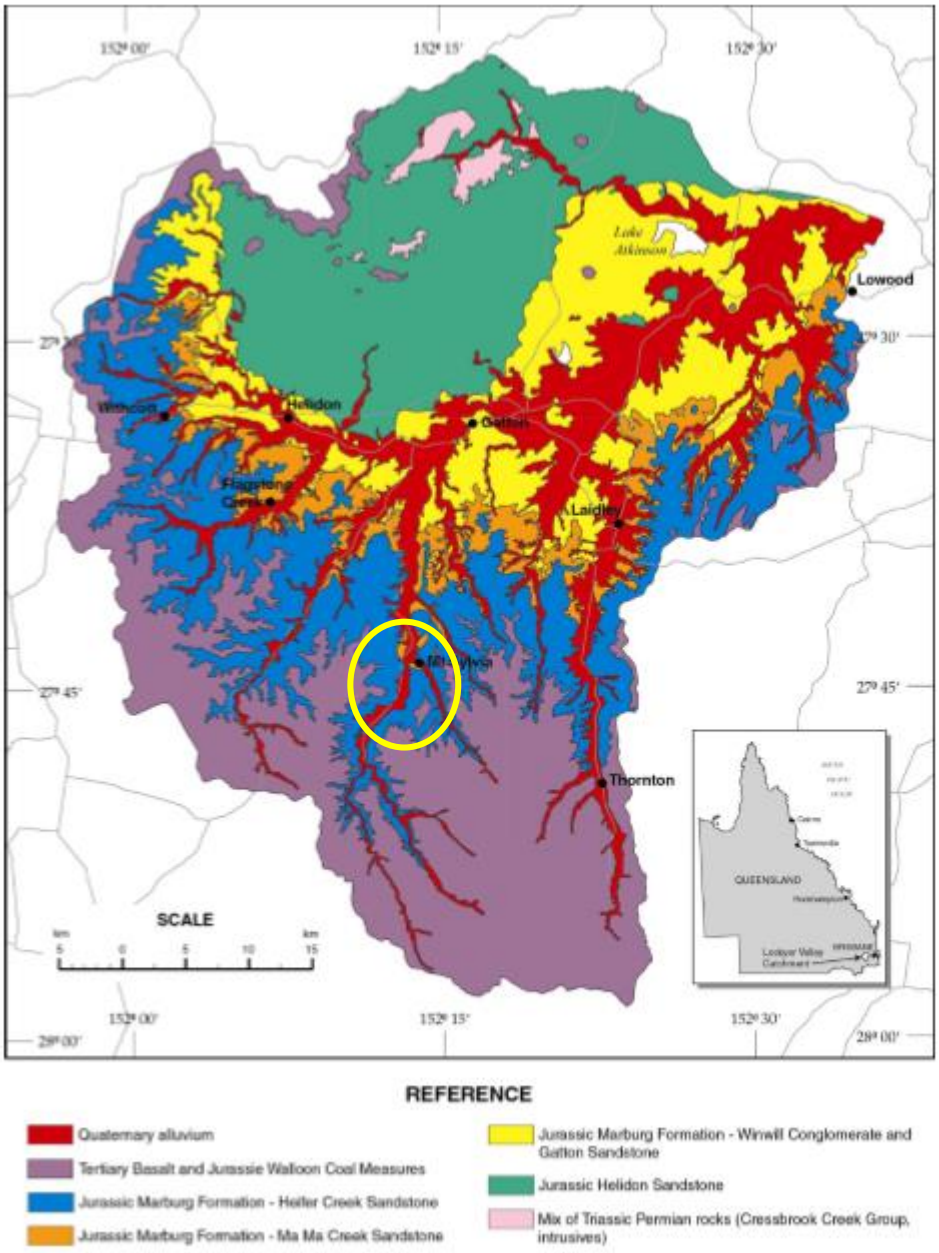

Figure 3.9: Soil Identification map
(Queensland Government Natural Resources and Mines 2002)

Knowing the type of soil is Alluvium, a clayey / sand with some gravel reasonable parameters were identified using Geotechdata.info (2008). Table 3.2 below illustrates the main material properties utilised for the FEA:

Table 3.2: Main Material Properties used for FEA

Material	Young's Modulus (MPa)	Poison's Ratio	Density (kg/m^3)	Friction Angle
Reinforced Concrete	30960	0.2	2400	N/A
Compacted Gravel sub base "Type 2.3"	200	0.3	2000	35°
Compacted Subgrade – 95% MDD	150	0.3	1900	30°
Rock Protection	100	0.3	1400	30°
Natural Earth	40	0.3	1700	25°

In determining the above parameters the following assumptions have been made:

- characteristic strength of concrete is 32 MPa
- Young's Modulus of compacted gravel sub base "Type 2.3" is the greatest of the four different soils, reducing in each layer approaching the natural earth
- rock protection will be modelled as a soil based on Strand7 limitations
- assume steel reinforcement included satisfies tensile strength requirements.

3.5 Forces

The forces utilised throughout the FEA have been determined based on first principles or in accordance with AS 5100.2-2004 (Standards Australia 2004). The different types of forces include hydrostatic, impact, drag, debris and lifting forces. When calculating based upon Australian Standards ultimate limit states

have been adopted for the scope of this project. Furthermore, AS 5100.2-2004 (Standards Australia 2004) states all force magnitudes must have a specific magnifier applied to it based on the ARI of flood in which a structure is designed for. According to current floodway guidelines, this ARI is based on 20 years (Austroads Ltd 2013; Department of Transport and Main Roads 2010; Main Road Western Australia 2006). Therefore, in keeping with AS 5100.2-2004 (Standards Australia 2004) all forces are magnified by a factor of 2, omitting hydrostatic forces.

3.5.1 Hydrostatic Forces

The hydrostatic forces the model was subjected to are shown in Figure 3.10 below:

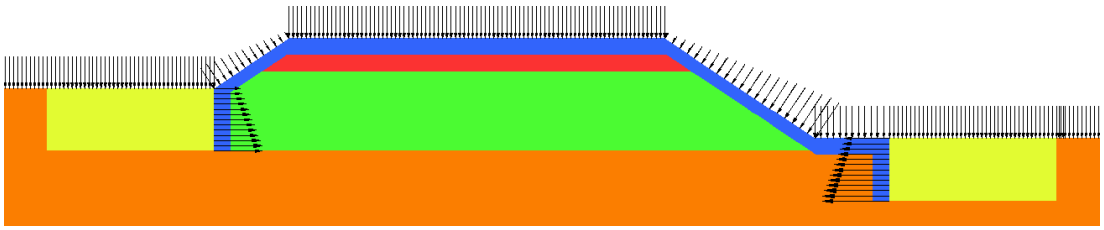

Figure 3.10: Hydrostatic Forces acting on Floodway

These forces act vertical on the surface of the ground upstream, downstream and across the roadway of the floodway structure itself. The downstream and upstream batters and vertical cut-off walls of the floodway are also subjected to hydrostatic forces. All forces are applied to the plates as an edge load pressure acting normal to the face of the plane in which it is in contact.

The hydrostatic forces are a linear function of the depth of flow and are calculated using Equation (2.6) below:

$$Hydrostatic\ Pressure = \rho g h \qquad (2.6)$$

Since the magnitude of these forces change with depth of flow, a summary table of some arbitrary water depths and their associated resultant hydrostatic pressures have been provided below in Table 3.3. Note: the 2D Plane Strain Strand7 model utilised applies pressure loads in terms of MPa and therefore this is what has been tabulated below:

Table 3.3: Applied Hydrostatic Pressure Summary

Depth of flow (m)	Hydrostatic Pressure (MPa)
0.2	1.962×10^{-3}
1	9.81×10^{-3}
2	1.962×10^{-2}
5	4.905×10^{-2}
10	9.81×10^{-2}

3.5.2 Drag Force

Drag forces (F_{drag}) have been applied to the upstream batter of the floodway acting in the same direction as the flow, shown in in Figure 3.11 below. A limitation in calculating this force is the relative submergence and proximity ratios required to determine the drag coefficient (C_d) for a bridge could not be directly applied to the floodway geometry. AS 5100.2-2004 (Standards Australia 2004) states the relative submergence is the ratio of the vertical distance from the girder soffit to the flood water surface upstream of the bridge (d_{wgs}) to the wetted depth of the superstructure (d_{sp}). To apply this to the floodway geometry d_{wgs} had to become the distance from the ground to the surface of the flood water. However, the proximity ratio could not be established utilising Figure 2.14 and therefore an average C_d of 1.4 was adopted. Applying this load to the upstream batter of the floodway meant the magnitude of this load had to be converted to equivalent

nodal forces acting over the perpendicular distance of 0.6 m, clearly demonstrated in Figure 3.11 below:

Figure 3.11: Drag Force

Equation (2.7) below shows how these forces were calculated with a summary of magnitudes with respect to flow velocities shown in Table 3.4. Full calculations can be found in Appendix E.

$$F_{drag} = 0.5 C_d {V_u}^2 A_s \qquad (2.7)$$

Note: All magnitudes shown it Table 3.4 have been magnified by 2 to satisfy ARI requirements.

Table 3.4: Applied Drag Force Summary

Mean Velocity (m/s)	Drag Force (kN)
1	0.84
3	7.56
5	21.0
6	30.24
7	41.16
8	53.76
10	84.0

3.5.3 Lifting Force

A lifting force has been applied to the roadway of the floodway structure in terms of a pressure which can be seen in Figure 3.12 below:

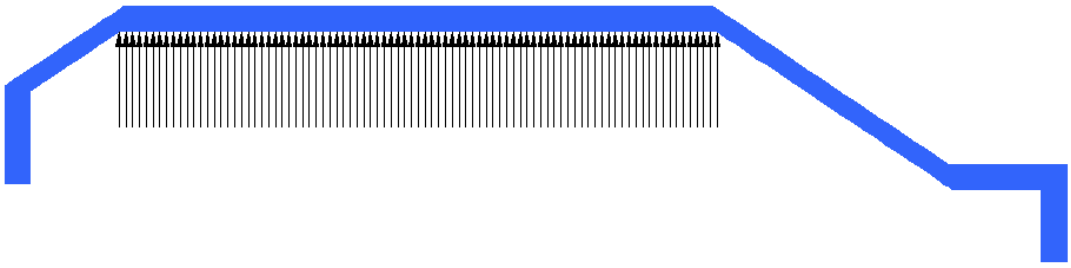

Figure 3.12: Lifting Force

Lifting forces are a function of both water velocity and depth of flow. Determining the relative submergence (S_r) of the floodway allows for the lifting coefficient (C_L) in both upward and downward directions to be established from Figure 2.18. Calculating for both, the resultant lifting force needs to be greater than the 43.19 kN self-weight of the floodway for an uplift to occur. If the resultant force is less than the floodways self-weight the force is applied in the downward direction. Calculating these lifting forces based on floodway geometry meant some assumptions were made. As explained in section 3.5.2 above the relative submergence required to determine lifting coefficient had to be adapted to suit floodways. Hence, lifting coefficients could then be determined from Figure 2.18.

Equation (2.10) below shows how the lifting forces were calculated with Table 3.5 showing a summary of the loads to be applied. Full calculations can be found in Appendix E.

$$F^*_{Lu} = 0.5 C_L V_u{}^2 A_L \qquad (2.10)$$

Note: All magnitudes shown it Table 3.5 have been magnified by 2 to satisfy ARI requirements.

Table 3.5: Applied Lifting Force Loads Summary

Depth (m)	0.2	1	2	5	10
Velocity (m/s)	F^*_{Lu} (MPa)				
1	-0.0001	0	0	0	0
3	0.018	0.0096	0	0	0
5	0.05	0.026667	0.02	0.02	0.02
6	0.072	0.0384	0.0288	0.0288	0.0288
7	0.098	0.052267	0.0392	0.0392	0.0392
8	0.128	0.068267	0.0512	0.0512	0.0512
10	0.2	0.106667	0.08	0.08	0.08

3.5.4 Log Impact

In accordance with AS 5100.2-2004 (Standards Australia 2004), log impact forces are calculated based on the velocity of the water, a 2,000 kg object and the slowdown distance associated with that object striking a solid concrete pile which is 0.075 m. Due to the arbitrary size and shape of floating debris it was assumed this load would act over an area of 0.2 m^2. Therefore the resultant pressure was divided into equivalent nodal forces in Strand7 acting over this area, as shown in Figure 3.13 for a log impact high and Figure 3.14 for a log impact low:

Figure 3.13: Log Impact High

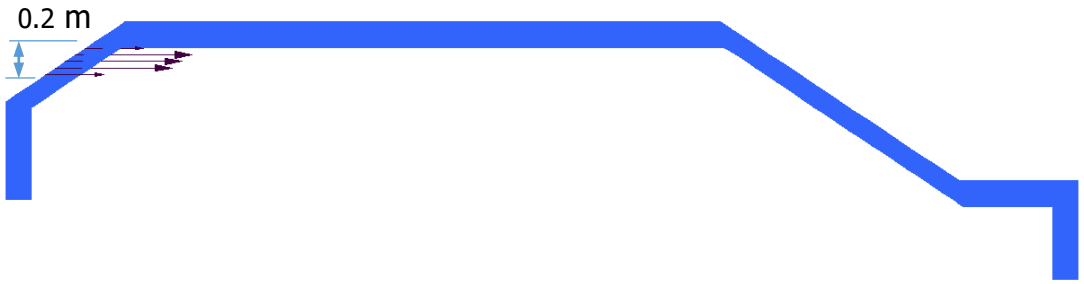

Figure 3.14: Log Impact Low

Equation (2.14) below shows how the log impact forces were calculated, with Table 3.6 showing a summary of the loads to be applied. Full calculations can be found in Appendix E. :

$$F_{Impact} = 0.5 \times 2000kg \times {V_u}^2/0.075m \qquad (2.14)$$

Note: All magnitudes shown it Table 3.6 have been magnified by 2 to satisfy ARI requirements.

Table 3.6: Applied Log Impact Force Summary

Flow Velocity (m/s)	Log Impact (kN)
1	26.67
3	240.0
5	666.67
6	960.0
7	1306.67
8	1706.67
10	2666.67

3.5.5 Debris Accumulation

Debris accumulation forces are calculated in a similar manner to drag forces. The drag coefficient (C_d) however is calculated differently, based on the product of

the mean velocity of water squared and the water depth identified in Figure 2.21. The area or debris mat which these loads act over for bridges is based on variables such as catchment vegetation, depth of flow and span of superstructure. However, the assumption is made for this project that debris can accumulate across the entire upstream batter. Therefore the overall area of 0.6 m^2 making up the upstream batter is considered a debris mat.

Figure 3.15: Debris Accumulation

Equation (2.12) below shows how the debris accumulation forces were calculated, with Table 3.7 showing a summary of the loads to be applied. Full calculations can be found in Appendix E:

$$F^*_{debris\ ultimate} = 0.5 C_d {V_u}^2 A_{deb} \qquad (2.12)$$

Note: All magnitudes shown it Table 3.7 have been magnified by 2 to satisfy ARI requirements.

Table 3.7: Applied Debris Accumulation Force Summary

Depth (m)	**0.2**	**1**	**2**	**5**	**10**
Velocity (m/s)	$F^*_{debris\ ultimate}$ (MPa)				
1	2.04	2.04	2.04	2.04	2.04
3	18.36	18.36	18.36	17.55	12.69
5	51	51	46.5	30.45	21.75

6	73.44	73.44	56.592	38.664	30.24
7	99.96	92.022	65.562	43.218	41.16
8	130.56	105.216	77.184	53.76	53.76
10	204	132	100.8	84	84

Furthermore, limitations within Strand7 meant these forces could not be applied as a pressure to the upstream batter as there line of action needed to be horizontal, not normal to the surface. Therefore, the pressure had to be converted to equivalent point loads acting over a surface area of 0.6 m^2.

3.6 Loading Combinations

The scope of this project investigates three different loading combinations. Each combination considers hydrostatic, lift and drag forces applied plus either a log impact or debris accumulation load. Table 3.8 below illustrates the forces included in each of the three combinations:

Table 3.8: Load Combination force inclusions

Force	Combination 1	Combination 2	Combination 3
Hydrostatic	✔	✔	✔
Lift	✔	✔	✔
Drag	✔	✔	✔
Log Impact (high)	✔	✖	✖
Log Impact (low)	✖	✔	✖
Debris Accumulation	✖	✖	✔

Combination 1 and 2 both consider log impact forces, however investigate different locations for the application of this load. Combination 1 considers a log impact hitting the top corner of the upstream batter of the floodway whilst

combination 2 applies the force in the middle. The reason for this is to determine which type of log impact would have the most adverse effect. Combination 3 investigates the impact of debris accumulation acting along the full length of the upstream batter.

3.7 Boundary Conditions

To determine accurate boundary conditions for the model it would require a costly soil investigations being undertaken at the site of the LHBR floodway. This in combination with acquiring works approval from LVRC means soil testing could not be included in the scope. Therefore it has been assumed the natural soil Alluvium surrounding the floodway is homogeneous to a width and depth of infinity. Based on this an iterative process was undertaken to identify satisfactory restraints for the model which would not influence the models outputs. The premise was to find a boundary where the resultant stresses in the soil did not interact with the boundary itself. To do this the model was subjected to an extreme loading combination which included hydrostatic, drag, lifting and log impact forces, all based on a flow velocity of 10 m/s and a water depth of 10 m. Whilst this load remained constant the distance of soil either side and below the model was increased in a stepwise fashion.

The resulting Mohr Coulomb stress contours of this process are shown in the four figures below. Figure 3.19 with a natural soil of 40 m wide and 14.1 m deep was identified as the point at which the boundary stopped influencing the resultant stresses in the soil. In each of the iterations below all unsatisfactory boundary interactions have been highlighted with a red cross. Knowing this, the boundary of this model could have fixed restraints applied on both sides and across the bottom. Based on the standard X, Y and Z axis orientation shown in Table 3.3, fixed supports restrict all translational and rotational movements with respect to all axis.

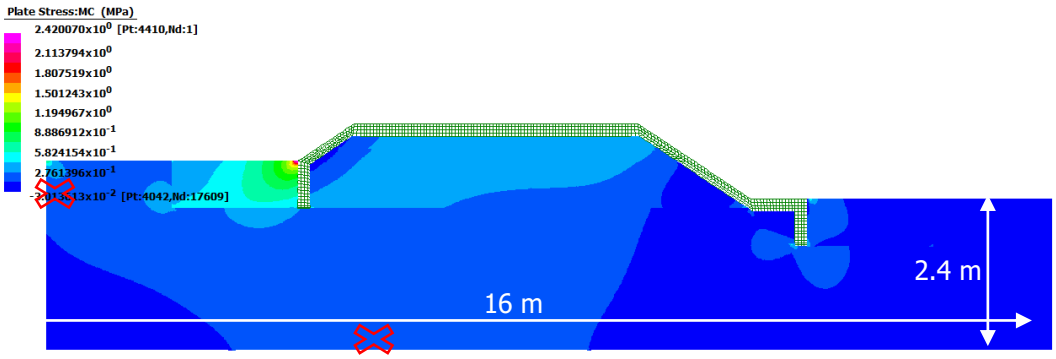

Figure 3.16: Boundary Iteration 1

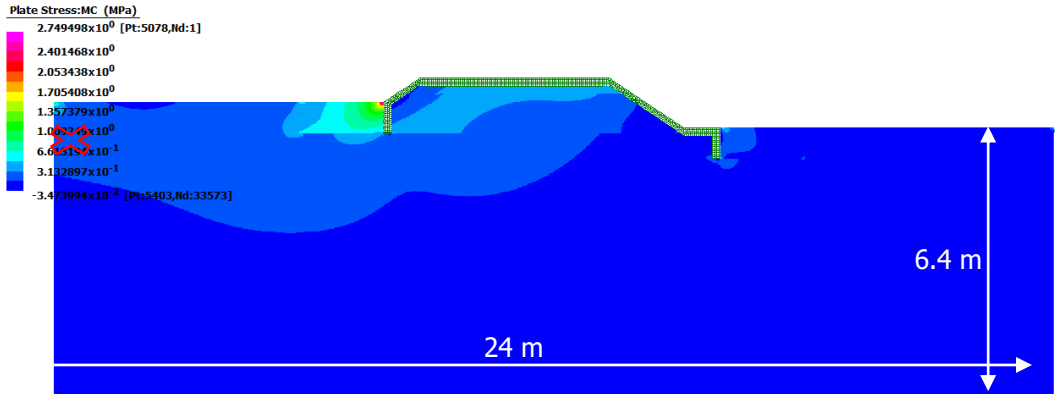

Figure 3.17: Boundary Iteration 2

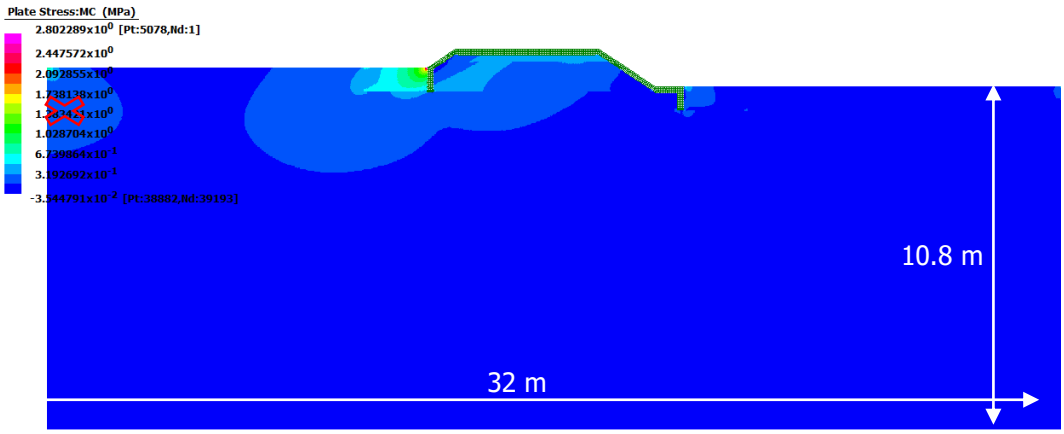

Figure 3.18: Boundary Iteration 3

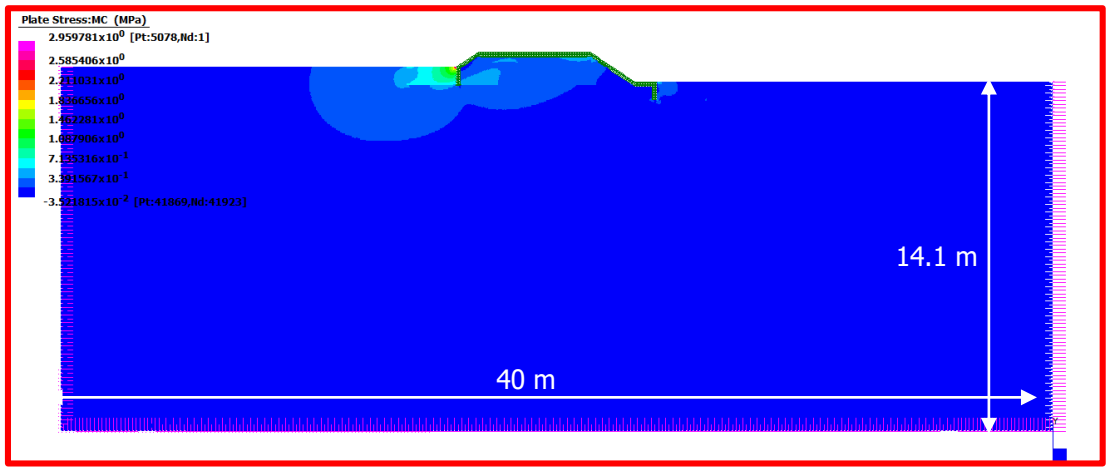

Figure 3.19: Boundary Iteration 4

3.8 Convergence Study

A convergence study was conducted to ensure the model was delivering accurate results whilst limiting the computational time it would take to calculate. To achieve this, the model was subjected to a constant 666 kN log impact load which was calculated based on a 5 m/s velocity. The iterative process recorded the stress (MPa) and displacement (mm) against the number of elements and nodes respectively. It was important to ensure the same element and node was analysed each time, more specifically element 24 and node 56 shown in Figure 3.20 below:

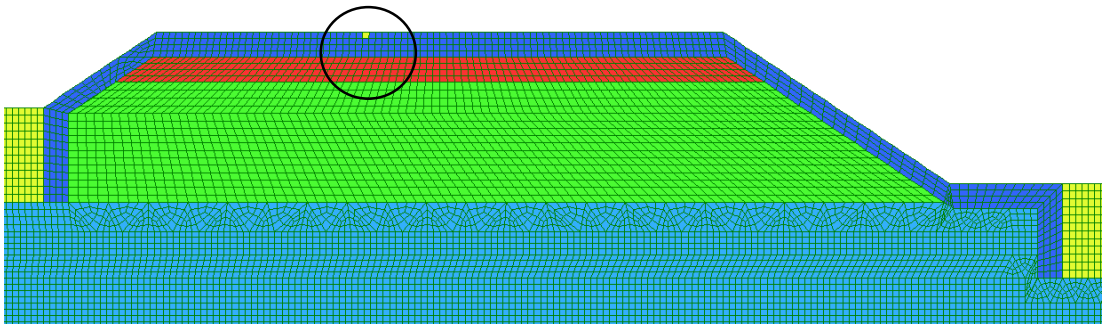

Figure 3.20: Node and element location

The premise is to identify the point at which the change in stress and displacement is within an acceptable tolerance of 5%, ultimately saying the

results are converging. Reducing the size of each element increases the overall number of elements and nodes that make up the mesh required for analysis. Based on a 25 mm x 25 mm element size the model requires 213,207 elements and a computational time of 19 minutes and 2 seconds. The stress recorded at element 24 for this iteration is 2.25 MPa. Increasing the element size to 50 mm x 50 mm reduces the number of elements to 63,497 giving a stress at element 24 of 2.15 MPa. The change in stress between these two locations is 4.65% meaning the lesser number of 63,497 elements with dimensions of 50 mm x 50 mm is adopted providing a more efficient computational time of 4 minutes and 55 seconds. Figure 3.21 below illustrates how the stress (MPa) is converging with respect to the number of elements:

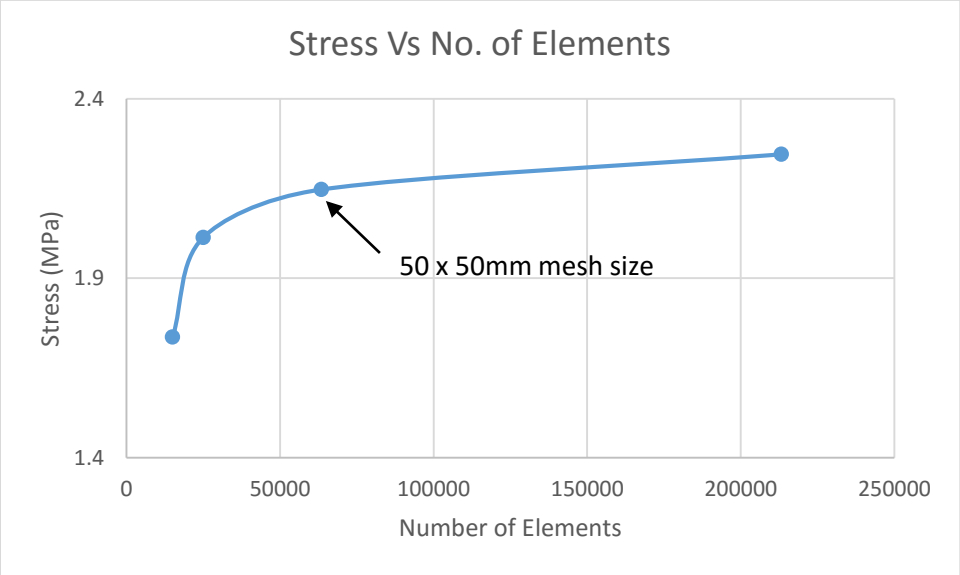

Figure 3.21: Stress Convergence Study

Similarly, Figure 3.22 below demonstrates the converging relationship between the number of nodes and the nodal displacement (mm). The change in displacement magnitude between 213,185 elements and 63,185 elements was less than 1%. Further indicating the adopted 50 mm x 50 mm element size yields accurate results, limiting the computational time required for analysis:

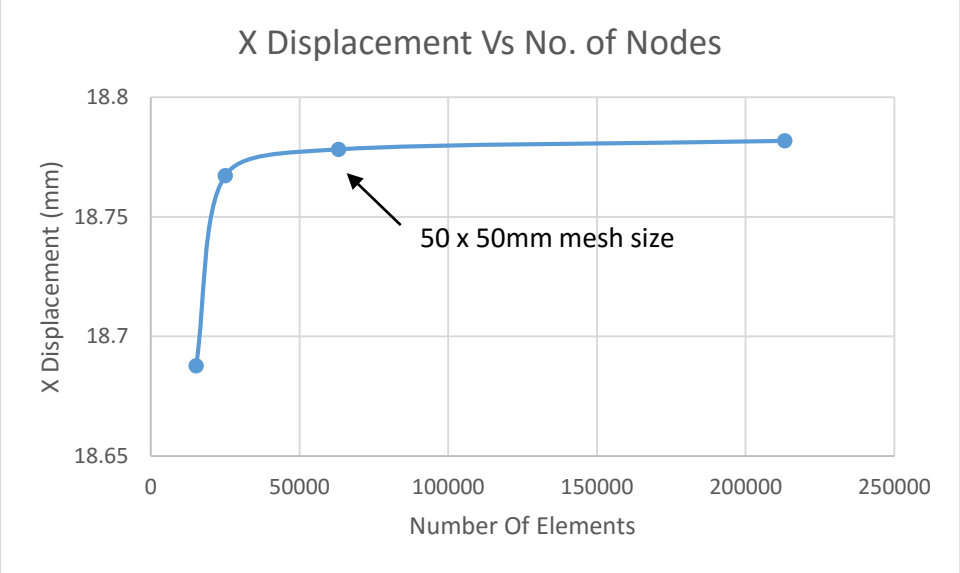

Figure 3.22: Displacement Convergence Study

CHAPTER 4. 2D FINITE ELEMENT ANALYSIS

4.1 Introduction

This chapter outlines the comprehensive parametric study which investigates the flow velocity and flow depth relationships with respect to three alternative loading combinations. Based on the worst load combination identified, the 2D FEA conducted in Strand7 examines the stresses and displacements within the floodway structure, rock protection and surrounding soil, identifying areas of vulnerabilities. This analysis is based upon constant flow velocity and changing flow depths and constant flow depth and changing flow velocity. Furthermore, a damage simulation is undertaken to understand the behaviour within the concrete floodway once damage to the downstream rock protection has been sustained. Finally, some limitations for this research with respect to Strand7, loadings and material properties are identified to ensure all aspects of the modelling process have been disclosed.

4.2 Parametric Study

Limited flood history data for the LHBR floodway area meant that a parametric study was necessary. This study was extensive and investigated the three different loading combinations previously discussed when subjected to water flow velocities of 1, 3, 5, 6, 7, 8 and 10 m/s and flow depths of 0.2, 1, 2, 5 and 10 m. For each of the different combinations the maximum stress and displacements were recorded for both the concrete floodway structure and the surrounding soil. A full summary table for each of the three different loading combinations can be found in Appendix F.

4.2.1 Stress Analysis

The data for loading combinations 1 and 2 consistently indicated the magnitude of stresses sustained by the concrete floodway were less as a result of the changing water depths and more directly related to the water flow velocities. This trend is clearly demonstrated in the column charts shown in Figure 4.1 and Figure 4.2 below. For instance, load combination 1 when calculated based on 5 m/s velocity only showed a change in stress from 6.01 MPa to 7.11 MPa for 0.2 m to 10 m water depth respectively, a change of 18.3%. However when we consider a constant depth of 5 m and a velocity change of 5 m/s to 6 m/s the stress increases from 6.01 MPa to 8.54 MPa. This yields a 42.1% increase in stress without any change in the depth of water flow.

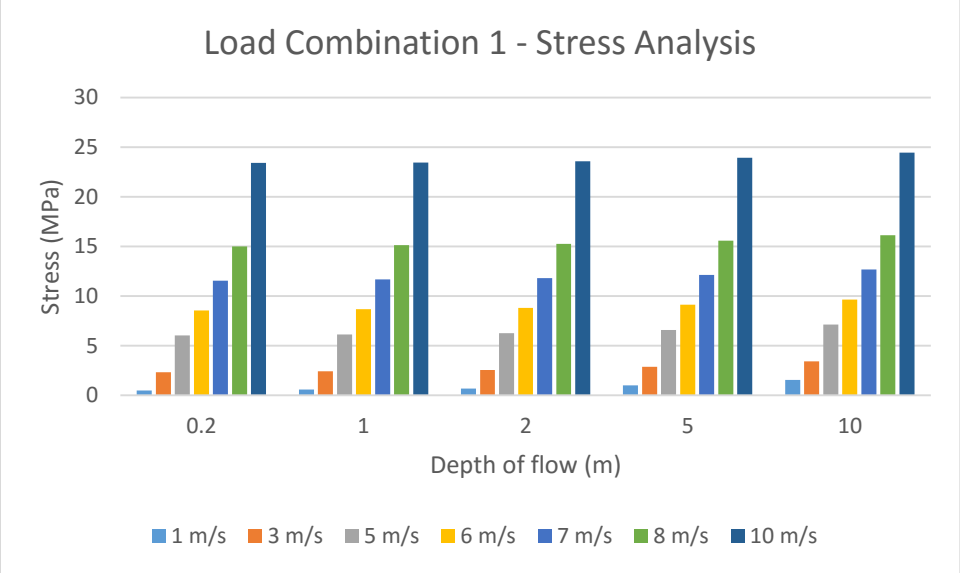

Figure 4.1: Load Combination 1 Stress Analysis

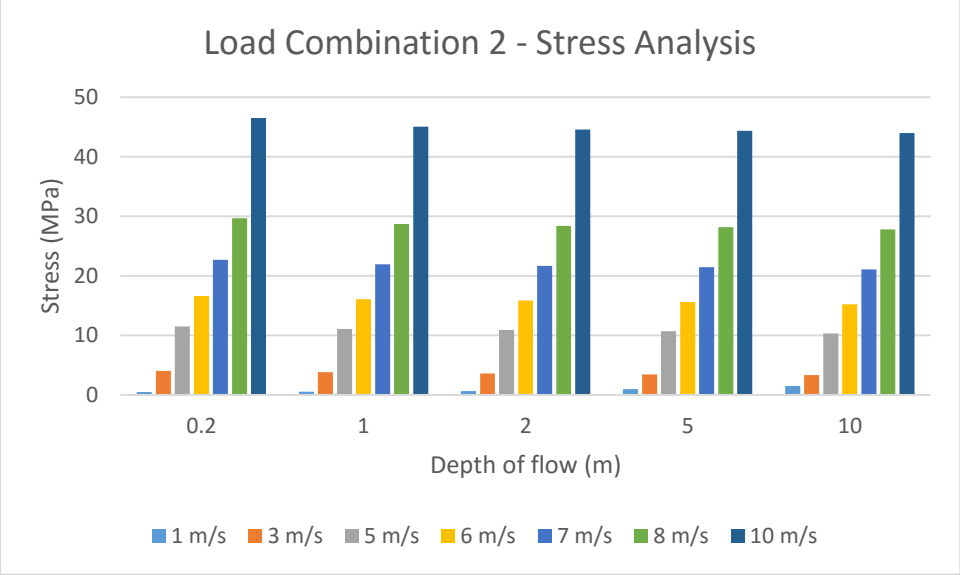

Figure 4.2: Load Combination 2 Stress Analysis

Load combination 3 data indicates the stress levels are a function of both water flow depth and velocities. Stress levels calculated based on 3 m/s or less velocities appear to increase as the depth of flow increases from 0.2 m to 10 m. At 5 m/s velocity, the stress profile reduces with respect to the increasing water depth, however between 2 m and 5 m water depth this behaviour changes further increasing as it approaches 10 m water depth. Stress levels associated with larger velocities 6, 7, 8 and 10 m/s transition from reducing with respect to water depth to increasing with depth once 5 m water depth is eclipsed. These behaviour patterns are shown in Figure 4.3 below:

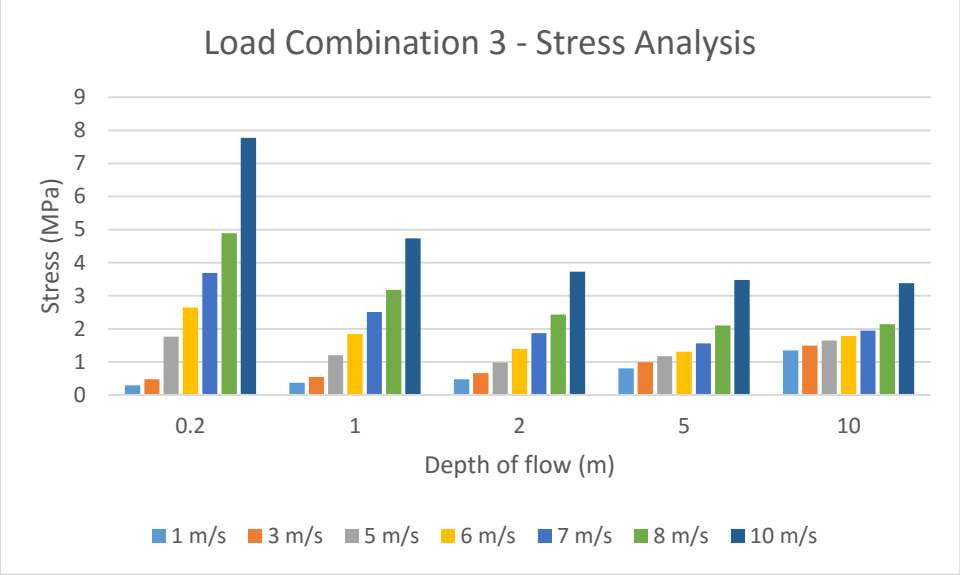

Figure 4.3: Load Combination 3 Stress Analysis

Of the three loading combinations considered in this parametric study, combination 3 demonstrated that debris accumulation consistently had the lowest resultant stress levels. Load combinations 1 and 2 had the same force magnitudes, however the change in location of the log impact dramatically influenced the stress levels incurred by the floodway structure. Combination 2 consistently demonstrated the highest resultant stresses, indicating this to be the worst loading combination as further demonstrated in Figure 4.4 below. This figure shows the relationship between stress and depth of flow for the three different load combinations with all loadings calculated based on a 5 m/s flow velocity. Therefore, further analysis focuses on load combination 2. Furthermore, all water flow depths combined with a 10 m/s flow velocity for load combination 2 identified as the only scenarios where the resultant stresses exceeded the 32 MPa compressive strength of the concrete structure. This implies that the concrete floodway structure could withstand all other potential loading combinations and that serious structural damage to the concrete floodway would most likely not occur without structural failure within the surrounding soil taking place.

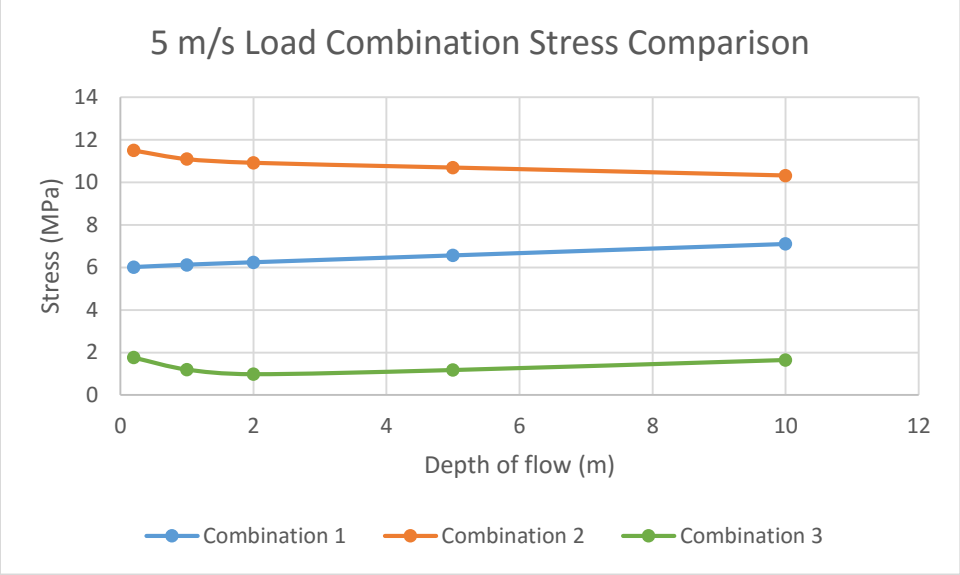

Figure 4.4: 5 m/s Load Combination Stress Comparison

4.2.2 Displacement Analysis

Similar to the stress analysis, the relationships between horizontal or X direction displacements and depth of flow have also been analysed. The data for loading combinations 1 and 2 consistently indicated the magnitude of displacements sustained by the concrete floodway were very similar for all scenarios, all within 0 - 3% of each other. Figure 4.5 and Figure 4.6 plots the maximum displacements under load combination 2 for different flow velocities and depths. Figures indicate only a minor increase in displacements with respect to changing flow depths. Over the 9.8 m change in water depth the horizontal displacement within the structure only increased from 4.88 mm to 4.97 mm, a change of only 1.84%. However, when the velocity changes and the flow depth remains constant the structural displacement increases as shown in Figure 4.6. For example, load combination 2 with forces calculated at a constant flow depth of 5 m and changing flow velocities revealed horizontal displacements of 0.89 mm and 52.1 mm for flow depths 0.2 m and 10 m respectively. This substantial increase in the rate of horizontal displacement, further concludes the concrete

floodway structure is more vulnerable to changes in water flow velocities than changes in water depth.

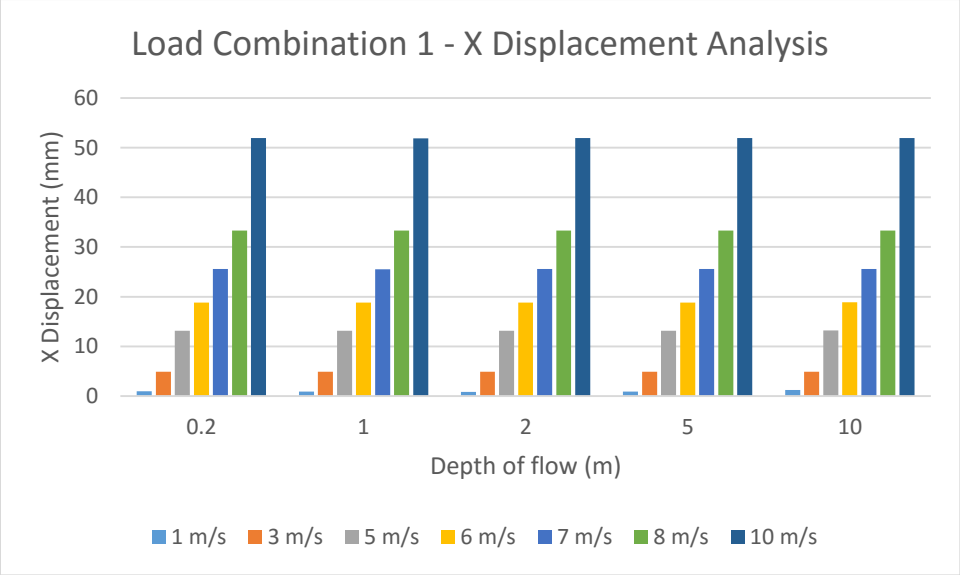

Figure 4.5: Load Combination 1 X Displacement Analysis

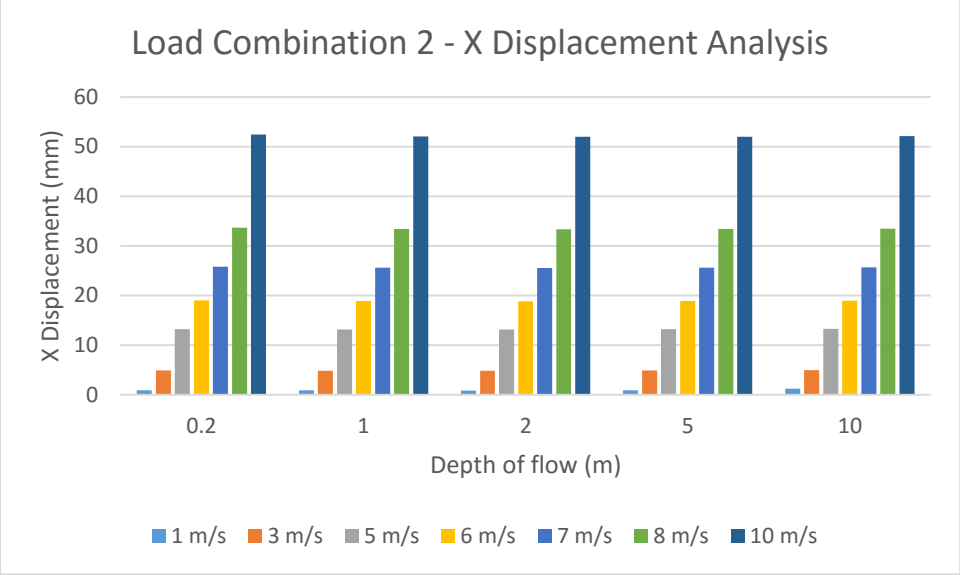

Figure 4.6: Load Combination 2 X Displacement Analysis

Load combination 3 data indicates that horizontal displacement magnitudes are a function of both water flow depth and velocities. Horizontal displacements appear to increase almost linearly when flow depth remains constant and flow velocities change. When considering a constant flow velocity of 3 m/s or less,

the magnitude of displacement appears to increase with the rise in flow depth. However, once these flow velocities equal or exceed 5 m/s the magnitude of horizontal displacement begins to decrease as the flow depth increases from 0.2 m to 5 m, only to again start increasing as the depth approaches 10 m. These behaviour patterns are shown in Figure 4.7 below:

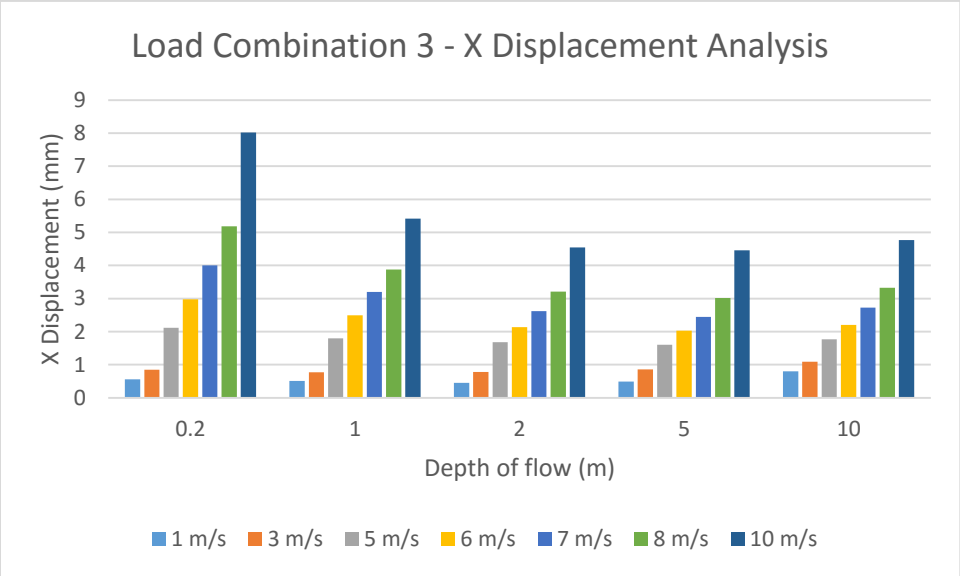

Figure 4.7: Load Combination 3 X Displacement Analysis

Of the three loading combinations considered in this parametric study, combination 3 demonstrated that debris accumulation caused the least amount of structural displacement in the horizontal direction. The worst horizontal displacement for this load combination was 8.02 mm, occurring at a flow velocity of 10 m/s and a flow depth of only 0.2 m. This worst case result was substantially lower than the horizontal displacements recorded for load combinations 1 and 2.

Load combinations 1 and 2 consistently demonstrated the highest horizontal displacements. Furthermore, irrespective of the location of the log impact associated with the combinations, the magnitude of displacements recorded where almost identical, as shown in Figure 4.8 below. This figure shows the relationship between horizontal displacement and depth of flow for the three different load combinations with all loadings calculated based on a 5 m/s flow

velocity. Whilst it is evident that load combinations 1 and 2 yield the greatest displacements, quantifying the significance of this displacement is difficult without Australian Standards for design to compare to.

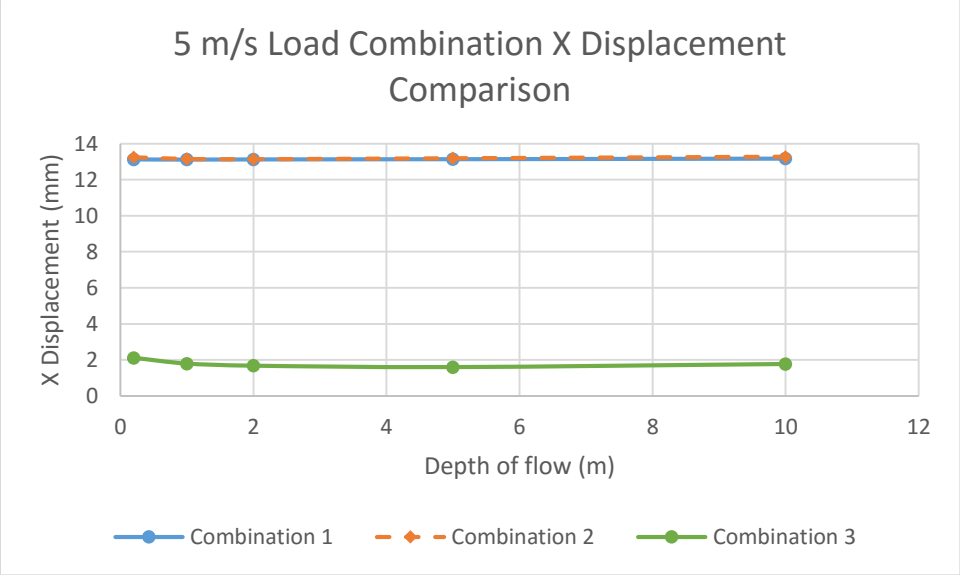

Figure 4.8: 5 m/s Load Combination X Displacement Comparison

4.3 Stress and Displacement Analysis

This analysis investigates the relationships between stress and displacement with respect to the effects of water flow velocity and flow depth. In addition to the contour plots being shown each type of analysis, all other stresses and displacements will be tabulated for the remaining depths and velocities included in the study for a complete comparison to be formed.

4.3.1 Change in Stress at Different Flow Depths

Utilising the worst case load combination 2, this analysis investigates the structural performance of the floodway when subjected to loadings calculated based upon a constant flow velocity of 3 m/s and changing flow depths. The stress and displacement contour plots shown for this analysis focus on a very low

and extremely high flow depth, 1 m and 10 m respectively for visual comparisons to be made.

The von Mises stress failure criterion demonstrated that the greatest stress for each of the different flow depths occurred at two different locations within the concrete structure. The magnified portions of Figure 4.9 and Figure 4.10 show that this particular loading combination at 1 m flow depth was subjected to a maximum stress of 3.85 MPa located at the upstream batter of the floodway where the log impact occurred. However, as the water depth increased to 10 m a maximum recorded stress of 3.34 MPa was located at the downstream batter of the floodway. Therefore, at a 3 m/s flow velocity the downstream side of the structure is more vulnerable to increased stresses as a result of rising flow depth than the upstream side, but still well below the 32 MPa compressive strength of the concrete floodway. In addition, the contour plots show that the corners or intersecting points of the floodways geometry appear to be the most vulnerable areas for which these concentrated stresses seem to occur. Across the roadway itself the analysis shows a stress of 0.666 MPa at the central location based on 1 m flow depth. This only slightly increases to 1.03 MPa at a flow depth of 10 m, a rise of 54.7 %.

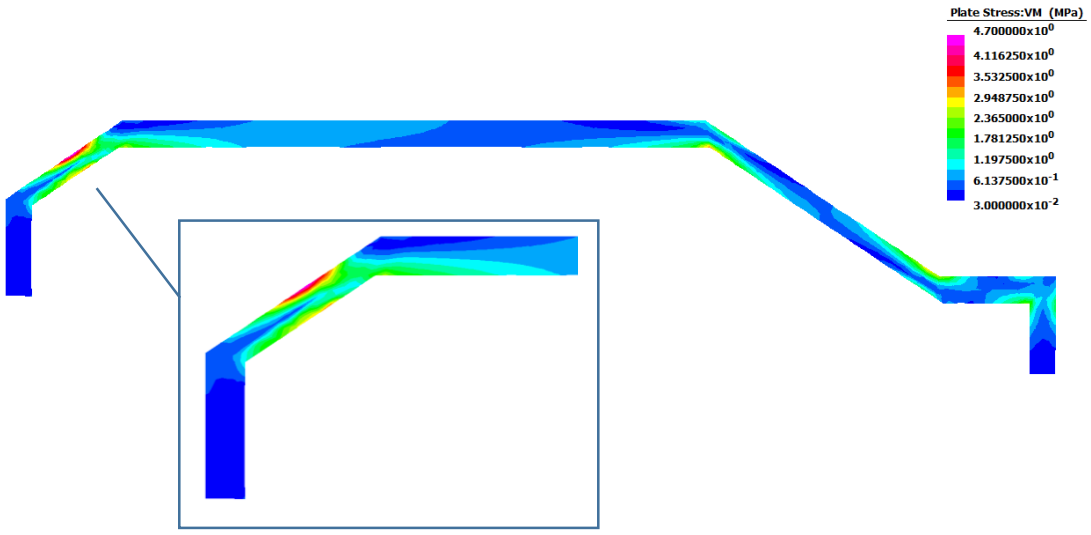

Figure 4.9: Stress for 3 m/s Flow Velocity @ 1 m Flow Depth

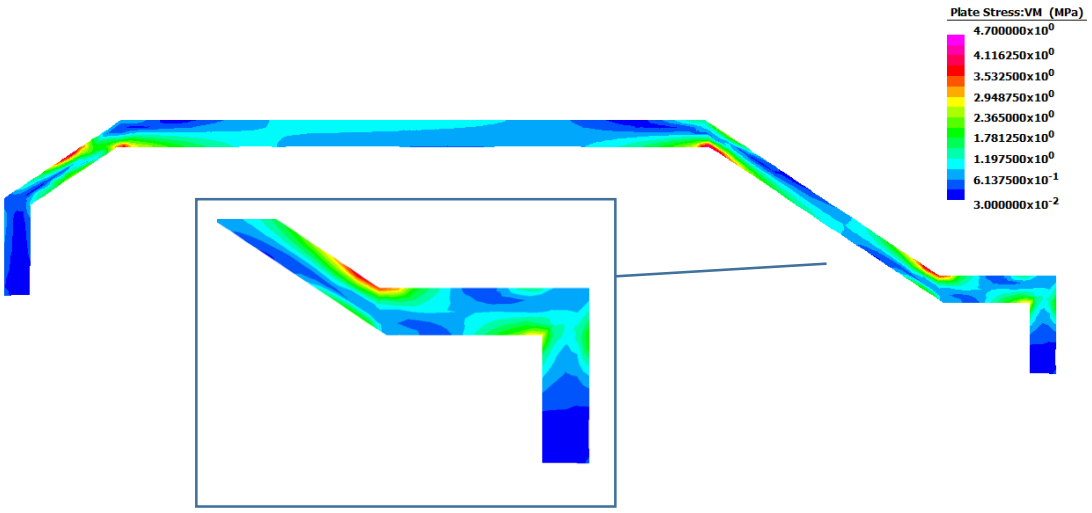

Figure 4.10: Stress for 3 m/s Flow Velocity @ 10 m Flow Depth

Table 4.1 and Table 4.2 below summarise the stresses recorded for each of the different flow depths included in this study. Each table represents the maximum stress concentrations at both the upstream and downstream batters of the floodway. This data indicates under these loading conditions the concentrated stresses upstream would decrease by 24% with a 9.8 m increase in water depth. Interestingly, the downstream side of the structure would simultaneously experience an increase in stress of 48.4%. Figure 4.11 below provide a visual representation of this behaviour for comparison:

Table 4.1: Stress for Constant 3 m/s Velocity – Upstream Data

Constant 3 m/s Velocity – Upstream Data					
Depth (m)	0.2	1	2	5	10
Max. Stress (MPa)	4.04	3.85	3.63	3.41	3.07

Table 4.2: Stress for Constant 3 m/s Velocity – Downstream Data

Constant 3 m/s Velocity – Downstream Data					
Depth (m)	0.2	1	2	5	10
Max. Stress (MPa)	2.25	2.35	2.47	2.79	3.34

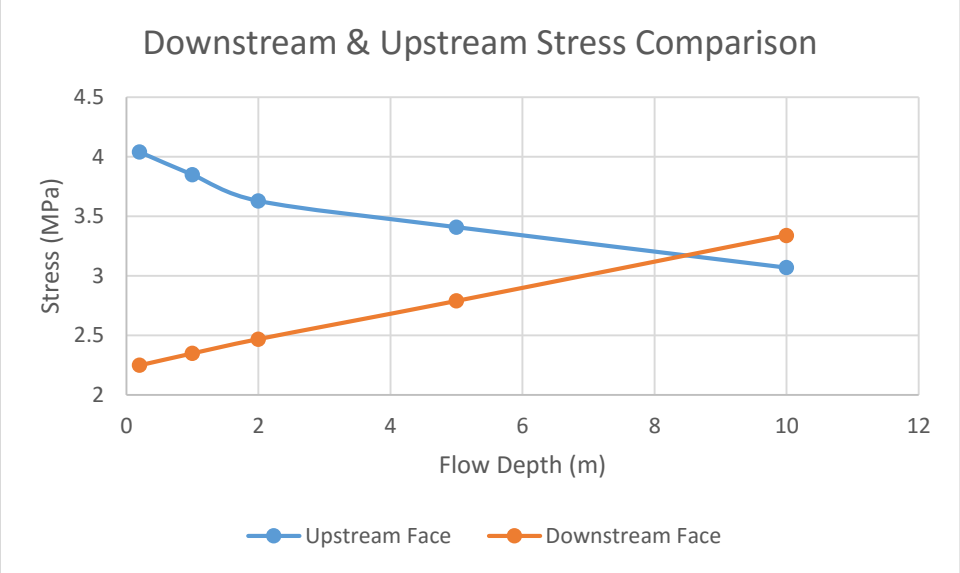

Figure 4.11: Velocity Downstream and Upstream Stress Comparison

4.3.2 Change in Displacement at Different Flow Depths

The maximum displacement in the X direction was recorded at 4.84 mm and 4.97 mm for flow depths of 1 m and 10 m respectively, an increase of 2.69%. Figure 4.12 and Figure 4.13 below show the X direction displacement comparison for the two different flow depths. The wireframe floodway image within these figures, shows the original location of the floodway with all displacement contour plots magnified by 1% for visual representation. For both scenarios the maximum X displacements occurs at the upstream batter of the floodway, however spread downwards onto the upstream cut-off wall and advances across the roadway towards the downstream with the increase in flow depth. This demonstrates that based on this particular loading scenario an increase in water depth will increase the floodways horizontal displacement, even without any change in flow velocity.

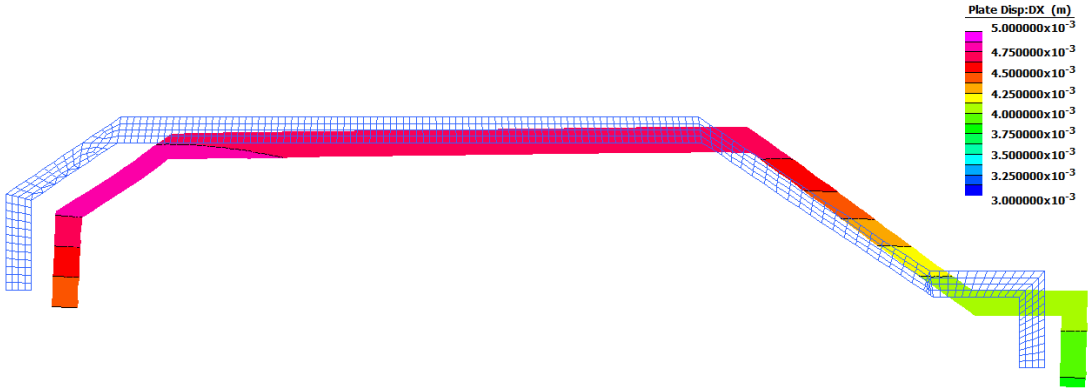

Figure 4.12: X Displacement for 3 m/s Flow Velocity @ 1 m Flow Depth

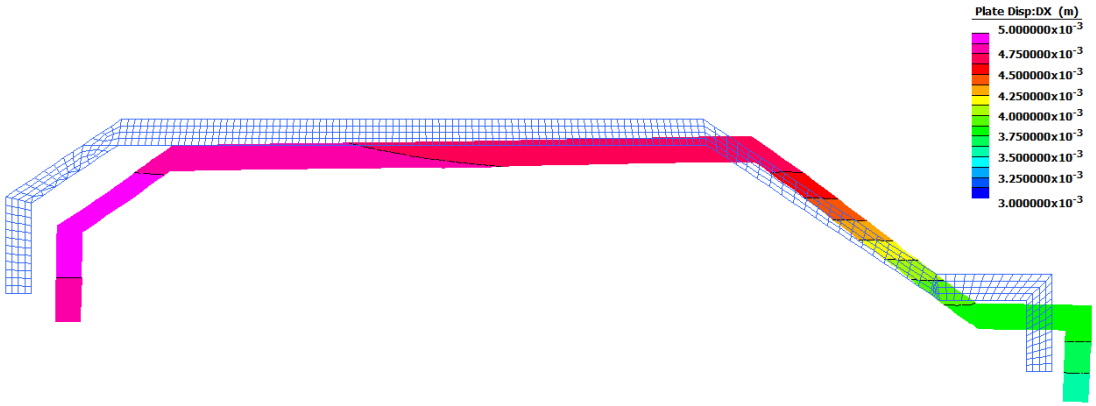

Figure 4.13: X Displacement for 3 m/s Flow Velocity @ 10 m Flow Depth

Table 4.3 below summarises the maximum X direction displacements recorded for each of the different flow depths included in this study. Figure 4.14 below provides a visual representation of the tabulated data for comparison. From this graph we can identify that with this particular loading scenario and a flow velocity of 3 m/s the X direction displacement actually decreases between 0.2 m and 2 m flow depths. Once the flow depth exceeds 2 m the horizontal displacement begins to increase, almost in a linear fashion.

Table 4.3: X Displacement for Constant 3 m/s Velocity Data

Constant 3 m/s Velocity					
Depth (m)	0.2	1	2	5	10
Max. X Disp.(mm)	4.87	4.84	4.8	4.86	4.96

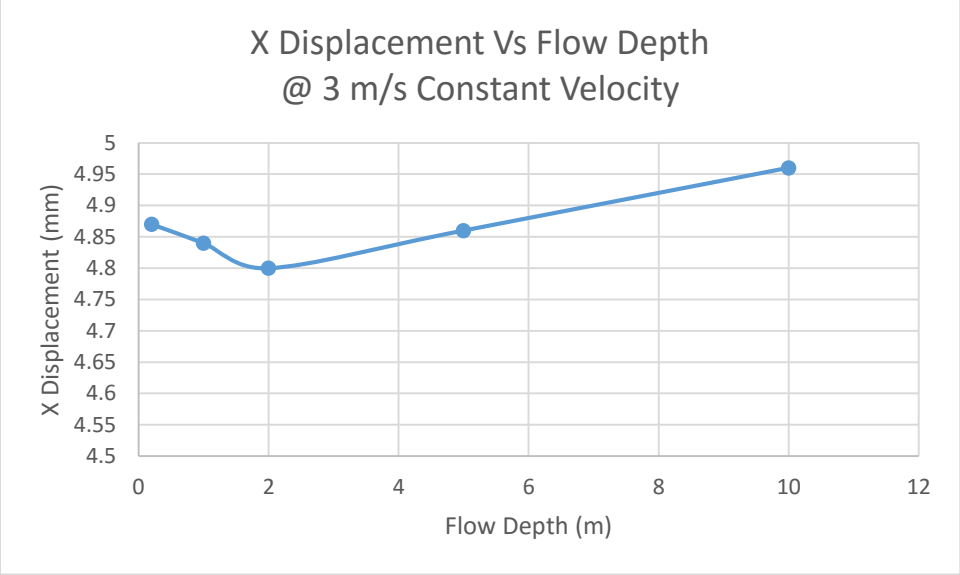

Figure 4.14: X Displacement vs Flow Depth @ 3 m/s Constant Velocity

The maximum displacement in the Y direction was recorded at 1.91 mm and 3.03 mm for flow depths of 1 m and 10 m respectively, an increase of 58.6%. Figure 4.15 and Figure 4.16 below show the Y direction displacement comparison for the two different flow depths. The largest Y displacements occur at both the upstream and downstream cut-off walls of the floodway, with the maximum displacements presenting at the downstream cut-off walls for both scenarios. This demonstrates that based on this particular loading combination and constant flow velocity of 3 m/s, the vertical displacement within the floodway would increase as a result of the increasing flow depth.

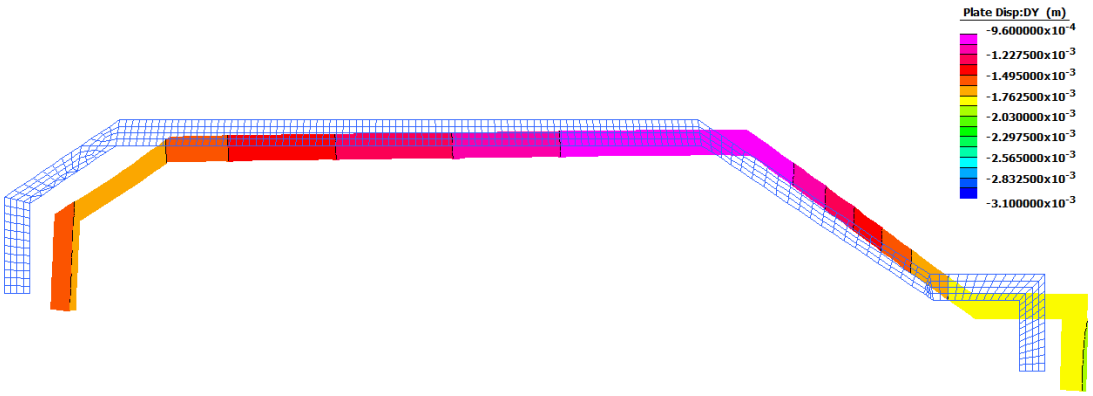

Figure 4.15: Y Displacement for 3 m/s Flow Velocity @ 1 m Flow Depth

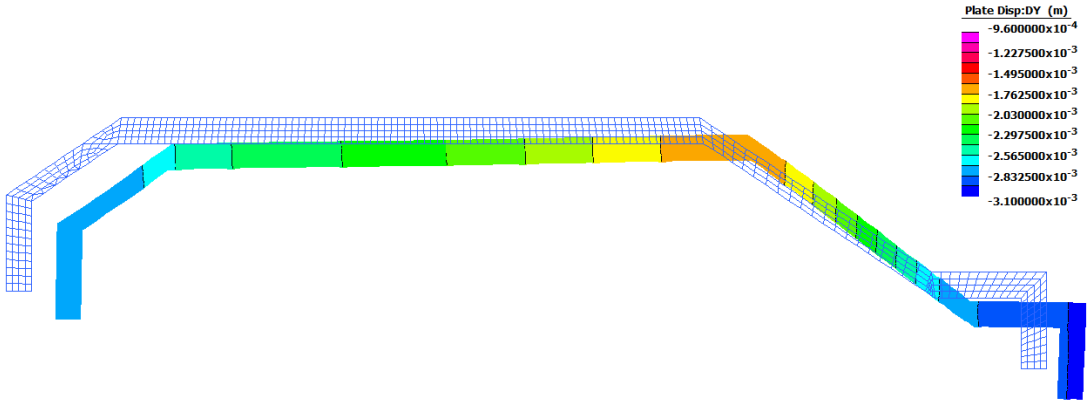

Figure 4.16: Y Displacement for 3 m/s Flow Velocity @ 10 m Flow Depth

Table 4.4 below summarises the maximum Y displacements recorded for each of the different flow depths included in this study. Figure 4.17 below provides a visual representation of the tabulated data for comparison. From this graph we can identify that with this particular loading scenario and a flow velocity of 3 m/s the Y direction displacement continually increases as the depth increases from 0.2 m to 10 m.

Note: Negative values only indicate the displacement is acting in the downwards direction.

Table 4.4: Y Displacement for Constant 3 m/s Velocity Data

Constant 3 m/s Velocity					
Depth (m)	0.2	1	2	5	10
Max. Y Disp.(mm)	-1.72	-1.91	-2.23	-2.47	-3.03

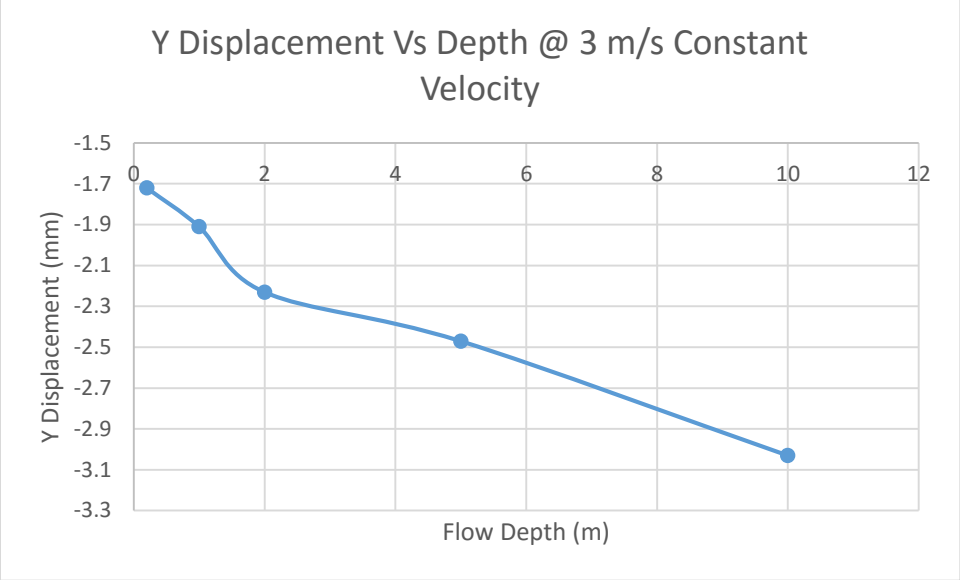

Figure 4.17: Y Displacement vs Flow Depth @ 3 m/s Constant Velocity

4.3.3 Change in Stress at Different Flow Velocities

This analysis investigates the structural behaviour of the floodway when the flow depth remains constant at 5 m and the flow velocities change. The stress and displacement contour plots for this analysis considers 1 m/s and 7 m/s flow velocities for comparison.

Figure 4.18 and Figure 4.19 below show the stress contour comparison throughout the concrete floodway based on the above flow depth velocities. Results show that a flow velocity of 1 m/s at a depth of 5 m delivers a maximum stress of 1.01 MPa to the downstream batter of the floodway. Increasing the flow velocity to 7 m/s yields a maximum stress of 21.5 Mpa, but this time acts on the upstream batter of the floodway shown in the magnified image within Figure 4.19 below. The two contour plots also demonstrate a greater variation in stress levels throughout the floodway when the flow velocity increases from 1 m/s to 7 m/s. Once again neither case resulted in stress levels that exceeded the 32 MPa compressive strength of the floodway.

This significant increase in stress at both ends of the floodway demonstrates the substantial impacts flow velocities have on this type of structure. Therefore based on this particular loading combination and a constant flow depth of 5 m, it can be concluded that stress levels are influenced more greatly by flow velocities as opposed to flow depth.

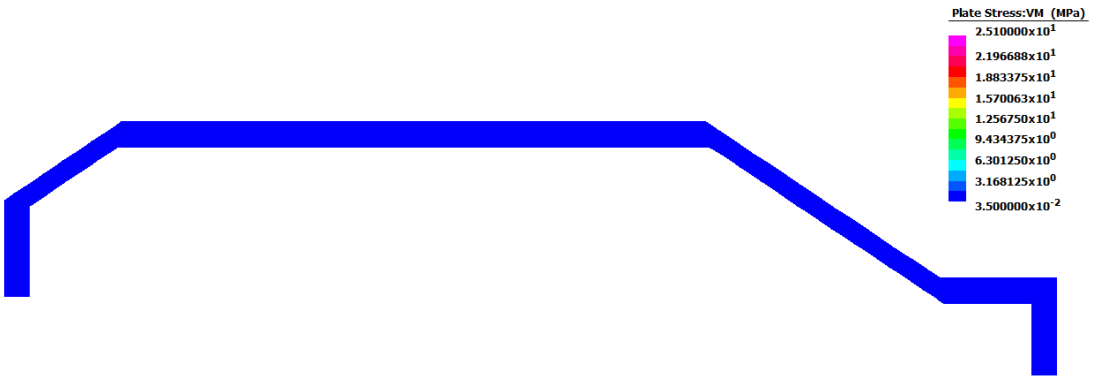

Figure 4.18: Stress for 1 m/s Flow Velocity @ 5 m Flow Depth

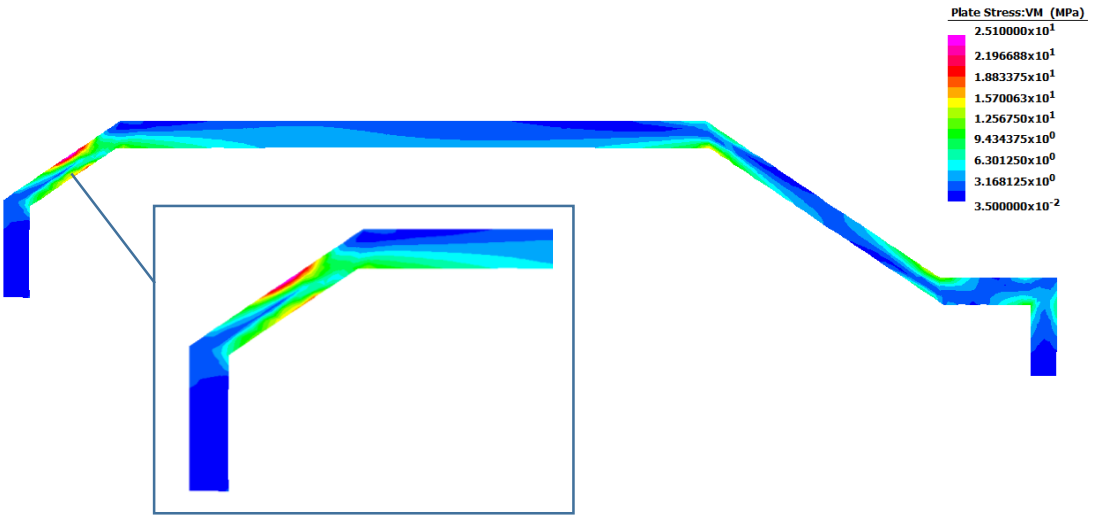

Figure 4.19: Stress for 7 m/s Flow Velocity @ 5 m Flow Depth

Table 4.5 and Table 4.6 below summarise the stresses recorded for each of the different flow velocities included in this study. Each table represents the maximum stress concentrations at both the upstream and downstream batters of the floodway. Figure 4.20 below demonstrates the tabulated data highlighting the behaviour of the stress at both the upstream and downstream batters as the flow velocity increases from 1 m/s to 7 m/s and the flow depth remains constant

at 5 m. The upstream batter which takes the full force of the log impact increases at a greater rate than the stress on the downstream batter, which is to be expected.

Table 4.5: Stress for Constant 5 m Flow Depth Upstream Data

Constant 5 m Flow Depth – Upstream Data							
Velocity (m/s)	1	3	5	6	7	8	10
Max. Stress (MPa)	0.19	3.41	10.70	15.63	21.46	28.19	44.35

Table 4.6: Stress for Constant 5 m Flow Depth Downstream Data

Constant 5m Flow Depth – Downstream Data							
Velocity (m/s)	1	3	5	6	7	8	10
Max. Stress (MPa)	1.01	2.79	6.34	8.79	11.68	15.02	23.03

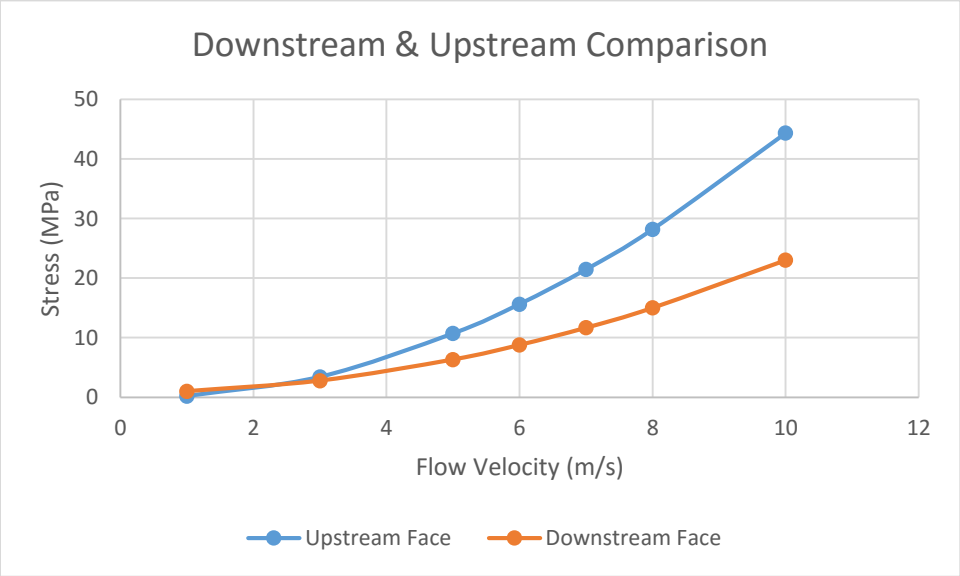

Figure 4.20: Depth Downstream and Upstream Comparison

4.3.4 Change in Displacement at Different Flow Velocities

The maximum displacement in the X direction was recorded at 0.89 mm and 25.6 mm for flow velocities of 1 m/s and 7 m/s respectively. Figure 4.21 and Figure

4.22 below show the X direction displacement comparison for the two different flow velocities. The wireframe floodway image within these figures, shows the original location of the floodway with all displacement contour plots magnified by 1% for visual representation. At a flow velocity of 1 m/s and a flow depth 5 m, Figure 4.21 indicates a full blue contour, meaning there is very little variation in the horizontal displacement throughout the floodway in comparison to the contour for a 7 m/s flow velocity. However, when the flow velocity increases to 7 m/s for the same depth of flow the floodway experiences horizontal displacements of 16 mm or above throughout. At 7 m/s flow velocity the maximum X displacement occurs on the upstream batter of the floodway and continues across the roadway. This demonstrates that based on this particular loading scenario an increase in flow velocity will increase the floodways horizontal displacement, even without any change in the depth of flow.

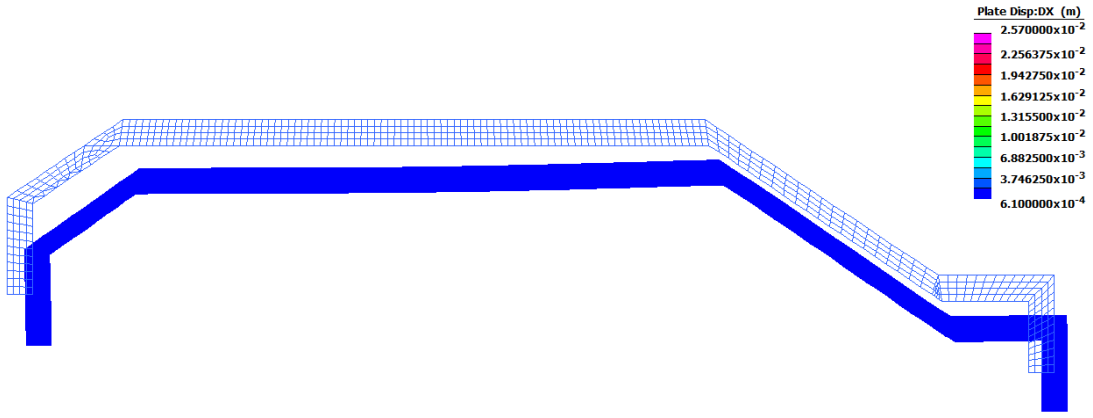

Figure 4.21: X Displacement for 1 m/s Flow Velocity @ 5 m Flow Depth

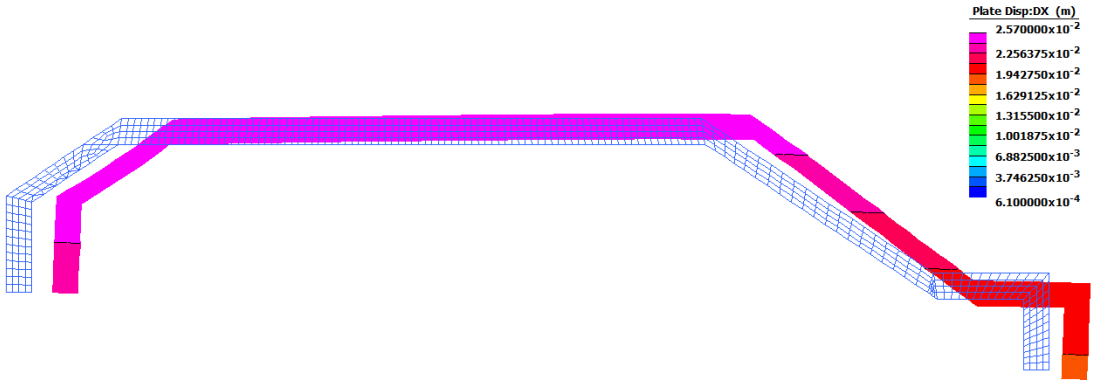

Figure 4.22: X Displacement for 7 m/s Flow Velocity @ 5 m Flow Depth

Table 4.7 below summarises the maximum X direction displacements recorded for each of the different flow velocities included in this study. Figure 4.23 below provides a visual representation of the tabulated data for comparison. From this graph we can identify that the with this particular loading scenario and a flow depth of 5m the X direction displacement actually increases exponentially with the increasing flow velocity.

Table 4.7: X Displacement for Constant 5 m Flow Depth Data

Constant 5m Flow Depth							
Velocity (m/s)	1	3	5	6	7	8	10
Max. X Disp.(mm)	0.89	4.88	13.20	18.90	25.60	33.40	52.0

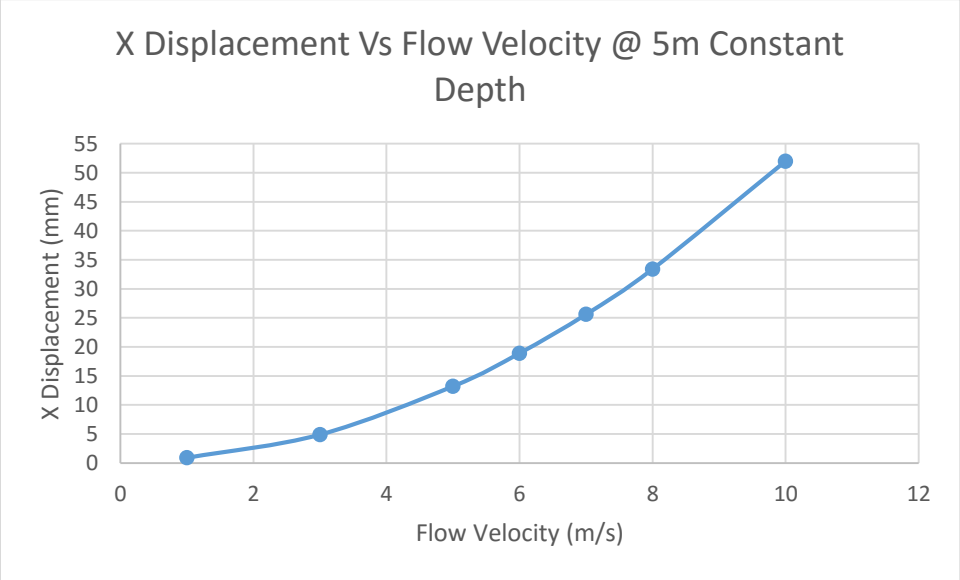

Figure 4.23: X Displacement vs Flow Velocity @ 5 m Constant Depth

The maximum displacement in the Y direction was recorded at -2.39 mm and -9.07 mm for flow velocities of 1 m/s and 7 m/s respectively. Figure 4.24 and Figure 4.25 below show the Y direction displacement comparison for the two different flow velocities. Most notable is the increase in vertical displacement throughout the floodway with respect to the increasing flow velocity. At a 1 m/s velocity the vertical displacement is very uniform throughout, quite different to

the contour plot for a flow velocity of 7 m/s showing much more variation and greater magnitudes.

The largest Y displacements occur at both the upstream and downstream cut-off walls of the floodway, with the maximum displacements presenting at the downstream cut-off walls for both scenarios. This demonstrates that based on this particular loading combination and constant flow velocity of 3 m/s, the vertical displacement within the floodway would increase as a result of the increasing flow depth, with the downstream being most vulnerable to increases.

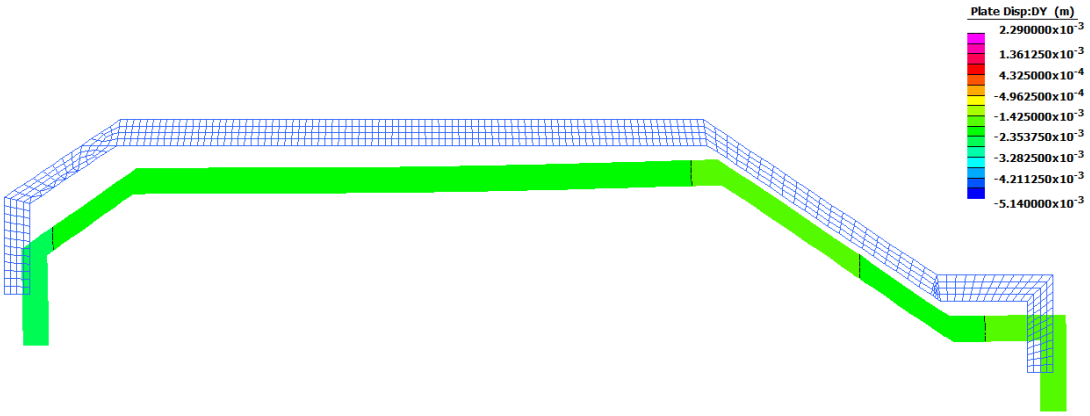

Figure 4.24: Y Displacement for 1 m/s Flow Velocity @ 5 m Flow Depth

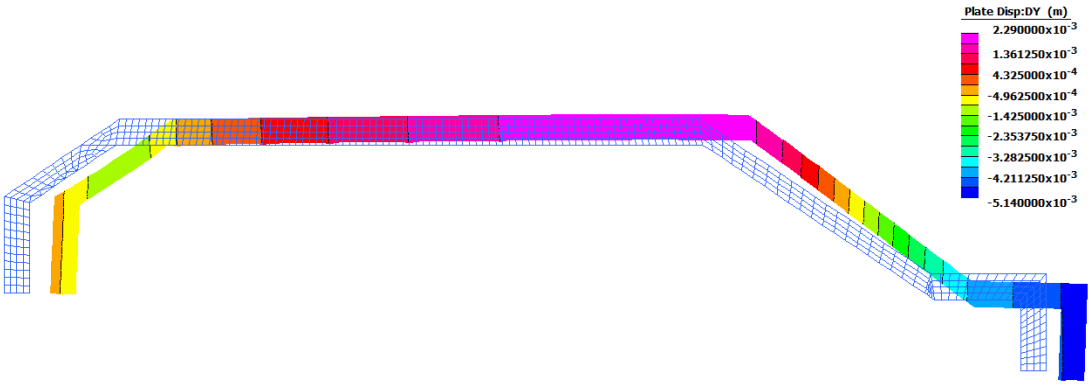

Figure 4.25: Y Displacement for 7 m/s Flow Velocity @ 5 m Flow Depth

Table 4.8 below summarises the maximum Y direction displacements recorded for each of the different flow velocities included in this study. Figure 4.26 below provides a visual representation of the tabulated data for comparison. From this

graph we can identify that the with this particular loading scenario and a flow depth of 5m the Y direction displacement actually increases exponentially with respect to increasing flow velocities.

Note: Negative values only indicate the displacement is acting in the downwards direction.

Table 4.8: X Displacement for Constant 5 m Flow Depth Data

Constant 5m Flow Depth							
Velocity (m/s)	1	3	5	6	7	8	10
Max. Y Disp.(mm)	-2.39	-2.83	-5.37	-7.06	-9.07	-11.40	-17.0

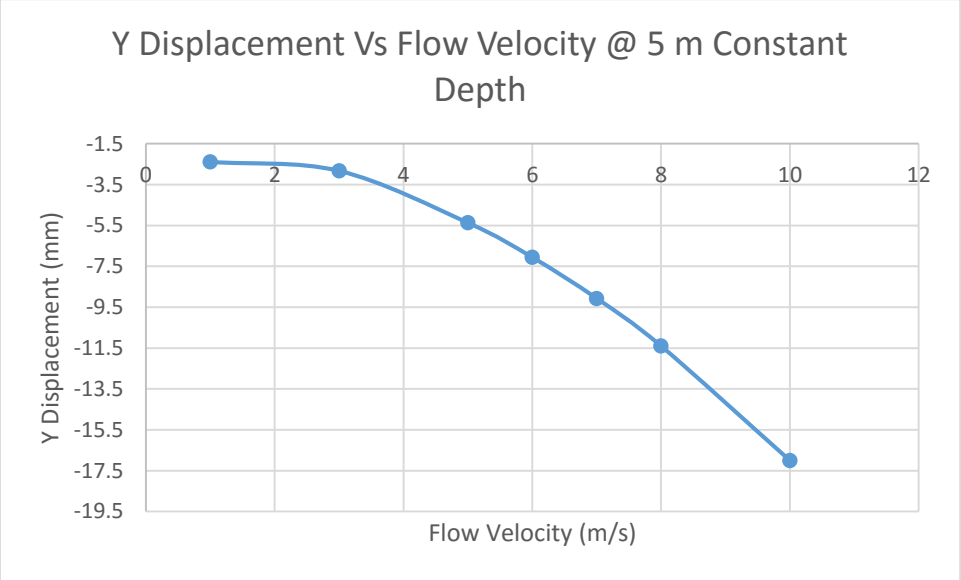

Figure 4.26: Y Displacement vs Flow Velocity @ 5 m Constant Depth

4.4 Soil Analysis

A linear static analysis was conducted on the rock protection and soils surrounding the floodway again utilising the worst loading combination, load combination 2. Like previous types of analysis, this investigates the structural performance of the rock protection and soils surrounding the floodway based on

a constant submerged flow depth of 5 m and two different flow velocities, 3 m/s and 5 m/s. Analysing the two different flow velocities allows comparisons to be made between contour plots for both soil stress and displacements.

To perform this type of analysis it had to be assumed that the natural soil surrounding the floodway is homogeneous to a width and depth of infinity. Also, soil behaviour is generally nonlinear which means the linear analysis being conducted has limitations. Strand7 therefore will not provide exact stresses within the soil, but a more general overview of areas of vulnerability. This limitation could be address with a nonlinear analysis, however this was outside the scope of this project.

4.4.1 Stress Analysis

The contour plots shown in Figure 4.27 and Figure 4.28 below represent the Mohr Coulomb stress within the soils for the two different flow velocities, 3 m/s and 5 m/s. Within the legend the positive or negative stresses shown represent either structural failure or adequacy not actual stress magnitudes. Mohr Coulomb failure criterion utilised by Strand7 states all negative values are considered safe, all positive values represent soil failure. With zero representing the change from adequacy to failure, the greater distance a number is from zero the more significant this adequacy or failure becomes.

The results shown below indicate that the majority of the soil surrounding the floodway structure is structurally sound. However, the magnified sections at both upstream and downstream shown in Figure 4.27 and Figure 4.28 illustrate there is potential for soil strength limits to be exceeded, with contours represented by positive values. These figures also show that the affected area dramatically increases in size when the flow velocity increases from 3 m/s to 5 m/s. These areas align with literature stating extensive erosion occurs at both these

locations. Whilst this research can identify theses areas of vulnerability, a more extensive nonlinear dynamic FEA would be required to acquire more exact results.

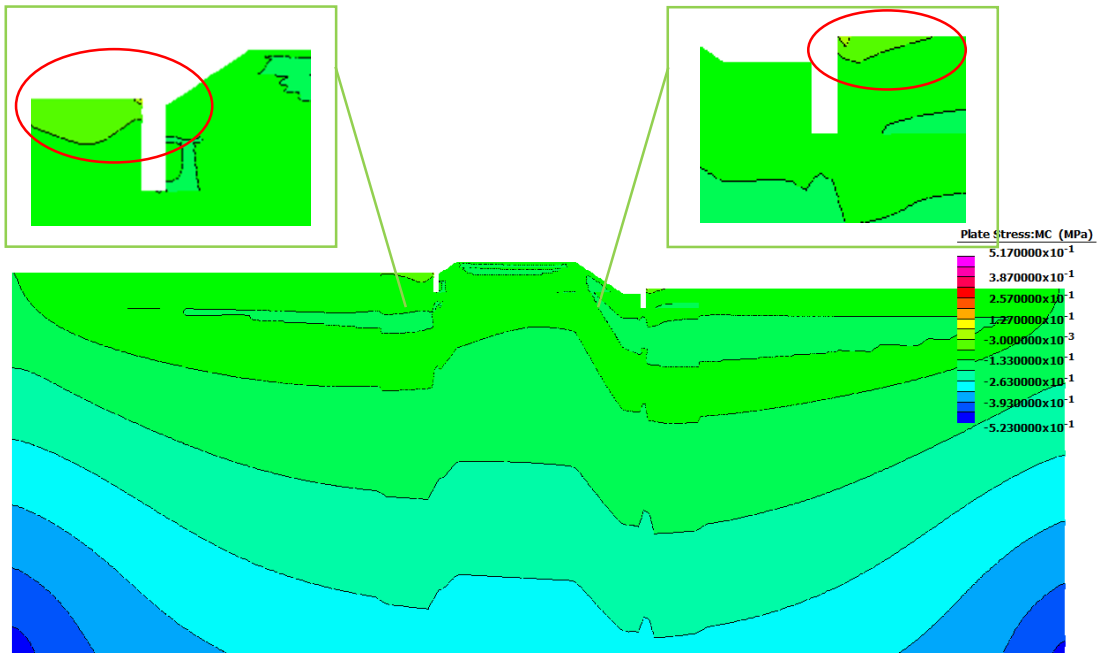

Figure 4.27: Mohr Coulomb Stress Pattern @ 5 m Depth 3 m/s Velocity

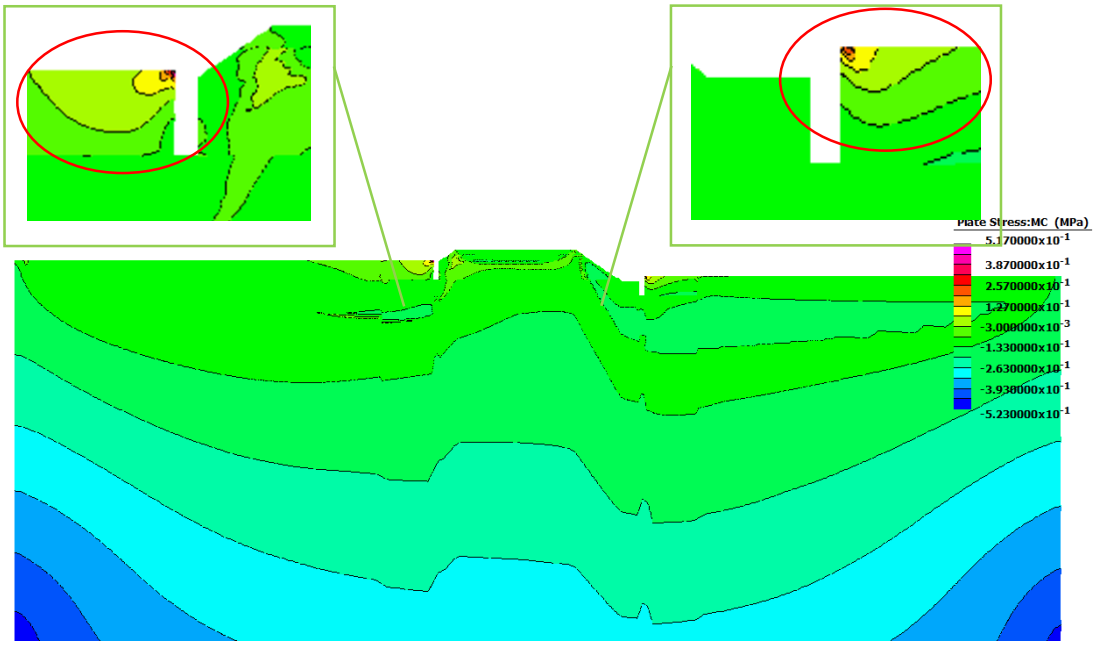

Figure 4.28: Mohr Coulomb Stress Pattern @ 5 m Depth 5 m/s Velocity

4.4.2 Displacement Analysis

Horizontal displacement within the soils intensifies around the floodway when the flow velocity increases from 3 m/s to 5 m/s shown in Figure 4.29 and Figure 4.30. Immediately upstream of the floodway the horizontal displacement was 4.81 mm and 12.9 mm for flow velocities 3 m/s and 5 m/s respectively. Downstream the displacements are slightly less at 4.05 mm and 10.6 mm for the same velocities but there proportional increase is almost the same. Below the centre of the floodway where the purple and red contours meet in Figure 4.30 the displacement increases from 4.45 mm to 11.8 mm with the change in velocity from 3 m/s to 5 m/s. Quantifying the significance of this displacement requires further research since Australian Standards are not available for evaluating.

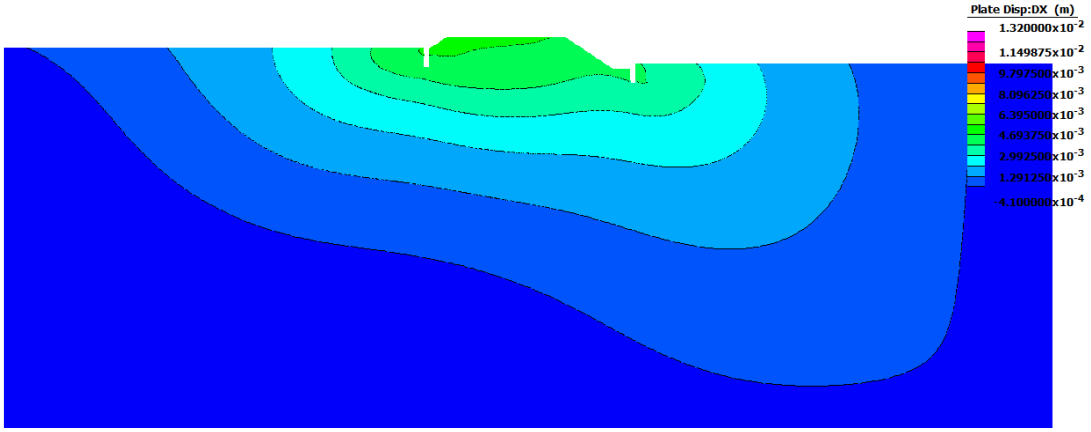

Figure 4.29: X Displacement Pattern @ 5 m Depth 3 m/s Velocity

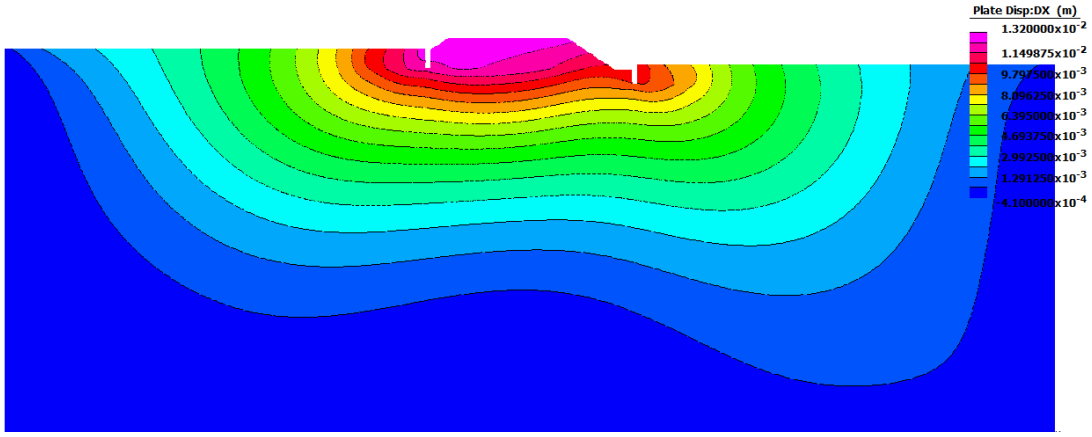

Figure 4.30: X Displacement Pattern @ 5 m Depth 5 m/s Velocity

Vertical displacement within the soils intensifies approximately 5 – 10 m upstream of the floodway and at the downstream cut-off wall of the floodway shown when the flow velocity increases from 3 m/s to 5 m/s, shown in Figure 4.31 and Figure 4.32. However, the downstream vertical displacement is of most interest as this aligns with literature reporting majority of damage occurs on the downstream side of the floodway. At the downstream cut-off wall circled in red, the vertical displacement increases from -2.45 mm to -3.43 mm, increasing by 40% with the change in flow velocity. This demonstrates that when the flow velocity increases, vertical displacements increase both upstream and downstream. Once again, quantifying the significance of this displacement requires further research since Australian Standards are not available.

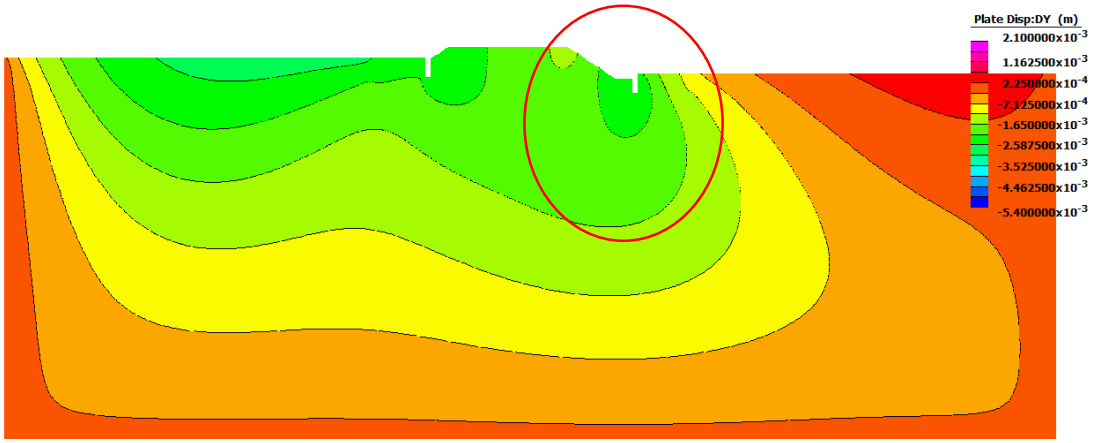

Figure 4.31: Y Displacement Pattern @ 5 m Depth 3 m/s Velocity

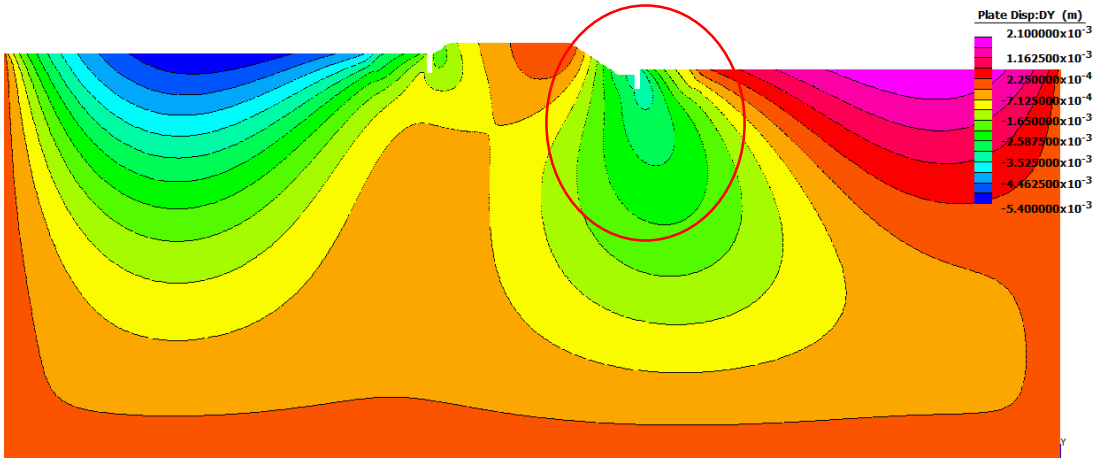

Figure 4.32: Y Displacement Pattern @ 5 m Depth 5 m/s Velocity

Combining the horizontal and vertical displacements together gives a better understanding of the overall displacement behaviour within the soil. The XY displacement contours shown in Figure 4.33 and Figure 4.34 have an almost identical contour pattern to the X displacement shown in Figure 4.29 and Figure 4.30. This indicates that the greatest influence on soil displacement for this particular loading combination comes from the horizontal force components. Again the largest displacements are occurring in close proximity to the floodway highlighted in purple, red, orange and yellow contours in Figure 4.34. Within this region the magnitudes of the combined displacements range from 7 mm to 13 mm. Once again, quantifying the significance of this displacement requires further research since Australian Standards are not available.

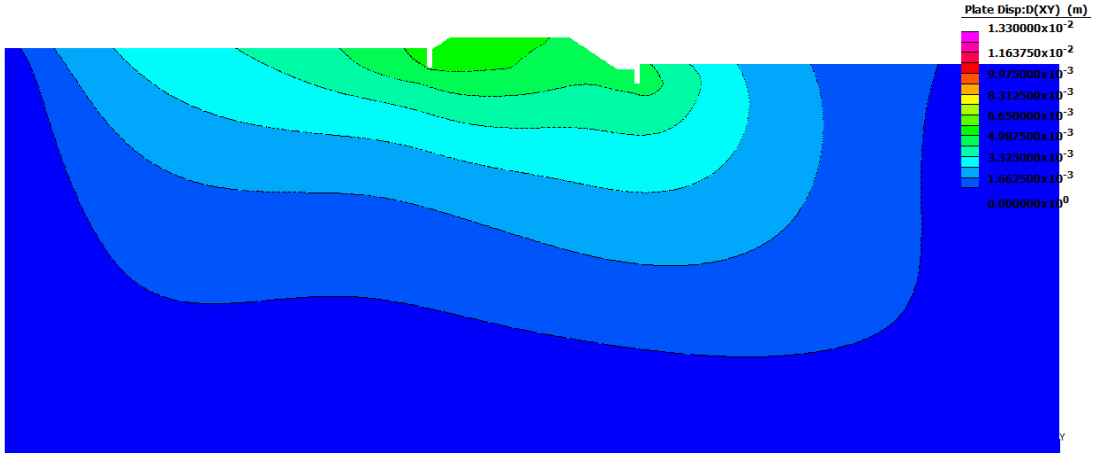

Figure 4.33: XY Displacement Pattern @ 5 m Depth 3 m/s Velocity

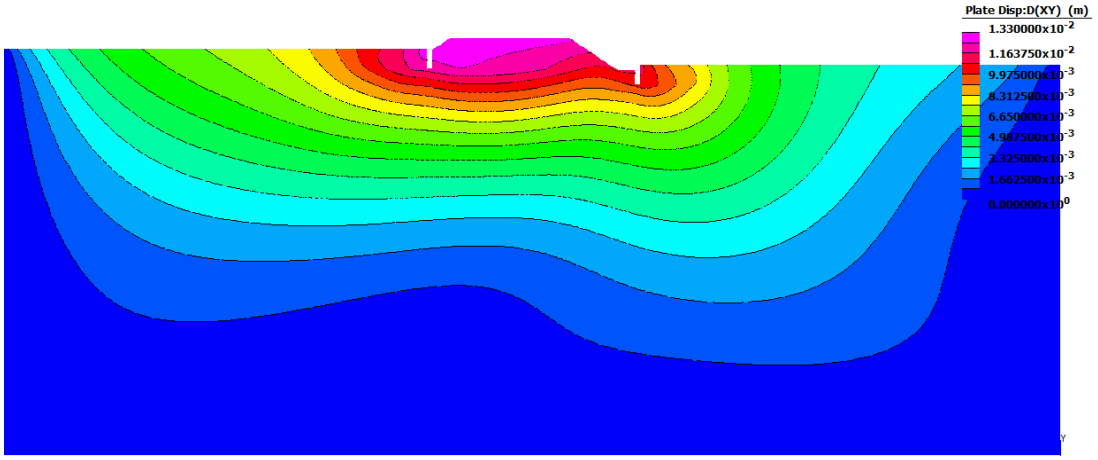

Figure 4.34: XY Displacement Pattern @ 5 m Depth 5 m/s Velocity

4.5 Damage Simulation

Literature shows that in many cases erosion at the downstream rock protection of the floodway is a big contributing factor to floodway damage post extreme flooding. This type of analysis identifies the relationships the resultant stresses and displacements within the structure have to increasing damage sustained at the downstream rock protection. Since load combination 2, log impact hitting the middle of the upstream batter of the floodway is the worst loading case yielding the greatest stresses and displacements, this combination is utilised for this damage simulation. The aim is to subject the model to a constant load combination 2 calculated based on 5 m/s flow velocity and 5 m depth of flow. The rock protection downstream then has its Young's modulus reduced in a stepwise method, 100%, 75%, 50%, 25% and 5% respectively. This damaged region is represented by the purple zone in Figure 4.35 below. The stress and displacement results of each reduction is recorded against the percentage of Young's modulus. This approach requires the element and node for which this data is collected to remain constant, these being node 193 and element 42069. This node and element were selected as they recorded the greatest stress and displacement pre failure.

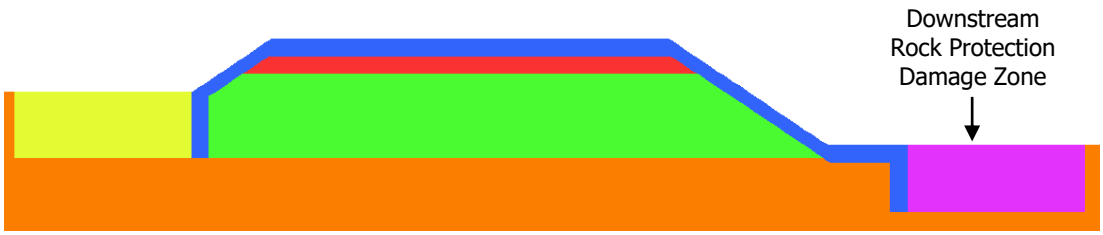

Figure 4.35: Downstream Rock Protection Damage Zone

4.5.1 Stress Analysis

The contour plots below in Figure 4.36 - Figure 4.40 illustrate the change in stress throughout the concrete floodway as the level of simulated damage increases. Visually, there is very little change in the stress distribution throughout the

concrete floodway as a result of this damage simulation. The maximum stress recorded pre failure at the upstream batter where the log impact occurs was 9.96 MPa increasing to 10.2 MPa at 95% failure of the downstream rock protection. Limitations within Strand7 meant 100% failure could not be analysed using this method. Overall this was a modest increase in the maximum stress recorded of 2.4%. This result indicates that the LHBR floodway structure both pre and post flood event would not incur any stress greater than the 32 MPa compressive strength of the concrete. In fact, should this loading combination and downstream rock protection damage occur simultaneously, the integrity of the concrete floodway would still be considered safe by a factor of safety (FOS) of 3.2.

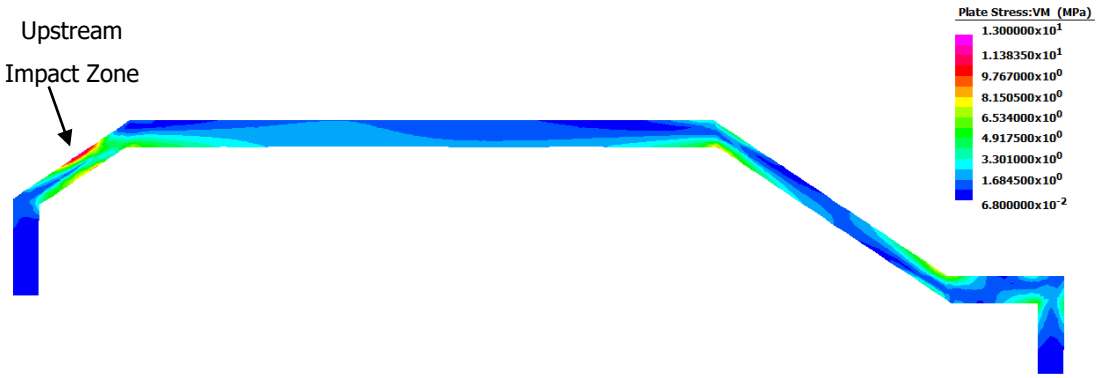

Figure 4.36: No Damage to Rock Protection Downstream (Stress)

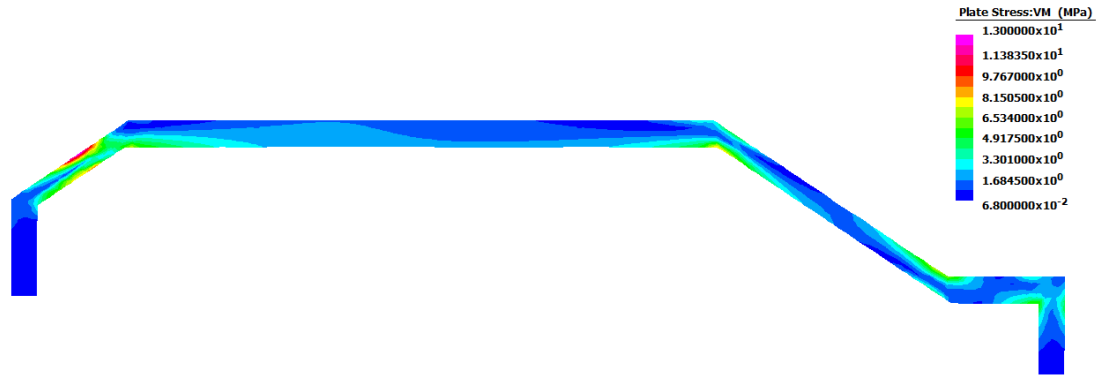

Figure 4.37: 25% Damage to Rock Protection Downstream (Stress)

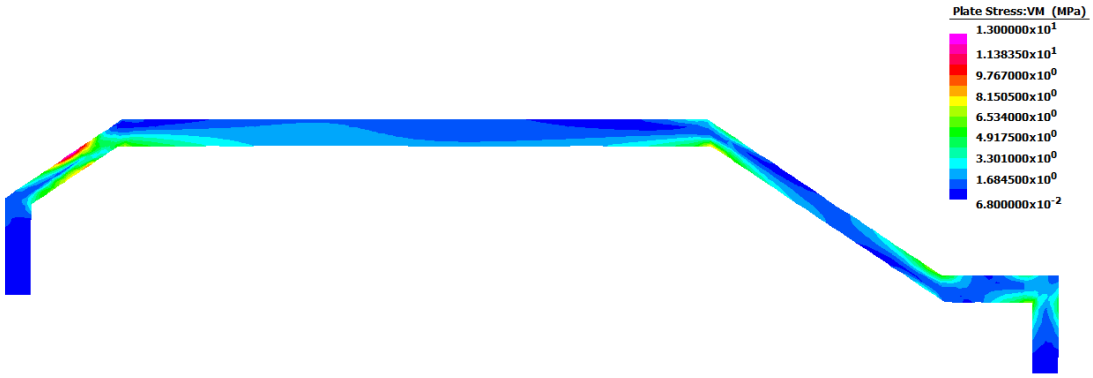

Figure 4.38: 50% Damage to Rock Protection Downstream (Stress)

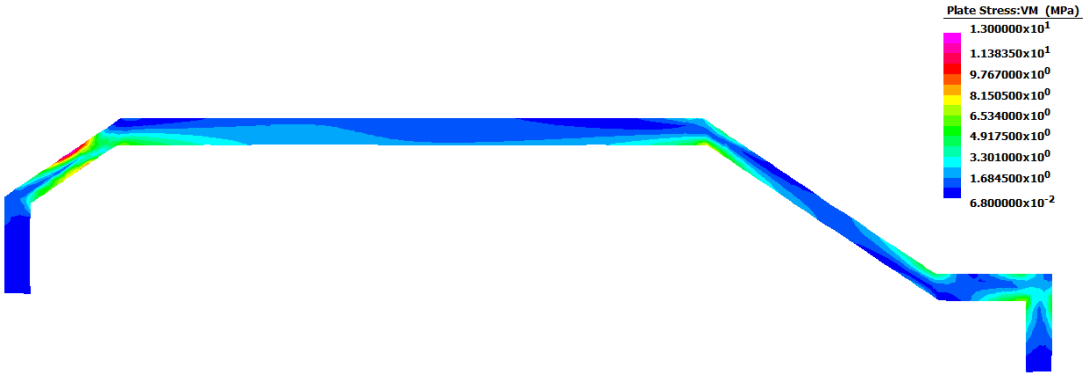

Figure 4.39: 75% Damage to Rock Protection Downstream (Stress)

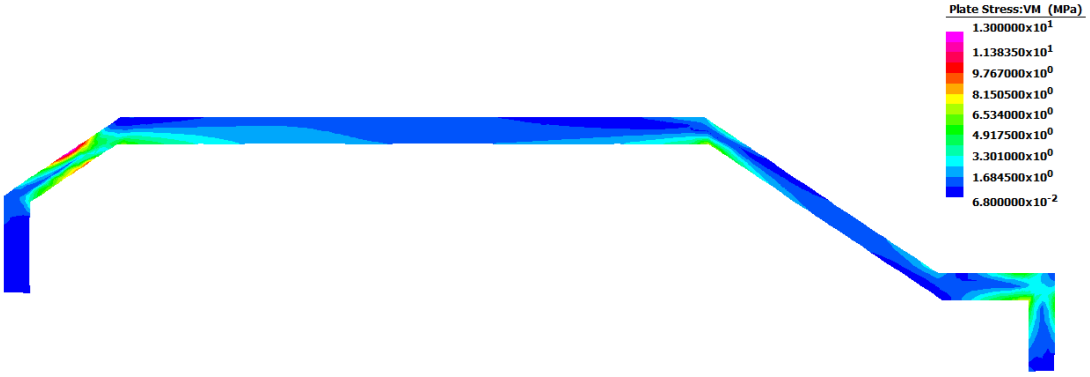

Figure 4.40: 95% Damage to Rock Protection Downstream (Stress)

Figure 4.41 is a visual representation of the relationship between stress within the concrete floodway and the percentage of damage sustained. The graph shows that up to 50% damage the rate at which the stress increases appears to behave linearly. Above 50% the stress begins to increase exponentially with respect the increasing damage.

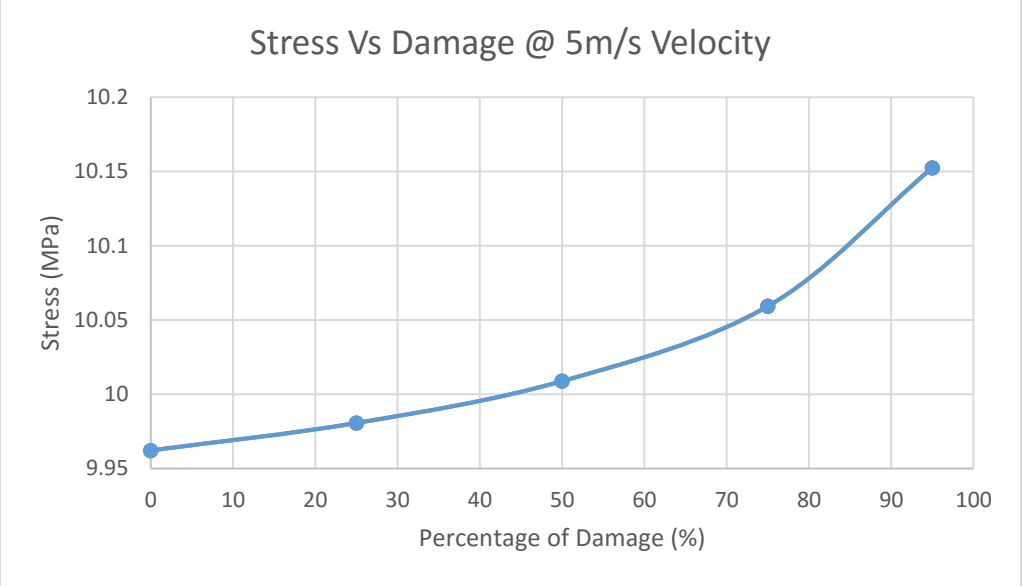

Figure 4.41: Stress Vs Damage Relationship

Table 4.9 below shows a summary of damage results for when the floodway is subjected to alternative flow velocities 3 m/s, 5 m/s and 7 m/s in combination with a 5 m flow depth. The comparisons show that the rate at which the stresses increase is primarily dependent upon the velocity of the water, not water depth. Again increases in stress distributions are moderate irrespective of the water velocities tested and therefore the structural stresses incurred do not exceed the compressive strength of concrete at 32 MPa. Velocities above 7 m/s begin to detract from real world scenarios and therefore if analysed may exceed the 32 MPa compressive strength of the concrete.

Finally, the rates at which these stresses increase with respect to changing velocities appears to be very similar. Whilst the magnitudes of stress obviously increase with the rising level of damage, the profile of the increasing stress rates appear to be relatively similar irrespective of velocity changes, as shown in Figure 4.42, Figure 4.43 and Figure 4.44 below. This indicates that the relationship between stress and damage incurred in the floodway are reasonably proportional to each other.

Table 4.9: Stress Summary with respect to Damage

Velocity (m/s)	% of Damage	Stress (MPa)	% increase
3	0	3.47E+00	2.02
	25	3.47E+00	
	50	3.48E+00	
	75	3.50E+00	
	95	3.54E+00	
5	0	9.96E+00	2.41
	25	9.98E+00	
	50	1.00E+01	
	75	1.01E+01	
	95	1.02E+01	
7	0	1.97E+01	2.03
	25	1.97E+01	
	50	1.98E+01	
	75	1.99E+01	
	95	2.01E+01	

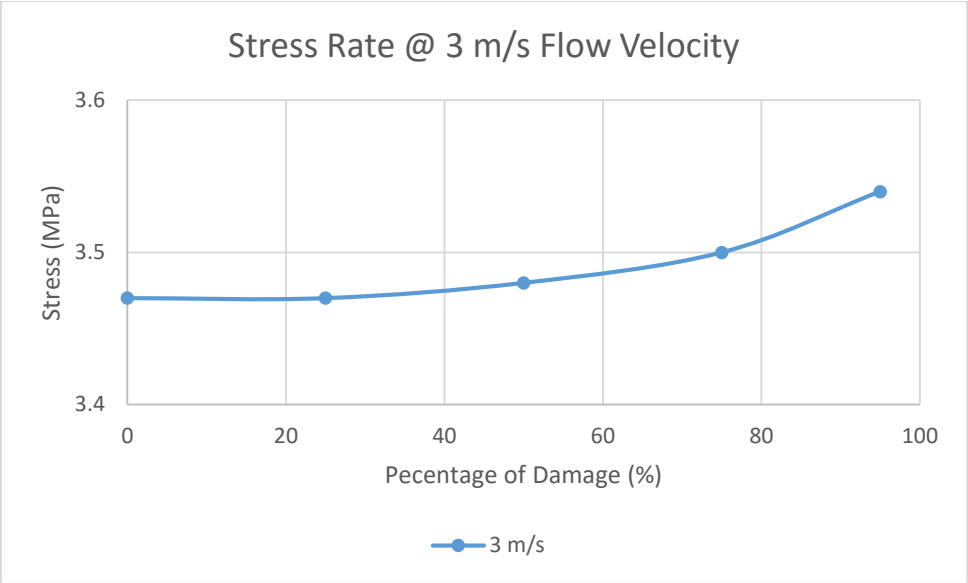

Figure 4.42: Stress Rate @ 3 m/s Flow Velocity

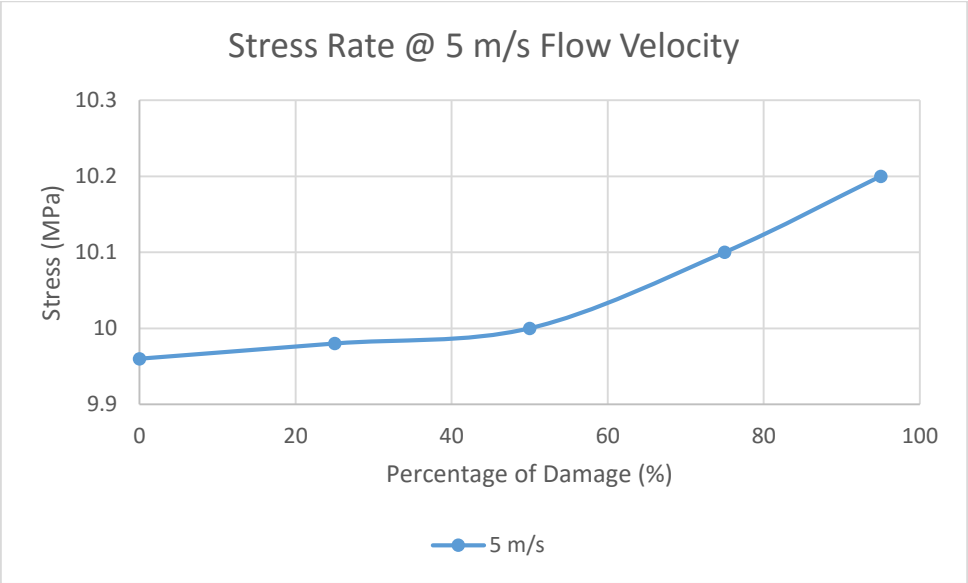

Figure 4.43: Stress Rate @ 5 m/s Flow Velocity

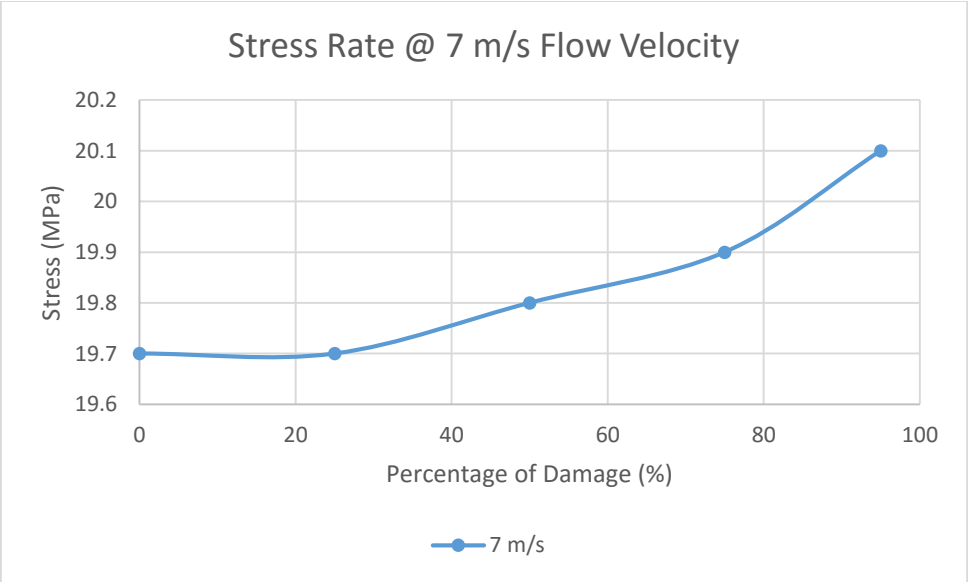

Figure 4.44: Stress Rate @ 7 m/s Flow Velocity

4.5.2 Displacement Analysis

The contour plots below illustrate the change in nodal displacement throughout the concrete floodway as the level of simulated damage increases. The focus of this analysis is the displacement in the horizontal or X direction, as this is most significant. Included in the images is an undeformed wireframe of the floodway

and a 1% magnified contour highlighting areas subjected to the greatest deformation for comparison.

Pre failure, the maximum displacement in the X direction was 13.2 mm acting at the point of impact on the upstream batter of the floodway. Once 95% failure of the downstream rock protection has occurred, the displacement on the upstream batter increased to 14.7 mm, a rise of 11.4% overall. Unlike the stresses recorded based on the same loading conditions the displacement is more significant.

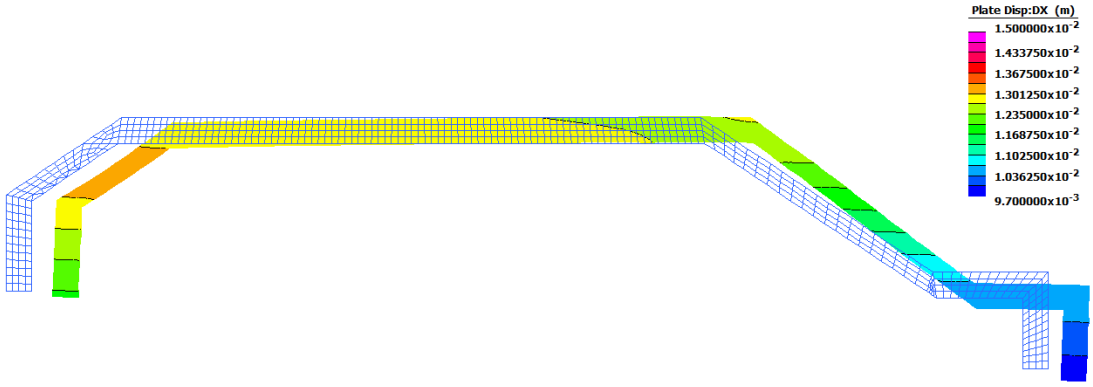

Figure 4.45: No Damage to Rock Protection Downstream (Displacement)

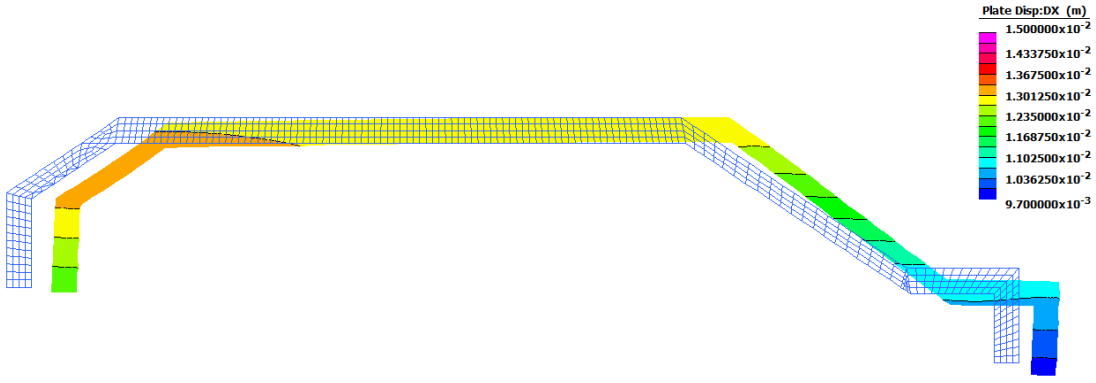

Figure 4.46: 25% Damage to Rock Protection Downstream (Displacement)

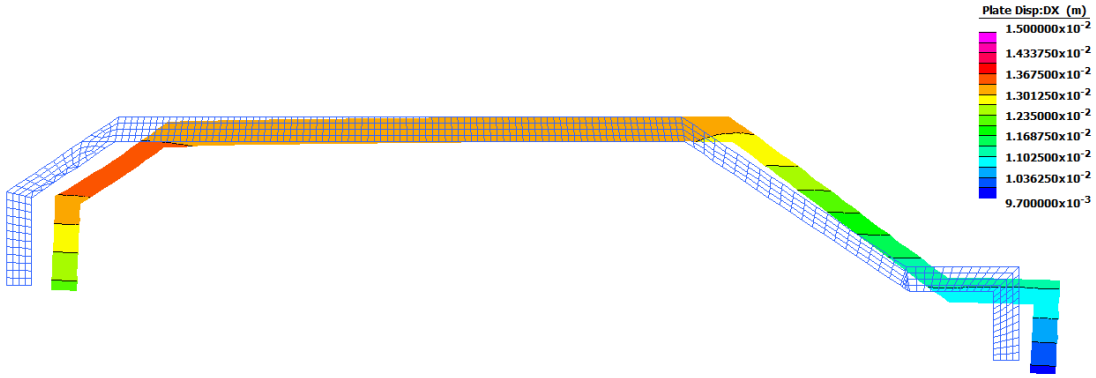

Figure 4.47: 50% Damage to Rock Protection Downstream (Displacement)

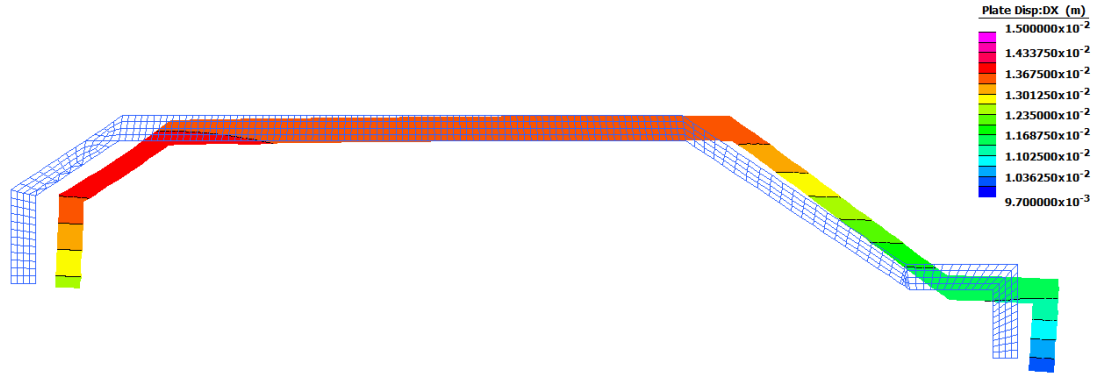

Figure 4.48: 75% Damage to Rock Protection Downstream (Displacement)

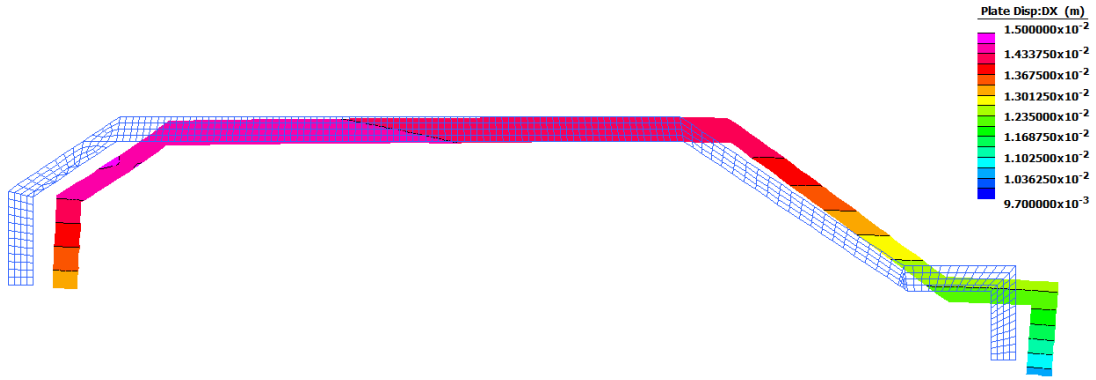

Figure 4.49: 95% Damage to Rock Protection Downstream (Displacement)

Figure 4.50 is a visual representation of the relationship between the displacement in the X direction within the concrete floodway and the percentage of damage sustained. The graph shows that after 75% sustained damage, the X direction displacements begin to increase exponentially with respect to the

increasing damage. Interestingly, when analysing the vertical or Y direction displacements it was found that under the same loading conditions the displacement reduced as the level of damage at the downstream rock protection increased. This behaviour is shown in Figure 4.51 below which demonstrates a very minor reduction in vertical displacement from 1.7 mm to 1.57 mm.

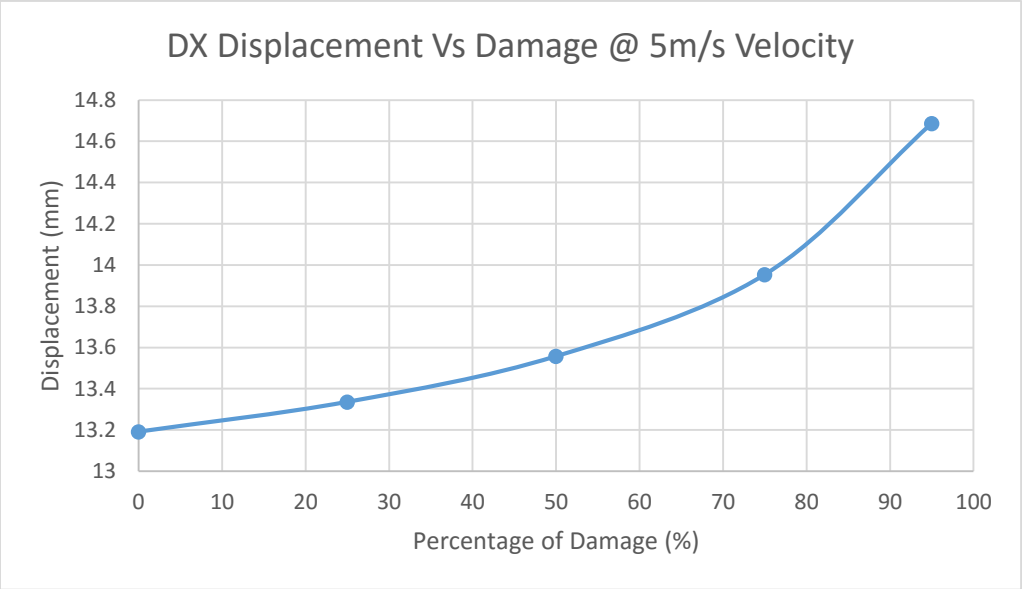

Figure 4.50: X Displacement Vs Damage Relationship

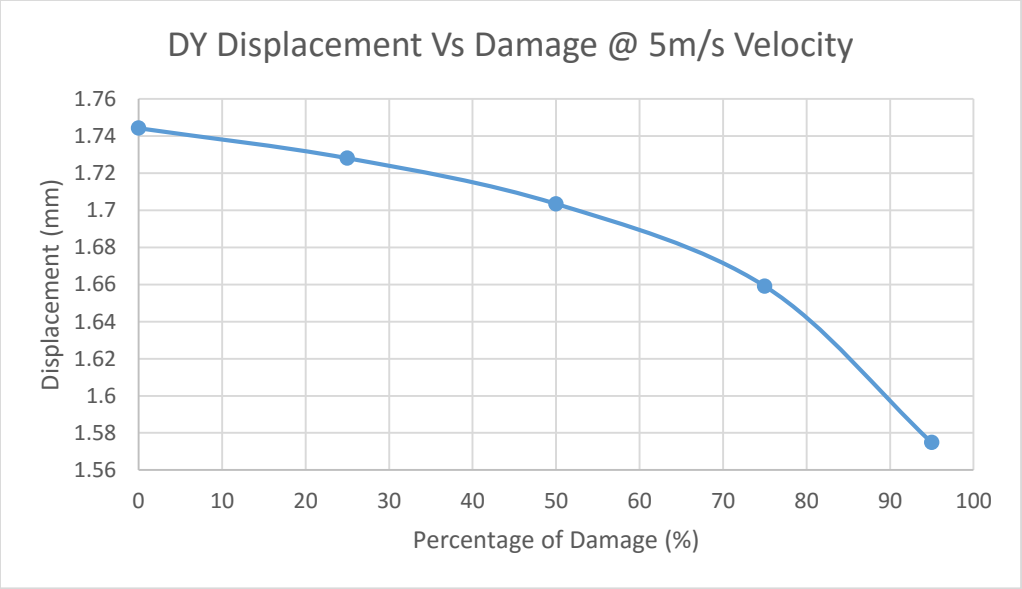

Figure 4.51: Y Displacement Vs Damage Relationship

Similar to Table 4.9 above, Table 4.10 below shows a summary of damage results for X Displacement when the floodway is subjected to 3 m/s, 5 m/s and 7 m/s flow velocities combined with a 5 m flow depth. The comparisons show that the rate at which the horizontal displacements increases is dependent upon the velocity of the water. However, the results also suggests that the rate of change of displacement associated with 5 m/s velocity loadings is the same as the 7 m/s velocity loadings. Whilst there is obvious differences in X displacement between the two, the slight reduction in the rate of change could most likely be attributed to the increasing hydrostatic pressures, cancelling out some of the effects of the horizontal forces within this loading combination. Similar to the stress vs damage analysis above, Figure 4.52, Figure 4.53 and Figure 4.54 again demonstrate that the rate of change in horizontal displacement does not changes significantly with the increasing flow velocities.

Table 4.10: X Displacement Summary with respect to Damage

Velocity (m/s)	% of Damage	Disp. X (mm)	% increase
3	0	4.88	10.30
	25	4.93	
	50	5.02	
	75	5.16	
	95	5.44	
5	0	13.2	10.20
	25	13.3	
	50	13.6	
	75	14.0	
	95	14.7	
7	0	25.6	10.20
	25	25.9	
	50	26.3	
	75	27.1	

Velocity (m/s)	% of Damage	Disp. X (mm)	% increase
	95	28.5	

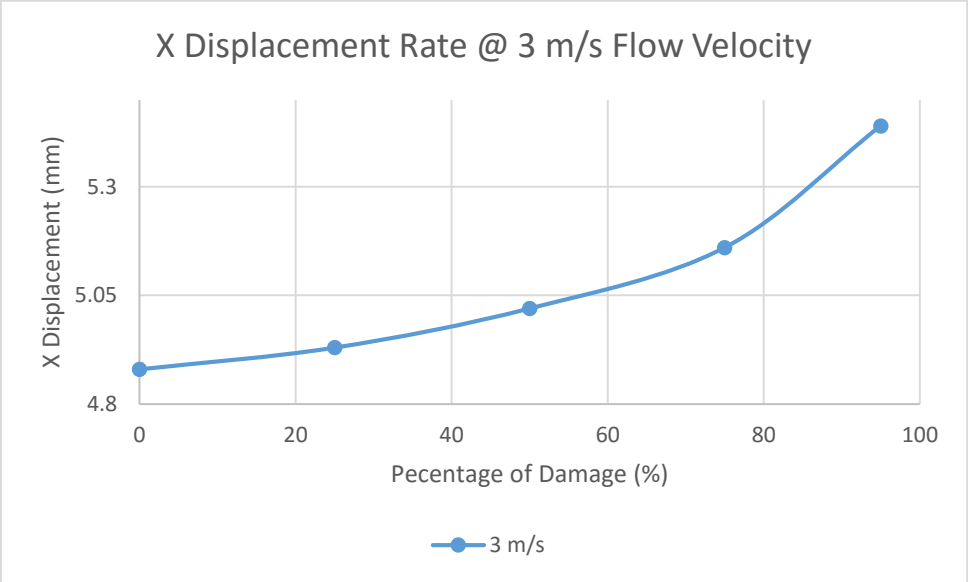

Figure 4.52: Stress Rate @ 3 m/s Flow Velocity

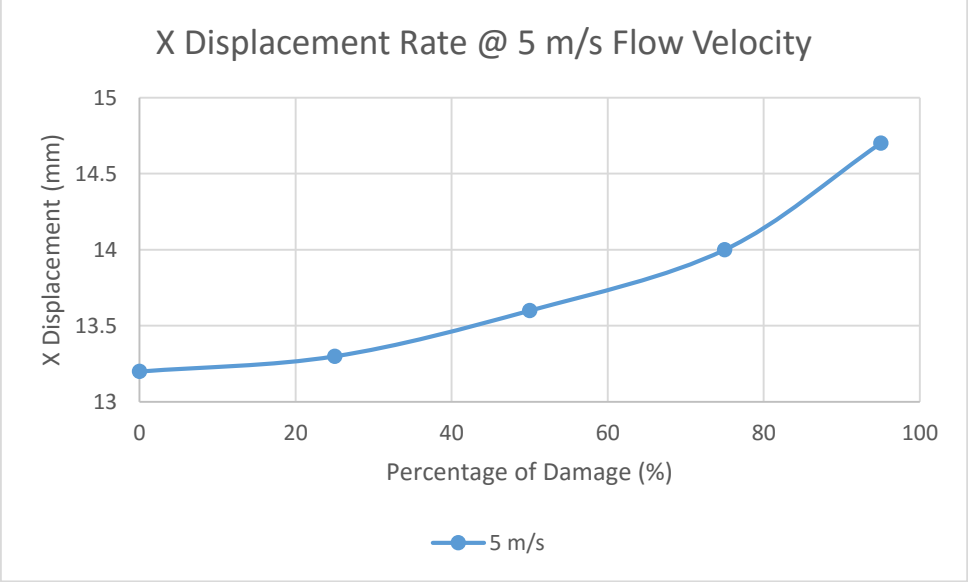

Figure 4.53: Stress Rate @ 5 m/s Flow Velocity

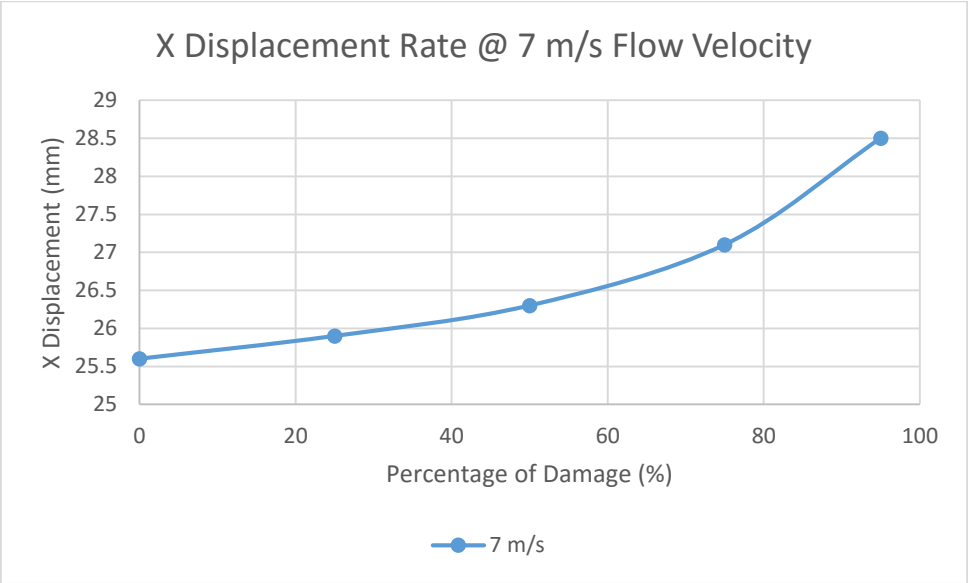

Figure 4.54: Stress Rate @ 7 m/s Flow Velocity

4.6 Finite Element Analysis Limitations

The 2D linear static analysis used for this research presented multiple limitations. Firstly, all loadings have been applied statically and do not have the ability to reflect the dynamic aspects associated with water flow. For example, flow velocities across the floodway would be dynamic and therefore not be considered a constant. Flow profiles would also experience transitional periods with flow velocity profiles changing combined with different type of flows i.e. laminar or turbulent. Secondly, the results presented for the soil investigation can only identify the potential stress and displacement patterns that may be expected under the loading conditions considered. The nonlinear behaviour of soil means accurate results cannot be achieved without a full nonlinear dynamic FEA taking place. Finally, the rock protection had to be assigned soil properties for the linear analysis to work. This meant adopting the most relevant soil parameters that could best represent rocks. However, whilst this approach is the only available option using Strand7 FEA some limitations would still be present.

4.7 Discussion

The three different loading combinations analysed considered hydrostatic, debris, drag, impact and lifting forces in accordance with AS 5100.2-2004 (Standards Australia 2004). Of these, the parametric study determined that load combination 2 which considers a log impact hitting the middle of the upstream batter yielded the most critical stresses and displacements. It was also established that for all alternative flow velocities and flow depths only one loading combination would exceed the 32 MPa compressive strength of the concrete floodway. At a flow velocity of 10 m/s, analysis of all flow depths for load combination 2 showed stress levels exceeding 32 MPa, potentially causing structural failure. This however is a very extreme water velocity used for analysis purposes and most likely would not reflect practical flood velocities throughout the Mt Sylvia region. Therefore it can be said that the LHBR floodway would not sustain any structural damage based on the loading combinations analysed without structural failure occurring within the surrounding soils.

When considering the stress relationships between a constant flow velocity of 3 m/s and changing water depths both the upstream and downstream sides of the floodway were analysed for comparison. It was revealed that as the water level increased from 0.2 m to 10 m the rate of stresses upstream decreased from 4.04 MPa to 3.07 MPa, a reduction of 24%. Interestingly the downstream side of the floodway sustained a 48.4% increase in stress from 2.25 MPa to 3.34 MPa under the same conditions. This increase downstream is most likely attributed to the geometry of the floodway. The additional horizontal surface area on the downstream apron means vertical hydrostatic forces have a greater influence compared to upstream. Overall, stress levels throughout the concrete floodway indicate variation in flow depth has marginal impact on the resultant stress levels within the concrete floodway.

Alternatively, when the flow depth remains constant at 5 m and the flow velocities change the floodway structure behaves very differently. It was revealed that as the flow velocity increased from 1 m/s to 10 m/s the rate of stress within the

structure both upstream and downstream increased. Upstream experienced a change in stress from 0.19 MPa to 44.35 MPa. Similarly, downstream stress had an increase from 1.01 MPa to 23.03 MPa. These significant increases indicate that under load combination 2 conditions stress levels within the concrete floodway are more influenced by changes in flow velocity rather than flow depth.

Analysis of the horizontal X displacement was conducted in the same manner as the stress analysis discussed above, utilising load combination 2. When subjecting the floodway to a constant flow velocity of 3 m/s, maximum displacements are recorded at 4.84 mm and 4.97 mm for flow depths 1 m and 10 m respectively. For both of these flow depths the maximum displacements occurred at the upstream batter of the floodway. When analysing all flow depths included in the study, it was revealed that the horizontal displacement decreases between flow depths of 0.2 m and 2 m. Once the flow depth exceeds 2 m the horizontal displacement begin to increase in a linear fashion. The very modest change in displacement indicates that changing flow depths have minimal influence over horizontal displacement.

Similarly, when considering a constant flow depth of 5 m and alternative velocities horizontal displacements have been analysed. This analysis revealed displacements increased from 0.89 mm to 25.6 mm when the flow velocity increased from 1 m/s to 7 m/s. At 7 m/s flow velocity the maximum X displacement occurs on the upstream batter of the floodway and continues across the roadway. The analysis concluded that regardless of the flow depth, an increase in flow velocity would have the most significant influence over the horizontal displacement sustained by the floodway.

A preliminary soil analysis was also conducted utilising a constant submerged flow depth of 5 m and two different flow velocities, 3 m/s and 5 m/s. Results indicated majority of the soil and rock protection was structurally adequate. However, contour plots demonstrated that rock protection immediately upstream

and downstream of the floodway might be vulnerable to soil failure. When the flow velocity increased from 3 m/s to 5 m/s this area of vulnerability increases in size.

Similarly, as flow velocities increase the horizontal X displacement upstream and downstream rises from 4.81 mm to 12.9 mm and 4.05 mm and 10.6 mm respectively. The contour plots illustrate as the flow velocity increases the intensity of the displacement contours surrounding the floodway structure magnifies. Contour plots also show the vertical Y displacement is less influenced by the increase in flow velocity in comparison to horizontal X displacement. These contours revealed a potential area of vulnerability within the soil below the downstream rock protection. Here the displacement increased from -2.45 mm to -3.43 mm an increase of 40%. In addition, approximately 10 m upstream another area of vulnerability is identified at the surface of the natural soil. Contour plots of the combined horizontal and vertical displacements revealed strong, almost identical contours to those in the X displacement analysis. This correlation further emphasises how changing velocity has more influence over horizontal displacement compared to vertical displacement within the model.

A damage simulation was conducted to represent erosion of the downstream rock protection utilising load combination 2, based on 5 m/s velocity and 5 m depth of flow. Results indicate there is minimal change in the stress distribution throughout the concrete floodway from pre-failure to 95% damage, with an increase from 9.96 MPa to 10.2 MPa respectively. Similarly, pre-failure recorded a maximum horizontal X displacement of 13.2 mm acting at the point of impact of the upstream batter of the floodway. At 95% sustained damage this displacement increased to 14.7 mm. Comparatively, pre-failure recorded a maximum vertical or Y displacement of 1.7 mm within the structure, decreasing to 1.57 mm at 95% sustained damage. Based on this scenario the results indicate the LHBR floodway structure both pre and post flood event would not incur any stress greater than the 32 MPa compressive strength of the concrete.

Quantifying the significance of all these displacements is very difficult and cannot be investigated without the aid of Australian Standard, for which there is currently none available. Although this is a limitation in the research, important behavioural patterns have still been established.

CHAPTER 5. CONCLUSIONS

5.1 Summary

This research conducted a 2D Strand7 FEA based on the LHBR floodway with the intention of determining the behaviour of the floodway when subjected to extreme flood loadings. Given current floodway design guidelines primarily focus on hydraulic design aspects they fails to consider additional loadings such as drag, debris, impact and lifting forces. Therefore, the loadings utilised in this research were adapted from AS 5100.2-2004.

Limitations in historical flood data for this region meant a parametric study was conducted and identified the worst loading combination with respect to flow velocities and flow depths. This combination was load combination 2 which considers a log impact hitting the middle of the upstream batter of the floodway. Based on this loading combination Strand7 FEA identified the potential failure mechanisms and areas of vulnerability within floodway structure and surrounding soils. It was established that the design of the LHBR floodway could adequately withstand all stresses resulting from flow velocities less than 10 m/s.

Displacement analysis conducted within the structure, rock protection and surrounding soils identified a number of areas of vulnerability. Quantifying the significance of this displacement is difficult without an Australian Standard for floodway design to compare to. The most critical failure mechanisms are most likely attributed to erosion or scour in and around the immediate area of the floodway.

5.2 Project Outcomes

The aim of this project was to investigate the performance of current floodway designs when subjected to extreme flood loadings. In order to do this the following aims were achieved:

1. *Conduct a literature review to identify current floodway design characteristics and practices*

The literature identified three prominent guidelines currently being utilised by various states in Australia for the design of floodways. All guidelines determine a floodways adequacy based on hydraulic aspects and as previously stated fail to consider additional critical loadings. The literature review identified limited information regarding the application of additional loadings to floodways such as hydrostatic, drag, debris and lifting forces and therefore AS 5100.2-2004 for bridge design was adopted.

2. *Conduct a 2D plane strain Strand7 FEA*

Chapter 3 focused on constructing the 2D plane strain finite element model based on cross section B of the LHBR floodway. Appropriate material parameters, forces and boundary conditions were determined to ensure accuracy of the results. A final convergence study was undertaken to maximise model efficiency without sacrificing this accuracy.

3. *Conduct a parametric study to investigate the behaviour of the floodway when subjected to additional loadings*

Chapter 4 conducted a parametric study and investigated three different loading combinations. Each of the loading combinations maximum stresses and displacements were recorded with respect to a combination of different flow

velocities and flow depths. This study identified the effects different flow velocities and flow depths have on the stress and displacement within the structure and surrounding soils.

4. *Identify the structural adequacy of the LHBR floodway when subjected to these additional loadings*

Results from the FEA identified all three loading combinations would not yield stresses which exceed the 32 MPa compressive strength of the concrete floodway. However there was one exception. At 10 m/s flow velocity all flow depths yielded stresses in excess of 32 MPa. This however is an extremely high flow velocity for analytical purposes and would not reflect real world situations. Structural displacements were also identified however, due to no Australian Standard to analyse the significance of the displacements, preliminary analysis could only be conducted.

5.3 Further Work

Further research should consider a nonlinear dynamic FEA based on the same geometry to validate the results of this research. To improve the results this additional research should consider alternative FEA software such as Abaqus. This will allow for water flow velocities, profiles and potential vortices to be considered in parallel with the forces discussed in this research.

Furthermore, to improve upon the results of this research soil testing at the LHBR floodway should be undertaken. This will validate the soil parameters utilised in this research. These parameters combined within a nonlinear analysis will provide a more accurate understanding of the structural integrity of the rock protection and surrounding soils. In addition, further research should investigate

further the impacts of scour and lifting forces to determine these impacts on a floodway.

Finally, further research should investigate avenues which may allow the structural displacements identified in this research for both the structure and the soil to be quantified. This could not be achieved in this research as there is currently no Australian Standards available to compare to.

REFERENCES

Akan, A 2006, *Open Channel Hydraulics*, Butterworth-Heinemann, Jordan Hill, Great Britain, viewed 15 September 2015 <http://site.ebrary.com/lib/qut/docDetail.action?docID=10186158>.

Austroads Ltd 2013, *Guide to Road Design Part 5B: Drainage – Open Channels, Culverts and Floodways*, Austroad Ltd, NSW.

Crisafulli, D, (Minister for Local Government, Community Recovery and Resilience) 2014, *Notorious floodway to be fixed*, Media Statement, The Queensland Cabinet and Ministerial Directory, 10 January, viewed 15 March 2015, <http://statements.qld.gov.au/Statement/2014/1/10/notorious-floodway-to-be-fixed>.

Department of Transport and Main Roads 2010, *Road Drainage Manual: Chapter 10 Floodway Design*, viewed 3 April 2015 <http://www.tmr.qld.gov.au/~/media/busind/techstdpubs/Road%20drainage%20manual/Recent/Recent%20Aug/RoadDrainageManualChap10Appendix10A.pdf>.

Department of Transport and Main Roads 2013, *Bridge Scour Manual*, viewed 24 May 2014 <http://www.tmr.qld.gov.au/~/media/busind/techstdpubs/Bridge%20scour%20manual/BridgeScourManual.pdf>.

Department of Transport and Main Roads 2015, *Queensland Road Crash Weekly Report*, viewed 15 March 2014, <https://www.webcrash.transport.qld.gov.au/webcrash2/external/daupage/weekly/roadsense.pdf>.

Dhatt, G, Lefrançois, E & Touzot, G 2013, *Finite Element Method*, 1 edn, Wiley, Hoboken N.J; London, viewed 15 April 2014 <http://QUT.eblib.com.au/patron/FullRecord.aspx?p=1120636>.

Engineers Australia 2010, *Our code of ethics*, viewed 24 October 2015, <http://www.engineersaustralia.org.au/sites/default/files/shado/About%20Us/Overview/Governance/codeofethics2010.pdf>.

Engineers Edge Solution By Design 2015, *Von Mises Criterion (Maximum Distortion Energy Criterion) Strength (Mechanics) of Materials*, viewed 26 October 2015, <http://engineersedge.com/material_science/von_mises.htm>.

Geotechdata.info 2008, *Geotechnical Parameters*, viewed 15 September 2015, <http://www.geotechdata.info/parameter/parameter.html>.

Gold Coast Bulletin 2014, *Gold Coast hammered with massive downpour closing roads and downing powerlines*, viewed 28 March 2014 <http://www.goldcoastbulletin.com.au/news/gold-coast/gold-coast-hammered-with-massive-downpour-closing-roads-and-downing-powerlines/story-fnj94idh-1226867153966>.

Haehnel, R & Daly, S 2004, 'Maximum Impact Force of Woody Debris on Floodplain Structures', *Journal of Hydraulic Engineering*, vol. 130, no. 2, pp. 112-120, viewed 28 September 2014, <http://ascelibrary.org/doi/abs/10.1061/%28ASCE%290733-9429%282004%29130%3A2%28112%29>.

Hamill, L 1999, *Bridge hydraulics*, E. & F.N. Spon, London.

Liu, GR 2003, *The finite element method : a practical course*, Butterworth-Heinemann, Oxford.

Lockyer Valley Regional Council 2009, *LVRC Locality map*, viewed 24 October 2015, <http://www.lockyervalley.qld.gov.au/our-region/about-the-lockyer-valley/Documents/Getting%20Around/LVRC%20Locality%20Map.pdf>.

Lockyer Valley Regional Council 2012a, *2011/2012 Annual Report*, viewed 15 March 2015 <http://www.lockyervalley.qld.gov.au/images/PDF/about_council/our%20recovery.pdf >.

Lockyer Valley Regional Council 2012b, *Lockyer Valley restores more floodways*, viewed 15 March 2015 <http://www.lockyervalley.qld.gov.au/news-events/news/1459-lockyer-valley-restores-more-floodways->.

Lockyer Valley Regional Council 2014, *Submission to the Australian Government Productivity Commission Inquiry into Natural Disaster Funding Arrangements*, viewed 15 March 2015 <http://www.pc.gov.au/inquiries/completed/disaster-funding/submissions/submissions-test/submission-counter/sub108-disaster-funding.pdf>.

Main Road Western Australia 2006, *Floodway Design Guide*, viewed 23 May 2015 <https://www.mainroads.wa.gov.au/Documents/Floodway%20Design%20Guide.PDF>.

Moore, K 2013, *ENV2103 Hydraulics 1: Study Book*, University of Southern Queensland, Toowomba.

Nalluri, C & Featherstone, R 2009, *Nalluri & Featherstone's civil engineering hydraulics* 5th edn, Wiley-Blackwell, Oxford.

Pritchard, R 2013, '2011 to 2012 Queensland floods and cyclone events: Lessons learnt for bridge transport infrastructure', *Australian Journal of Structural Engineering*, vol. 14, no. 2, pp. 167-176, viewed 14 September 2014, <http://search.informit.com.au.ezp01.library.qut.edu.au/documentSummary;dn=560445065519015;res=IELENG>.

Queensland Bridge and Civil 2015, *Black Duck Creek Road Floodways*, viewed 15 March 2015, <http://www.qbcivil.com.au/projects/current-projects/91-black-duck>.

Queensland Government n.d., *Lockyer Valley Regional Council - Sandy Creek on Woodlands Road*, viewed 15 March 2015 <http://www.qldreconstruction.org.au/the-queensland-betterment-fund-building-resilience/lockyer-valley-regional-council-woodlands-road/>.

Queensland Government Natural Resources and Mines 2002, *Soils and Irrigated Land Suitability of the Lockyer Valley Alluvial Plains, South-East Queensland* viewed 15 September 2015, <https://publications.qld.gov.au/storage/f/2014-11-20T06%3A45%3A01.356Z/loc-qnrm0121-locker-valley-alluvial-plains-soils-land-suitability.pdf>.

Queensland Reconstruction Authority n.d., *Toowoomba Regional Council*, viewed 24 May 2015, <http://qldreconstruction.org.au/the-queensland-betterment-fund-building-resilience/toowoomba-regional-council >.

Schmocker, L & Hager, W 2013, 'Scale Modeling of Wooden Debris Accumulation at a Debris Rack', *Journal of Hydraulic Engineering*, vol. 139, no. 8, pp. 827-836, <http://ascelibrary.org/doi/abs/10.1061/%28ASCE%29HY.1943-7900.0000714>.

Standards Australia 2004, *AS 5100.2-2004 Bridge design Part 2: Design loads* Standards Australia, NSW, viewed 25 October 2015, <www-saiglobal-com.ezproxy.usq.edu.au/PDFTemp/osu-2015-10-26/9558020697/5100.2-2004(+A1).pdf>.

Standards Australia 2013, *SA/SNZ HB 436:2013 (Guidelines to AS/NZS ISO 31000:2009) : Risk management guidelines - Companion to AS/NZS ISO 31000:2009*, Standards Australia, NSW, viewed 15 March 2014, <www-saiglobal-com.ezproxy.usq.edu.au/PDFTemp/osu-2015-10-26/9558020697/HB436-2013.pdf>.

State Government of Victoria 2015, *Computer-related injuries*, viewed 30 May 2015, <http://www.betterhealth.vic.gov.au/bhcv2/bhcarticles.nsf/pages/Computer-related_injuries>.

Strand7 Pty Ltd n.d.a, *Mohr-Coulomb Yield Criterion (Webnote)*, viewed 26 October 2015, <http://www.strand7.com/webnotes/serve/download/p9yy2hhjvbp6a7hq/ST7-1.57.10.1%20Mohr-Coulomb%20Yield%20Criterion.pdf>.

Strand7 Pty Ltd n.d.c, *Plate Elements*, viewed 20 October 2015, <http://www.strand7.com/html/plateelements.htm>.

topographic-map.com n.d., *Mount Sylvis*, viewed 15 September 2015, <http://en-ca.topographic-map.com/places/Mount-Sylvia-378112/>.

U.S. Department of Transportation 2012, *Hydraulic Design of Safe Bridges*, Hydraulic Design Series Number 7, viewed 23 May 2015 <www.fhwa.dot.gov/engineering/hydraulics/pubs/hif12018.pdf>.

Wahalathantri, B, Lokuge, W, Karunasena, W & Setunge, S 2015, 'Vulnerability of Floodways under Extreme Flood Events', *Natural Hazards Review*, vol. 04015012, pp. 1-12, viewed 17 October 2015, <http://dx.doi.org.ezproxy.usq.edu.au/10.1061/(ASCE)NH.1527-6996.0000194>.

Zienkiewicz, O, Taylor, R & Zhu, J 2015, *Finite Element Method - Its Basis and Fundamentals* 6th edn, Elsevier, viewed 15 September 2015 <http://app.knovel.com/hotlink/toc/id:kpFEMIBFEA/finite-element-method/finite-element-method>.

APPENDIX A. PROJECT SPECIFICATION

University of Southern Queensland
Faculty of Health, Engineering and Sciences
ENG 4111/4112 Research Project
PROJECT SPECIFICATION

FOR: Shane Cummings

TOPIC: ***Case Study***: Modelling the behaviour of floodways subjected to flood loadings.

SUPERVISORS: Professor Karu Karunasena

Dr Weena Lokuge

Dr Buddhi Wahalathantri

PROJECT AIM: To determine how floodways behave under the loading conditions given in AS 5100.2 – 2004.

PROGRAMME: (Issue A, 5th March 2015)

1) Investigate the damage sustained to floodways in the Lockyer Valley region post the 2010/11 and 2013 extreme flood events.
2) Identify the critical parameters required for the Strand7 2D Finite Element Analysis (FEA). These include, material properties and geometric design specifications.
3) Research loadings in accordance with AS 5100.2-2004 including: drag, debris accumulation, impact and lifting forces and their impacts upon floodway structures.
4) Outline the LHBR floodway design specifications, as a case study.
5) Construct 2D Strand7 Plane Strain model.
6) Determine adequate boundary conditions for the 2D Strand7 Model.
7) Conduct convergence study to improve the models performance and accuracy.
8) Undertake a parametric study for three different loading combinations, considering different water velocities and water depths.
9) Conduct FEM analysis to determine stresses and displacements under submerged conditions for the above loading combinations.
10) Analyse and discuss final analysis results.
11) Outline any future research.
12) Submit an academic dissertation of the research.

AGREED_____(Student) _____
(Supervisor)

DATE: / /2015 DATE: / /2015

Examiner / Co-examiner_____

APPENDIX B. RESEARCH CONSEQUENTIAL EFFECTS

Due to the infancy of this type of research, the information contained within, whilst purposeful should only be considered supplementary to a wider and more detailed research project. Understanding this ensures ethical behaviour is adopted at all times to protect the local communities who utilise these floodway structures (Engineers Australia 2010). Adopting incomplete research has the potential to limit the benefits associated with improving the quality and efficiency of future design standards. As a consequence the current financial and community risks may not be improved upon, which is one of the main objective of this research.

The large scope of this research means the possibility to identify all failure mechanisms may not be achieved within this one project. Therefore, outcomes are put forward on the understanding that other potential failure mechanisms may not have been identified and should be further investigated. This is important as communities entrust engineers to design adequate and safe structures and in doing so expect complete and thorough research to be undertaken (Engineers Australia 2010).

APPENDIX C. RISK ASSESSMENT

A risk assessment for this research project has been assessed utilising an approach adapted from SA SNZ HB 436:2013 Risk Management Guidelines Companion to AS NZS ISO 31000:2009 (Standards Australia 2013).

Personal Risk Assessment

Table C.1: Personal Risk Assessment

Hazard	Risk	Mitigation Strategies
Increase risk of vehicle incident/accident due to traffic and / or distance travelled.	Low	• Ensure route is appropriately planned • Ensure appropriate rest stops are scheduled • Ensure all road rules are obeyed • Always drive to road conditions. (Department of Transport and Main Roads 2015).
Death (i.e. Drowning) as a result of a site visit/s.	Medium	• Ensure family and friends are aware of all site visits • Ensure all site visit participants have first aid training to assist should a situation arise • Participate in a buddy system when and if a potentially dangerous scouting operation is required • Ensure appropriate Personal Protective Equipment (PPE) is maintained when conducing site visits.

Hazard	Risk	Mitigation Strategies
Injury (cuts, abrasions) from falling on uneven ground as a result of a site visit/s.	Low	• Partake in activities which are deemed safe in accordance with Workplace Health and Safety provisions • Ensure first aid kit is available during all site visits to apply if required and to minimise further infections and / or injuries. • Ensure all site visit participants have first aid training to assist should a situation arise • Participate in a buddy system when and if a potentially dangerous scouting operation is required • Ensure appropriate Personal Protective Equipment (PPE) is maintained when conducing site visits.
Extensive computer use can cause: • Eye stain • Muscular tenderness • Back Pain • Headaches.	Medium	• Ensure working environment: o Is well lit without direct light o Ensures screen are set to reduce glare o Make sure screen is at eye level and not too close. o Is ergonomically set up, • Ensure frequent breaks are taken away from the computer. (State Government of Victoria 2015).

Project Risk Assessment

Table C.2: Project Risk Assessment

Hazard	Risk	Mitigation Strategies
Limited relevant information available.	Medium	• Ensure a search strategy is developed to facilitate efficient search and retrieval • Ensure all databases have been utilised to source relevant information • Where resources are not directly related to floodways use the most applicable structure as a comparison.
Human errors made during calculations and / or modelling.	High	• Act diligently when entering data • Cross check Strand7 results with analytical results/hand calculations where possible • Follow a personal quality assurance process • Gain peer and supervisors review regularly.
Incomplete modelling.	High	• Partake in online tutorials for Strand7 to ensure a clear understanding in order to diagnose any potential issues efficiently • Collaborate with peers and supervisors for advice on estimated modelling times • Ensure sufficient time is allocated for the modelling process • Ensure the scope of the project is at the forefront when conducting modelling to reduce scope creep.

Hazard	Risk	Mitigation Strategies
Quality of material available.	Low	• Ensure a search strategy is developed to facilitate efficient search and retrieval • Ensure all material is analysed initially to determine suitability • Maintain a database of resources and their quality material categorisation.
Feedback and advice not received within agreed timeframes.	Low	• Ensure all participants roles and responsibilities are clearly defined • Ensure timeframes for responses are identified • Ensure all participants are included in any online communications.
Supervisor unavailability due to unforseen work or personal circumstances.	Low	• Advise of unavailable times where possible • Work with supervisors to ensure schedule is maintained where a delay has occurred • Contact project student as soon as possible as a result of an unforseen incident.
Delay in achieving milestones or deliverables due dates due to unforeseen work or personal circumstances.	Low	• Advise supervisors of unavailable times where possible • Contact supervisors as soon as possible to request extensions as required • Work with supervisors to ensure schedule is maintained where a delay has occurred • Contact supervisors as soon as possible as a result of an unforseen incident.
Technical failures i.e. computer, laptop or phone.	Medium	• Ensure contact details are maintained in multiple locations • Ensure assignment and research material and findings are stored in multiple locations and / or in a shared cloud environment such as ownCloud • Have a backup computer or phone to reduce downtime.

Hazard	Risk	Mitigation Strategies
System USQ outages including email and / or internet.	Low	• Ensure no outages are planned at times where deliverables are due • Establish alternative submission methods should systems not be available such as ownCloud or email.

APPENDIX D. LHBR FLOODWAY

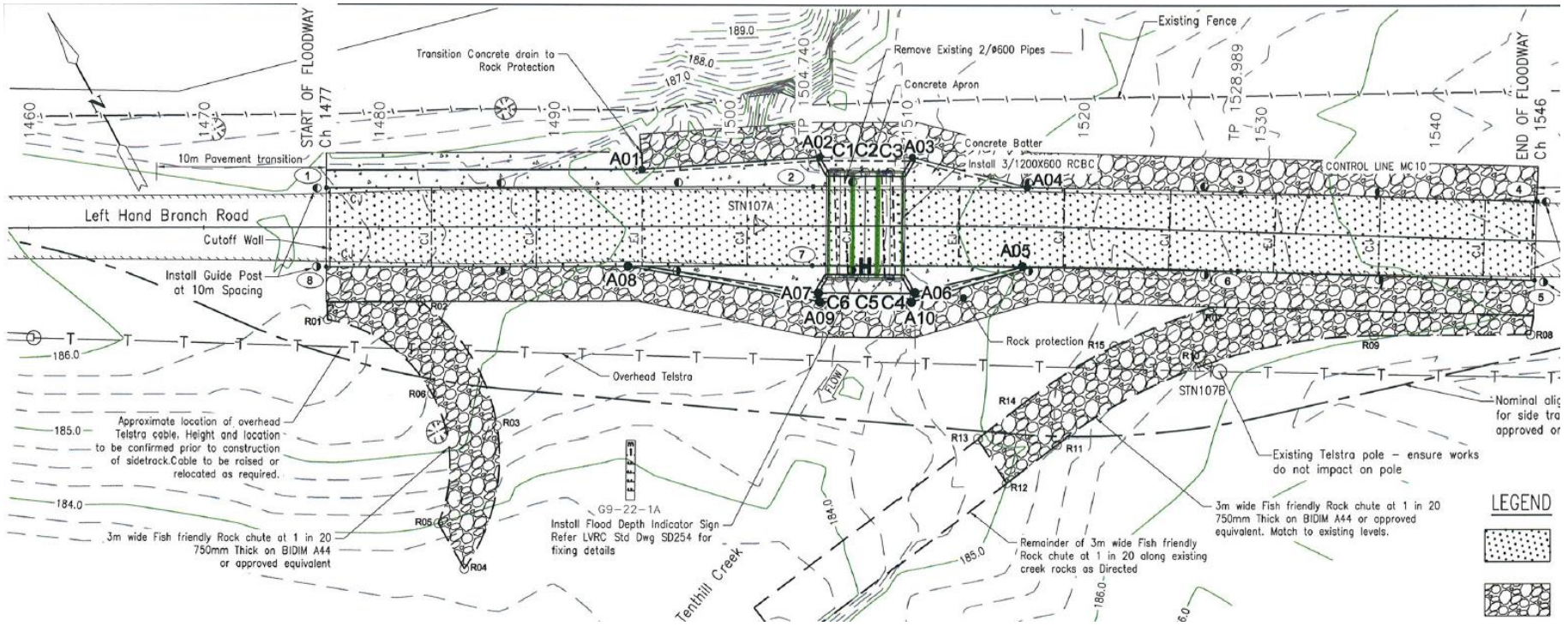

Figure D.1: LHBR Floodway Plan View

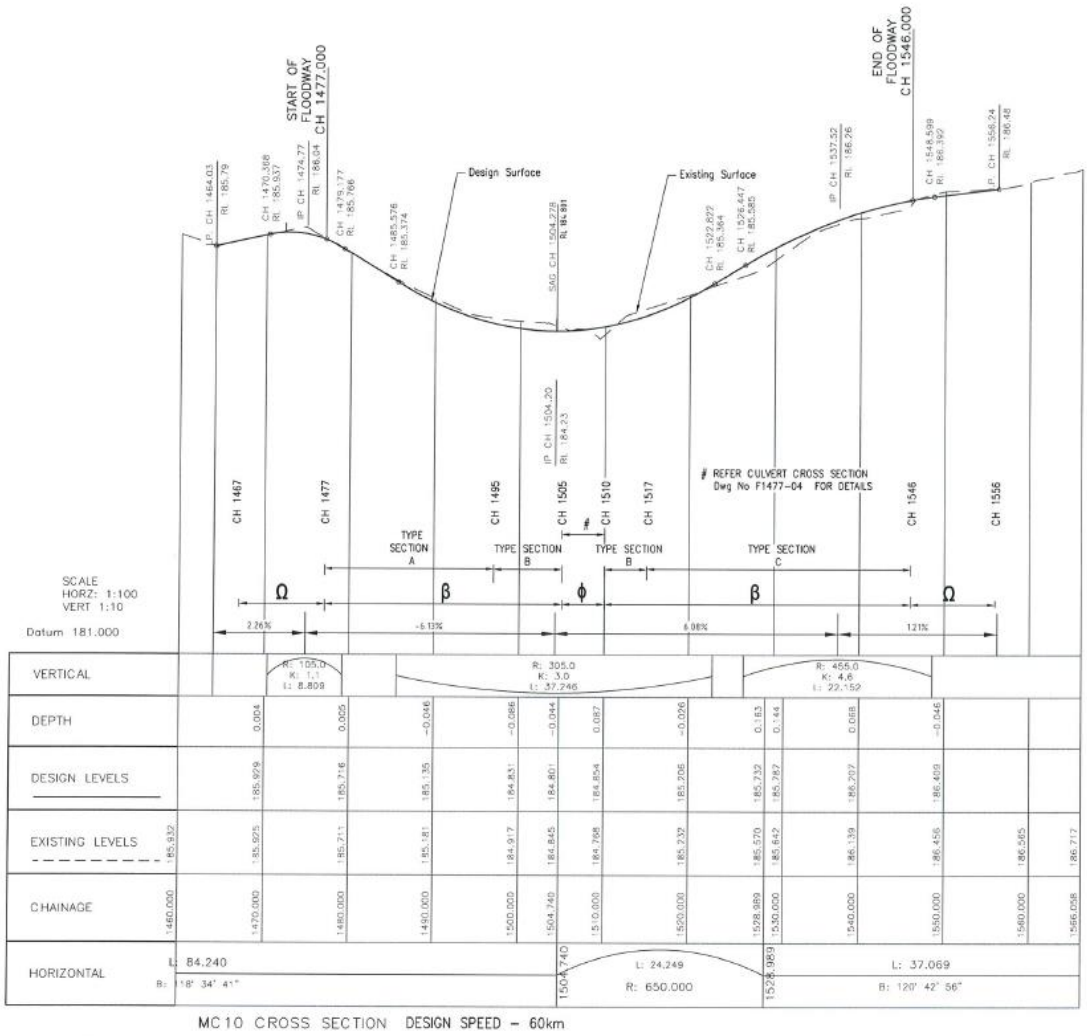

Figure D.2: LHBR Side View of Tenthill Creek Elevation

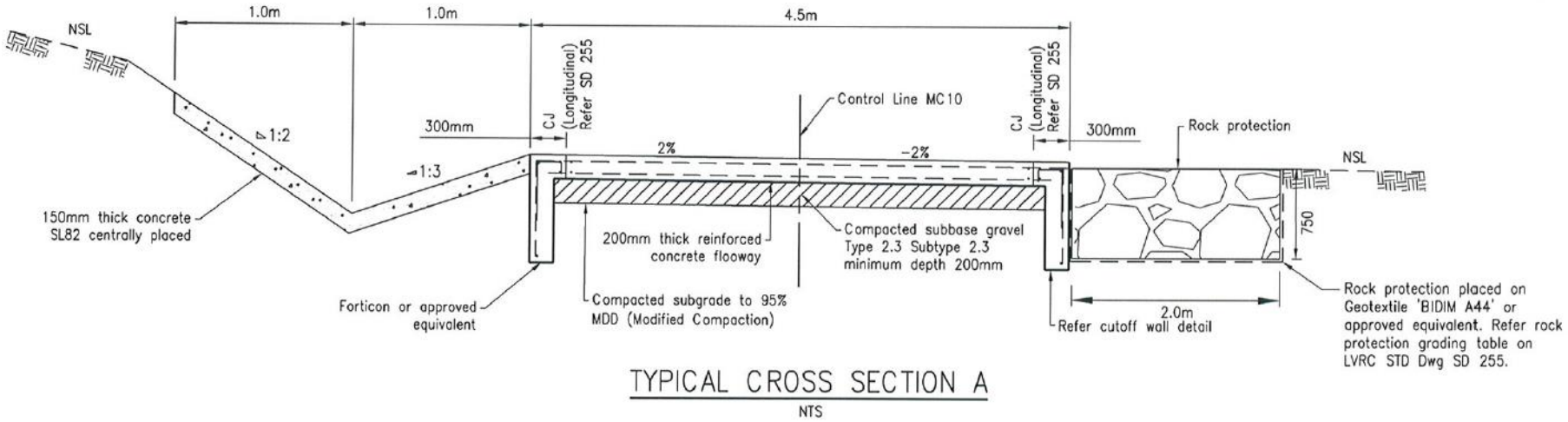

Figure D.3: Cross Section A

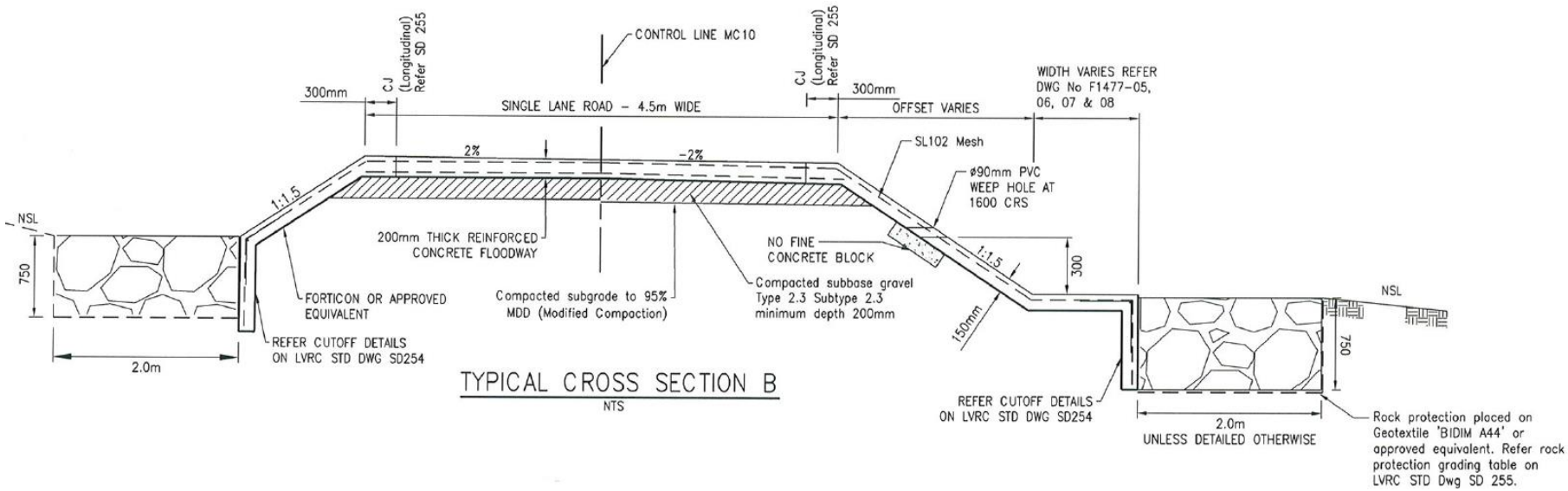

Figure D.4: Cross Section B

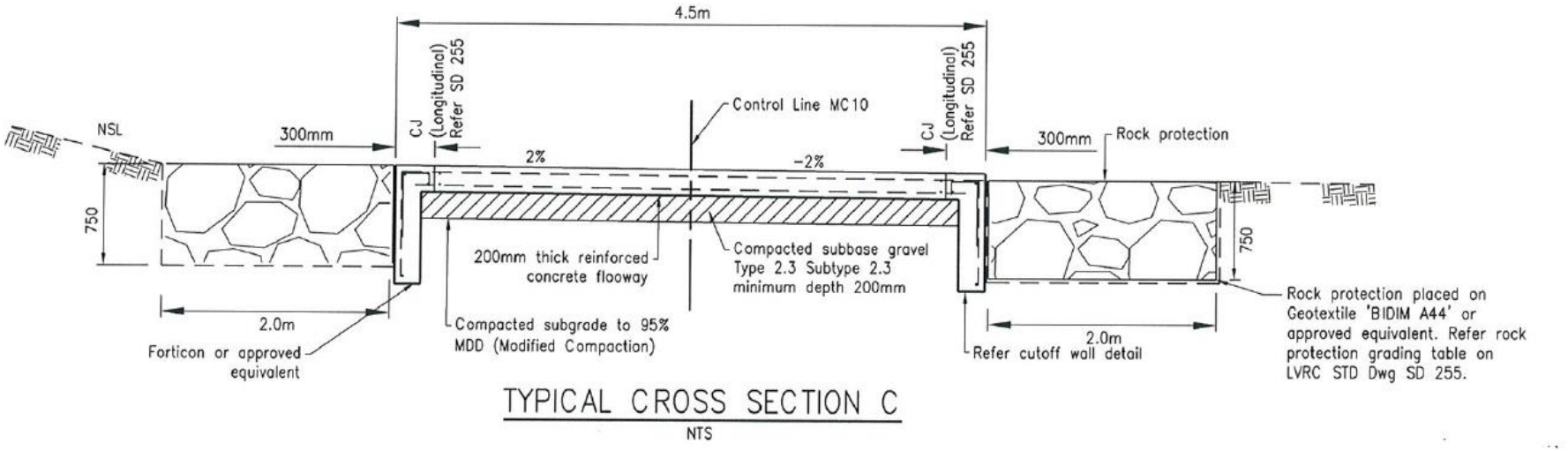

Figure D.5: Cross Section C

APPENDIX E. FORCE CALCULATIONS

Drag Force Calculations

Table E.1: Drag Force Spreadsheet

Velocity (m/s)	Force (kN)	F1	F2
1	0.8400	0.0350	0.0700
3	7.5600	0.3150	0.6300
5	21.0000	0.8750	1.7500
6	30.2400	1.2600	2.5200
7	41.1600	1.7150	3.4300
8	53.7600	2.2400	4.4800
10	84.0000	3.5000	7.0000

Note: F1 and F2 represent the force as equivalent point loads.

Lifting Force Calculations

Table E.2: Lifting Force Spreadsheet

Depth (m)	Velocity (m/s)	Vertical Dist. Dwgs	RS	CL Down	CL Up	Down (kN)	Up (kN)	Resultant	Convert to Mpa	Factor Up
0.2	**1**	0.8	1.3333	0.1	-2	0.456	-9.120	FALSE	0.000	0.000
0.2	**3**	0.8	1.3333	0.1	-2	4.104	-82.080	-82.080	-0.018	0.018
0.2	**5**	0.8	1.3333	0.1	-2	11.4	-228.000	-228.000	-0.050	0.050
0.2	**6**	0.8	1.3333	0.1	-2	16.416	-328.320	-328.320	-0.072	0.072
0.2	**7**	0.8	1.3333	0.1	-2	22.344	-446.880	-446.880	-0.098	0.098
0.2	**8**	0.8	1.3333	0.1	-2	29.184	-583.680	-583.680	-0.128	0.128
0.2	**10**	0.8	1.3333	0.1	-2	45.6	-912.000	-912.000	-0.200	0.200
1	**1**	1.6	2.6667	0	-1.0667	0	-4.864	FALSE	0.000	0.000
1	**3**	1.6	2.6667	0	-1.0667	0	-43.776	-43.776	-0.010	0.010
1	**5**	1.6	2.6667	0	-1.0667	0	-121.600	-121.600	-0.027	0.027
1	**6**	1.6	2.6667	0	-1.0667	0	-175.104	-175.104	-0.038	0.038
1	**7**	1.6	2.6667	0	-1.0667	0	-238.336	-238.336	-0.052	0.052
1	**8**	1.6	2.6667	0	-1.0667	0	-311.296	-311.296	-0.068	0.068
1	**10**	1.6	2.6667	0	-1.0667	0	-486.400	-486.400	-0.107	0.107
2	**1**	2.6	4.3333	0	-0.8	0	-3.648	FALSE	0.000	0.000
2	**3**	2.6	4.3333	0	-0.8	0	-32.832	FALSE	0.000	0.000
2	**5**	2.6	4.3333	0	-0.8	0	-91.200	-91.200	-0.020	0.020
2	**6**	2.6	4.3333	0	-0.8	0	-131.328	-131.328	-0.029	0.029
2	**7**	2.6	4.3333	0	-0.8	0	-178.752	-178.752	-0.039	0.039
2	**8**	2.6	4.3333	0	-0.8	0	-233.472	-233.472	-0.051	0.051

Depth (m)	Velocity (m/s)	Vertical Dist. Dwgs	RS	CL Down	CL Up	Down (kN)	Up (kN)	Resultant	Convert to Mpa	Factor Up
2	**10**	2.6	4.3333	0	-0.8	0	-364.800	-364.800	-0.080	0.080
5	**1**	5.6	9.3333	0	-0.8	0	-3.648	FALSE	0.000	0.000
5	**3**	5.6	9.3333	0	-0.8	0	-32.832	FALSE	0.000	0.000
5	**5**	5.6	9.3333	0	-0.8	0	-91.200	-91.200	-0.020	0.020
5	**6**	5.6	9.3333	0	-0.8	0	-131.328	-131.328	-0.029	0.029
5	**7**	5.6	9.3333	0	-0.8	0	-178.752	-178.752	-0.039	0.039
5	**8**	5.6	9.3333	0	-0.8	0	-233.472	-233.472	-0.051	0.051
5	**10**	5.6	9.3333	0	-0.8	0	-364.800	-364.800	-0.080	0.080
10	**1**	10.6	17.6667	0	-0.8	0	-3.648	FALSE	0.000	0.000
10	**3**	10.6	17.6667	0	-0.8	0	-32.832	FALSE	0.000	0.000
10	**5**	10.6	17.6667	0	-0.8	0	-91.200	-91.200	-0.020	0.020
10	**6**	10.6	17.6667	0	-0.8	0	-131.328	-131.328	-0.029	0.029
10	**7**	10.6	17.6667	0	-0.8	0	-178.752	-178.752	-0.039	0.039
10	**8**	10.6	17.6667	0	-0.8	0	-233.472	-233.472	-0.051	0.051
10	**10**	10.6	17.6667	0	-0.8	0	-364.800	-364.800	-0.080	0.080

Log Impact Force Calculations

Table E.3: Log Impact Force Spreadsheet

Velocity (m/s)	Force (kN)	F1	F2
1	26.67	3.3333	6.6667
3	240.00	30.0000	60.0000
5	666.67	83.3333	166.6667
6	960.00	120.0000	240.0000
7	1306.67	163.3333	326.6667
8	1706.67	213.3333	426.6667
10	2666.67	333.3333	666.6667

Note: F1 and F2 represent the force as equivalent point loads.

Debris Accumulation Force Calculations

Table E.4: Debris Accumulation Force Spreadsheet

Depth (m)	Velocity (m/s)	V2 x Depth	Drag (Cd)	Force (kN)
0.2	1	0.2	3.4	2.04
0.2	3	1.8	3.4	18.36
0.2	5	5	3.4	51
0.2	6	7.2	3.4	73.44
0.2	7	9.8	3.4	99.96
0.2	8	12.8	3.4	130.56
0.2	10	20	3.4	204
1	1	1	3.4	2.04
1	3	9	3.4	18.36
1	5	25	3.4	51
1	6	36	3.4	73.44
1	7	49	3.13	92.022
1	8	64	2.74	105.216
1	10	100	2.2	132
2	1	2	3.4	2.04
2	3	18	3.4	18.36
2	5	50	3.1	46.5
2	6	72	2.62	56.592

Depth (m)	Velocity (m/s)	V2 x Depth	Drag (Cd)	Force (kN)
2	7	98	2.23	65.562
2	8	128	2.01	77.184
2	10	200	1.68	100.8
5	1	5	3.4	2.04
5	3	45	3.25	17.55
5	5	125	2.03	30.45
5	6	180	1.79	38.664
5	7	245	1.47	43.218
5	8	320	1.4	53.76
5	10	500	1.4	84
10	1	10	3.4	2.04
10	3	90	2.35	12.69
10	5	250	1.45	21.75
10	6	360	1.4	30.24
10	7	490	1.4	41.16
10	8	640	1.4	53.76
10	10	1000	1.4	84

APPENDIX F. PARAMETRIC STUDY

Load Combination 1

Table F.1: Load Combination 1 Structure Stress and Displacement Data

		Max Stress (Structure) Mpa						Structure Displacements (m)			
Velocity (m/s)	**Depth (m)**	**XX**	**YY**	**XY**	**XY Plate No.**	**VM (centroid)**	**VM Plate No.**	**Dx**	**Dx Node No.**	**Dy**	**Dy Node No.**
1	0.2	-5.45E-01	-4.29E-01	2.22E-01	25274	4.94E-01	200	9.28E-04	40528	-2.10E-03	40807
	1	-6.04E-01	-4.59E-01	2.57E-01	25274	5.81E-01	200	8.76E-04	20	-2.12E-03	40810
	2	-6.79E-01	-4.98E-01	3.00E-01	200	6.90E-01	200	8.14E-04	20	-2.15E-03	40813
	5	-9.92E-01	-6.14E-01	4.37E-01	200	1.02E+00	200	8.70E-04	15650	-2.35E-03	1
	10	-1.54E+00	-8.09E-01	6.76E-01	35746	1.56E+00	200	1.18E-03	15650	-2.81E-03	1
3	0.2	-2.24E+00	-1.52E+00	1.05E+00	25274	2.33E+00	200	4.85E-03	15872	-1.83E-03	41660
	1	-2.36E+00	-1.65E+00	1.10E+00	35746	2.43E+00	200	4.85E-03	2	-2.02E-03	41660
	2	-2.51E+00	-1.79E+00	1.19E+00	35746	2.55E+00	200	4.86E-03	2	-2.25E-03	61
	5	-2.83E+00	-1.91E+00	5.16E-01	34034	2.87E+00	200	4.88E-03	2	-2.58E-03	15667
	10	-3.37E+00	-2.10E+00	1.57E+00	35746	3.42E+00	200	4.90E-03	15872	-3.14E-03	25517
5	0.2	-6.15E+00	-3.76E+00	2.70E+00	25274	6.01E+00	200	1.31E-02	42070	-2.90E-03	41660
	1	-6.11E+00	-4.05E+00	2.83E+00	35746	6.12E+00	200	1.31E-02	25774	-3.26E-03	41660
	2	-6.16E+00	-4.16E+00	2.90E+00	35746	6.24E+00	200	1.31E-02	2	-3.45E-03	41660
	5	-6.48E+00	-4.27E+00	3.05E+00	35746	6.56E+00	200	1.31E-02	25774	-3.79E-03	15667
	10	-7.02E+00	-4.47E+00	3.29E+00	35746	7.11E+00	200	1.32E-02	15872	-4.35E-03	15667
6	0.2	-8.87E+00	-5.30E+00	3.84E+00	25274	8.54E+00	200	1.88E-02	42070	-3.63E-03	41660

Velocity (m/s)	Depth (m)	XX	YY	XY	XY Plate No.	VM (centroid)	VM Plate No.	Dx	Dx Node No.	Dy	Dy Node No.
	1	-8.84E+00	-5.69E+00	4.01E+00	35746	8.66E+00	200	1.88E-02	25774	-4.11E-03	41660
	2	-8.79E+00	-5.84E+00	4.10E+00	35746	8.78E+00	200	1.88E-02	2	-4.34E-03	41660
	5	-9.02E+00	-5.96E+00	4.25E+00	35746	9.11E+00	200	1.88E-02	25774	-4.68E-03	41660
	10	-9.55E+00	-6.15E+00	4.49E+00	35746	9.65E+00	200	1.89E-02	15872	-5.24E-03	15667
7	0.2	-1.21E+01	-7.11E+00	5.20E+00	35739	1.15E+01	200	2.56E-02	42070	5.27E-03	40745
	1	-1.21E+01	-7.64E+00	5.42E+00	35746	1.17E+01	200	2.55E-02	15872	-5.13E-03	41660
	2	-1.20E+01	-7.83E+00	5.52E+00	35746	1.18E+01	200	2.55E-02	2	-5.39E-03	41660
	5	-1.20E+01	-7.94E+00	5.66E+00	35746	1.21E+01	200	2.56E-02	25774	-5.73E-03	41660
	10	-1.25E+01	-8.14E+00	5.91E+00	35746	1.27E+01	200	2.56E-02	15872	-6.29E-03	41660
8	0.2	-1.58E+01	-9.21E+00	6.81E+00	35739	1.50E+01	200	3.33E-02	42070	7.49E-03	40745
	1	-1.58E+01	-9.89E+00	7.04E+00	35746	1.51E+01	200	3.33E-02	15872	-6.29E-03	41660
	2	-1.57E+01	-1.01E+01	7.15E+00	35746	1.53E+01	200	3.33E-02	2	-6.60E-03	41660
	5	-1.56E+01	-1.02E+01	7.30E+00	35746	1.56E+01	200	3.33E-02	25774	-6.94E-03	41660
	10	-1.60E+01	-1.04E+01	7.54E+00	35746	1.61E+01	200	3.33E-02	25774	-7.51E-03	41660
10	0.2	-2.47E+01	-1.42E+01	1.07E+01	35739	2.34E+01	25255	5.20E-02	42070	1.28E-02	15267
	1	-2.47E+01	-1.53E+01	1.09E+01	35746	2.34E+01	200	5.19E-02	15872	-9.09E-03	41660
	2	-2.46E+01	-1.56E+01	1.11E+01	35746	2.36E+01	200	5.19E-02	2	-9.52E-03	41660
	5	-2.45E+01	-1.57E+01	1.12E+01	35746	2.39E+01	200	5.19E-02	2	-9.85E-03	41660
	10	-2.43E+01	-1.59E+01	1.15E+01	35746	2.45E+01	200	5.20E-02	25774	-1.04E-02	41660

Table F.2: Load Combination 1 Soil Stress and Displacement Data

		Max Stress (Soil) Mpa		Soil Displacements (m)			
Velocity (m/s)	**Depth (m)**	**MC**	**MC Plate No.**	**Dx**	**Dx Node No.**	**Dy**	**Dy Node No.**
1	0.2	-2.67E-01	202	9.33E-04	40543	-2.10E-03	15297
	1	-3.10E-01	202	8.96E-04	58254	-2.12E-03	25029
	2	-3.63E-01	202	8.67E-04	55946	-2.15E-03	40812
	5	-5.22E-01	202	8.70E-04	15650	-2.35E-03	63170
	10	-7.87E-01	202	1.18E-03	15650	-2.83E-03	63146
3	0.2	-2.67E-01	202	4.84E-03	69	-2.74E-03	15181
	1	-3.10E-01	202	4.83E-03	40632	-2.65E-03	15182
	2	-3.63E-01	202	4.82E-03	15210	-2.56E-03	15185
	5	-5.22E-01	202	4.84E-03	24839	-2.80E-03	15186
	10	-7.87E-01	202	4.89E-03	9	-3.20E-03	61346
5	0.2	3.06E-01	63478	1.31E-02	69	-5.53E-03	15175
	1	-3.10E-01	202	1.31E-02	25059	-5.14E-03	15176
	2	-3.63E-01	202	1.31E-02	69	-5.09E-03	15176
	5	-5.22E-01	202	1.31E-02	40632	-5.32E-03	15177
	10	-7.88E-01	202	1.31E-02	24839	-5.70E-03	15177
6	0.2	4.93E-01	63478	1.88E-02	69	-7.47E-03	15174
	1	4.62E-01	63478	1.87E-02	25059	-6.88E-03	15175
	2	4.51E-01	63478	1.87E-02	25059	-6.77E-03	15175
	5	-5.22E-01	202	1.88E-02	69	-7.00E-03	15175
	10	-7.88E-01	202	1.88E-02	15210	-7.37E-03	15176
7	0.2	7.15E-01	63478	2.55E-02	69	-9.77E-03	15173
	1	6.73E-01	63478	2.55E-02	25059	-8.94E-03	15174

Velocity (m/s)	Depth (m)	MC	MC Plate No.	Dx	Dx Node No.	Dy	Dy Node No.
	2	6.59E-01	63478	2.54E-02	25059	-8.76E-03	15174
	5	6.51E-01	63478	2.55E-02	69	-8.99E-03	15174
	10	-7.88E-01	202	2.55E-02	40632	-9.36E-03	15175
8	0.2	9.70E-01	63478	3.33E-02	25059	-1.24E-02	15173
	1	9.17E-01	63478	3.32E-02	25059	-1.13E-02	15173
	2	8.99E-01	63478	3.32E-02	25059	-1.11E-02	15173
	5	8.91E-01	63478	3.32E-02	25059	-1.13E-02	15174
	10	8.77E-01	63478	3.32E-02	69	-1.17E-02	15174
10	0.2	1.58E+00	63478	5.19E-02	25059	-1.88E-02	15173
	1	1.50E+00	63478	5.17E-02	25059	-1.70E-02	15173
	2	1.48E+00	63478	5.17E-02	25059	-1.66E-02	15173
	5	1.47E+00	63478	5.17E-02	25059	-1.68E-02	15173
	10	1.45E+00	63478	5.18E-02	69	-1.72E-02	15173

Load Combination 2

Table F.3: Load Combination 2 Structure Stress and Displacement Data

		Max Stress (Structure) Mpa						Structure Displacements (m)			
Velocity (m/s)	**Depth (m)**	**XX**	**YY**	**XY**	**XY Plate No.**	**VM (centroid)**	**VM Plate No.**	**Dx**	**Dx Node No.**	**Dy**	**Dy Node No.**
1	0.2	-5.37E-01	-4.21E-01	2.18E-01	25274	4.85E-01	200	9.19E-04	40528	-2.08E-03	40807
	1	-5.95E-01	-4.51E-01	2.52E-01	25274	5.72E-01	200	8.68E-04	20	-2.10E-03	40810
	2	-6.70E-01	-4.90E-01	2.96E-01	200	6.81E-01	200	8.06E-04	20	-2.13E-03	40815
	5	-9.84E-01	-6.07E-01	4.33E-01	200	1.01E+00	200	8.91E-04	15650	-2.39E-03	1
	10	-1.53E+00	-8.01E-01	6.70E-01	35746	1.55E+00	200	1.20E-03	15650	-2.85E-03	1
3	0.2	-3.46E+00	1.65E+00	2.22E+00	63491	4.04E+00	63491	4.88E-03	42069	-1.72E-03	41660
	1	-3.43E+00	-1.58E+00	2.13E+00	63491	3.85E+00	63491	4.86E-03	42069	-1.91E-03	15667
	2	-3.39E+00	-1.72E+00	2.01E+00	63491	3.63E+00	63491	4.83E-03	15870	-2.23E-03	12
	5	-3.34E+00	-1.84E+00	1.89E+00	63491	3.47E+00	193	4.88E-03	42069	-2.47E-03	15667
	10	-3.25E+00	-2.03E+00	1.70E+00	63491	3.34E+00	200	4.97E-03	24850	-3.03E-03	25517
5	0.2	-9.58E+00	4.70E+00	6.33E+00	63491	1.15E+01	63491	1.32E-02	42069	-5.58E-03	15176
	1	-9.52E+00	4.53E+00	6.11E+00	63491	1.11E+01	63491	1.32E-02	42069	-5.19E-03	15176
	2	-9.49E+00	4.46E+00	6.02E+00	63491	1.09E+01	63491	1.31E-02	42069	-5.14E-03	15177
	5	-9.43E+00	4.34E+00	5.90E+00	63491	1.07E+01	63491	1.32E-02	42069	-5.37E-03	15177
	10	-9.34E+00	-4.28E+00	5.71E+00	63491	1.03E+01	63491	1.33E-02	42069	-5.75E-03	15178
6	0.2	-1.38E+01	6.79E+00	9.16E+00	63491	1.66E+01	63491	1.90E-02	42069	4.01E-03	24884
	1	-1.37E+01	6.57E+00	8.85E+00	63491	1.61E+01	63491	1.89E-02	42069	-3.68E-03	41660
	2	-1.37E+01	6.47E+00	8.73E+00	63491	1.59E+01	63491	1.88E-02	42069	-3.90E-03	41660
	5	-1.36E+01	6.35E+00	8.62E+00	63491	1.56E+01	63491	1.89E-02	42069	-4.24E-03	41660

Velocity (m/s)	Depth (m)	XX	YY	XY	XY Plate No.	VM (centroid)	VM Plate No.	Dx	Dx Node No.	Dy	Dy Node No.
	10	-1.35E+01	6.15E+00	8.42E+00	63491	1.53E+01	63491	1.90E-02	42069	-4.81E-03	15667
7	0.2	-1.88E+01	9.26E+00	1.25E+01	63491	2.27E+01	63491	2.58E-02	42069	6.18E-03	41660
	1	-1.87E+01	8.97E+00	1.21E+01	63491	2.20E+01	63491	2.56E-02	42069	-4.53E-03	41660
	2	-1.86E+01	8.86E+00	1.19E+01	63491	2.17E+01	63491	2.56E-02	42069	-4.80E-03	41660
	5	-1.86E+01	8.74E+00	1.18E+01	63491	2.15E+01	63491	2.56E-02	42069	-5.14E-03	41660
	10	-1.85E+01	8.54E+00	1.16E+01	63491	2.11E+01	63491	2.57E-02	42069	-5.70E-03	15667
8	0.2	-2.45E+01	1.21E+01	1.63E+01	63491	2.97E+01	63491	3.36E-02	42069	8.68E-03	40753
	1	-2.44E+01	1.18E+01	1.58E+01	63491	2.88E+01	63491	3.34E-02	42069	-5.52E-03	41660
	2	-2.43E+01	1.16E+01	1.56E+01	63491	2.84E+01	63491	3.33E-02	42069	-5.83E-03	41660
	5	-2.43E+01	1.15E+01	1.55E+01	63491	2.82E+01	63491	3.34E-02	42069	-6.17E-03	41660
	10	-2.42E+01	1.13E+01	1.53E+01	63491	2.78E+01	63491	3.35E-02	42069	-6.73E-03	41660
10	0.2	-3.83E+01	1.90E+01	2.56E+01	63491	4.65E+01	63491	5.25E-02	42069	1.47E-02	15271
	1	-3.81E+01	1.84E+01	2.48E+01	63491	4.50E+01	63491	5.21E-02	42069	8.51E-03	38
	2	-3.80E+01	1.82E+01	2.45E+01	63491	4.46E+01	63491	5.20E-02	42069	-8.31E-03	41660
	5	-3.80E+01	1.81E+01	2.44E+01	63491	4.43E+01	63491	5.20E-02	42069	-8.65E-03	41660
	10	-3.79E+01	1.79E+01	2.42E+01	63491	4.40E+01	63491	5.21E-02	42069	-9.21E-03	41660

Table F.4: Load Combination 2 Structure Stress and Displacement Data

		Max Stress (Soil) Mpa		Soil Displacements (m)			
Velocity (m/s)	**Depth (m)**	**MC**	**MC Plate No.**	**Dx**	**Dx Node No.**	**Dy**	**Dy Node No.**
1	0.2	-2.67E-01	202	9.25E-04	40544	-2.08E-03	15297
	1	-3.10E-01	202	8.90E-04	57488	-2.10E-03	25029
	2	-3.63E-01	202	8.63E-04	21767	-2.13E-03	15301
	5	-5.22E-01	202	8.91E-04	15650	-2.39E-03	63170
	10	-7.87E-01	202	1.20E-03	15650	-2.86E-03	63158
3	0.2	-2.67E-01	202	4.88E-03	12	-2.76E-03	15181
	1	-3.10E-01	202	4.85E-03	40674	-2.68E-03	15183
	2	-3.63E-01	202	4.83E-03	40674	-2.59E-03	39802
	5	-5.22E-01	202	4.87E-03	12	-2.83E-03	39807
	10	-7.87E-01	202	4.97E-03	24850	-3.23E-03	61360
5	0.2	-2.68E-01	202	1.32E-02	12	-5.58E-03	15176
	1	-3.10E-01	202	1.31E-02	40674	-5.19E-03	15176
	2	-3.63E-01	202	1.31E-02	40674	-5.14E-03	15177
	5	-5.22E-01	202	1.32E-02	40674	-5.37E-03	15177
	10	-7.88E-01	202	1.33E-02	12	-5.75E-03	15178
6	0.2	4.38E-01	63478	1.90E-02	12	-7.53E-03	15175
	1	4.07E-01	63478	1.88E-02	40674	-6.95E-03	15175
	2	3.96E-01	63478	1.88E-02	40674	-6.83E-03	15175
	5	-5.22E-01	202	1.89E-02	40674	-7.06E-03	15176
	10	-7.88E-01	202	1.90E-02	12	-7.44E-03	15176
7	0.2	6.39E-01	63478	2.58E-02	12	-9.85E-03	15174
	1	5.97E-01	63478	2.56E-02	40674	-9.03E-03	15174

Velocity (m/s)	Depth (m)	MC	MC Plate No.	Dx	Dx Node No.	Dy	Dy Node No.
	2	5.84E-01	63478	2.55E-02	40674	-8.85E-03	15174
	5	5.75E-01	63478	2.56E-02	40674	-9.07E-03	15175
	10	-7.88E-01	202	2.57E-02	40674	-9.45E-03	15175
8	0.2	8.71E-01	63478	3.36E-02	12	-1.25E-02	15173
	1	8.18E-01	63478	3.34E-02	40674	-1.14E-02	15174
	2	8.00E-01	63478	3.33E-02	40674	-1.12E-02	15174
	5	7.92E-01	63478	3.34E-02	40674	-1.14E-02	15174
	10	-7.88E-01	202	3.34E-02	40674	-1.18E-02	15174
10	0.2	1.43E+00	63478	5.25E-02	12	-1.90E-02	15173
	1	1.35E+00	63478	5.20E-02	40674	-1.72E-02	15173
	2	1.32E+00	63478	5.19E-02	40674	-1.68E-02	15173
	5	1.31E+00	63478	5.20E-02	40674	-1.70E-02	15173
	10	1.30E+00	63478	5.20E-02	40674	-1.74E-02	15174

Load Combination 3

Table F.5: Load Combination 3 Structure Stress and Displacement Data

		Max Stress (Structure) Mpa						Structure Displacements (m)			
Velocity (m/s)	**Depth (m)**	**XX**	**YY**	**XY**	**XY Plate No.**	**VM (centroid)**	**VM Plate No.**	**Dx**	**Dx Node No.**	**Dy**	**Dy Node No.**
1	0.2	-3.76E-01	-2.83E-01	1.29E-01	25274	2.99E-01	34020	5.62E-04	20	-2.09E-03	40802
	1	-4.35E-01	-3.13E-01	1.63E-01	25274	3.72E-01	200	5.10E-04	20	-2.11E-03	40805
	2	-5.10E-01	-3.52E-01	2.08E-01	200	4.81E-01	200	4.48E-04	20	-2.14E-03	40810
	5	-8.00E-01	-4.69E-01	-3.53E-01	35737	8.07E-01	200	4.90E-04	15650	-2.40E-03	1
	10	-1.35E+00	-6.81E-01	-6.15E-01	35737	1.35E+00	200	8.02E-04	15650	-2.86E-03	1
3	0.2	-4.26E-01	2.17E-01	2.62E-01	63499	4.81E-01	63499	8.52E-04	15650	-1.26E-03	1
	1	-5.22E-01	-3.37E-01	2.44E-01	25274	5.48E-01	200	7.70E-04	39962	-1.66E-03	1
	2	-6.59E-01	-4.81E-01	2.90E-01	200	6.67E-01	200	7.82E-04	20	-2.13E-03	40813
	5	-9.65E-01	-5.93E-01	4.24E-01	200	9.87E-01	200	8.55E-04	15650	-2.39E-03	1
	10	-1.48E+00	-7.60E-01	6.41E-01	35746	1.49E+00	200	1.09E-03	15650	-2.85E-03	1
5	0.2	9.76E-01	8.14E-01	9.60E-01	63499	1.76E+00	63499	2.11E-03	17	1.52E-03	40774
	1	-8.50E-01	5.34E-01	6.53E-01	63499	1.20E+00	63499	1.79E-03	15650	-1.21E-03	193
	2	-9.33E-01	-4.93E-01	5.31E-01	63499	9.82E-01	200	1.68E-03	15650	-1.39E-03	193
	5	-1.14E+00	-5.20E-01	5.10E-01	200	1.18E+00	200	1.60E-03	15650	-1.68E-03	15671
	10	-1.63E+00	-7.32E-01	7.07E-01	200	1.65E+00	200	1.77E-03	15650	-2.22E-03	25522
6	0.2	1.47E+00	1.23E+00	1.44E+00	63499	2.64E+00	63499	2.98E-03	17	3.10E-03	15282
	1	-1.08E+00	8.19E-01	1.00E+00	63499	1.84E+00	63499	2.50E-03	15650	-1.16E-03	193
	2	-1.07E+00	6.14E-01	7.65E-01	63499	1.40E+00	63499	2.13E-03	15650	-1.34E-03	41668
	5	-1.27E+00	5.40E-01	6.29E-01	63499	1.31E+00	200	2.03E-03	15650	-1.62E-03	15671

Velocity (m/s)	Depth (m)	XX	YY	XY	XY Plate No.	VM (centroid)	VM Plate No.	Dx	Dx Node No.	Dy	Dy Node No.
	10	-1.75E+00	-7.78E-01	7.66E-01	200	1.79E+00	200	2.20E-03	41622	-2.17E-03	25522
7	0.2	2.05E+00	1.72E+00	2.01E+00	63499	3.69E+00	63499	4.00E-03	17	4.97E-03	15282
	1	1.39E+00	1.12E+00	1.36E+00	63499	2.51E+00	63499	3.20E-03	41622	1.72E-03	24897
	2	-1.21E+00	8.33E-01	1.02E+00	63499	1.88E+00	63499	2.62E-03	15650	-1.27E-03	41668
	5	-1.37E+00	7.28E-01	8.59E-01	63499	1.56E+00	63499	2.44E-03	41622	-1.55E-03	15671
	10	-1.91E+00	-8.55E-01	8.40E-01	200	1.95E+00	200	2.72E-03	41622	-2.11E-03	25522
8	0.2	2.73E+00	2.29E+00	2.66E+00	63499	4.89E+00	63499	5.18E-03	17	7.12E-03	15282
	1	1.76E+00	1.44E+00	1.73E+00	63499	3.18E+00	63499	3.88E-03	17	2.86E-03	15280
	2	-1.38E+00	1.09E+00	1.33E+00	63499	2.44E+00	63499	3.21E-03	41622	1.61E-03	24897
	5	-1.53E+00	9.64E-01	1.16E+00	63499	2.11E+00	63499	3.01E-03	41622	1.51E-03	24897
	10	-2.08E+00	1.02E+00	1.12E+00	63499	2.14E+00	200	3.32E-03	41622	-2.04E-03	25522
10	0.2	4.34E+00	3.65E+00	4.23E+00	63499	7.77E+00	63499	8.02E-03	17	1.23E-02	24902
	1	2.64E+00	2.17E+00	2.58E+00	63499	4.74E+00	63499	5.42E-03	17	5.62E-03	40774
	2	2.06E+00	1.69E+00	2.03E+00	63499	3.73E+00	63499	4.55E-03	17	3.69E-03	40774
	5	-1.96E+00	1.60E+00	1.90E+00	63499	3.48E+00	63499	4.46E-03	41622	3.59E-03	15280
	10	-2.51E+00	1.60E+00	1.86E+00	63499	3.38E+00	63499	4.77E-03	41622	3.46E-03	15280

Table F.6: Load Combination 3 Structure Stress and Displacement Data

		Max Stress (Soil) Mpa		Soil Displacements (m)			
Velocity (m/s)	**Depth (m)**	**MC**	**MC Plate No.**	**Dx**	**Dx Node No.**	**Dy**	**Dy Node No.**
1	0.2	-2.85E-01	202	7.10E-04	17785	-2.09E-03	25024
	1	-3.28E-01	202	7.03E-04	45189	-2.11E-03	40804
	2	-3.81E-01	202	7.00E-04	43662	-2.14E-03	25029
	5	-5.40E-01	202	7.02E-04	9065	-2.40E-03	1
	10	-8.06E-01	202	8.02E-04	15650	-2.87E-03	63159
3	0.2	-5.75E-01	202	8.52E-04	15650	-1.71E-03	39822
	1	-6.17E-01	202	7.70E-04	39962	-1.68E-03	15202
	2	-6.70E-01	202	8.47E-04	21435	-2.13E-03	40812
	5	-8.15E-01	202	8.55E-04	15650	-2.39E-03	63170
	10	-9.94E-01	202	1.09E-03	15650	-2.87E-03	63159
5	0.2	-1.15E+00	202	2.11E-03	17	-2.49E-03	15181
	1	-1.19E+00	202	1.79E-03	15650	-2.13E-03	15185
	2	-1.17E+00	202	1.68E-03	15650	-2.08E-03	24444
	5	-1.04E+00	202	1.60E-03	15650	-2.25E-03	61360
	10	-1.15E+00	202	1.77E-03	15650	-2.61E-03	15191
6	0.2	-1.55E+00	202	2.98E-03	59959	3.10E-03	15281
	1	-1.59E+00	202	2.50E-03	15650	-2.49E-03	15182
	2	-1.35E+00	202	2.13E-03	15650	-2.32E-03	15184
	5	-1.19E+00	202	2.03E-03	15650	-2.47E-03	61332
	10	-1.31E+00	202	2.20E-03	41622	-2.83E-03	39802
7	0.2	-2.02E+00	202	4.02E-03	14569	4.97E-03	15281
	1	-1.92E+00	202	3.20E-03	41622	-2.89E-03	15180

Velocity (m/s)	Depth (m)	MC	MC Plate No.	Dx	Dx Node No.	Dy	Dy Node No.
	2	-1.51E+00	202	2.62E-03	15650	-2.60E-03	15182
	5	-1.27E+00	202	2.44E-03	41622	-2.73E-03	15183
	10	-1.50E+00	202	2.72E-03	41622	-3.11E-03	15184
8	0.2	-2.56E+00	202	5.21E-03	14569	7.12E-03	15281
	1	-2.15E+00	202	3.88E-03	17	-3.32E-03	15178
	2	-1.71E+00	202	3.21E-03	41622	-2.94E-03	15180
	5	-1.46E+00	202	3.01E-03	41622	-3.06E-03	15181
	10	-1.72E+00	202	3.32E-03	41622	-3.45E-03	15182
10	0.2	-3.86E+00	202	8.08E-03	14569	1.23E-02	25009
	1	-2.63E+00	202	5.43E-03	59959	5.62E-03	15281
	2	-2.13E+00	202	4.55E-03	17	-3.75E-03	15178
	5	-1.99E+00	202	4.46E-03	41622	-3.90E-03	15178
	10	-2.26E+00	202	4.77E-03	41622	-4.28E-03	15179